Hydrogen-transfer reactions, in which a proton, hydrogen atom, or hydride ion moves from a donor to an acceptor, are ubiquitous in physics, chemistry, and biology – indeed throughout the natural world. These processes occur at rates from vibrational periods to geological periods and are studied by essentially every available theory and technique. Their importance for fundamental science is enormous but they are also vital in industrial chemistry, molecular medicine, and modern pharmaceutical science.

This multivolume work provides interpretative reviews, written by the most active scientists in their fields, of hydrogen transfer in systems beginning with isolated molecules and traversing all levels of organization up to cellular biology. Beginners will find these volumes a clear and accessible introduction to a broad range of topics, while established experts will be pleased by provocative and authoritative presentations of the newest discoveries and ideas.

James T. "Casey" Hynes *was born in Miami Beach, Florida in 1943. He received his A.B. from Catholic University in 1965 and his Ph.D. from Princeton University in 1969. He was then an NIH postdoctoral fellow at MIT and in 1971 joined the faculty at the University of Colorado, Boulder, where he is currently Professor of Chemistry and Biochemistry. Since 1999, he has also been CNRS Director of Research in the Chemistry Department at Ecole Normale Superieure, Paris. His research interests include the theory of the rates and mechanisms of ground and excited state chemical reactions (including proton transfer), of intermolecular and intramolecular energy transfer, and of atmospheric heterogeneous reactions.*

Judith P. Klinman *was born in the city of Philadelphia, PA (USA) in 1941 and educated at the University of Pennsylvania (A.B. 1962 and Ph.D, 1966). She spent several years as a postdoctoral fellow at the Weizmann Institute in Israel and at the Fox Chase Cancer Research Center in Philadelphia. After beginning her independent career as a Research Scientist at Fox Chase, she moved to the University of California in 1978, where she is now Professor of Chemistry and Professor of Molecular and Cell Biology. Her lifelong fascination with enzymes has led her to investigate a wide range of different enzyme systems, with one particular focus being the study of isotope effects as applied to the properties of enzymatic C-H activation.*

Hans-Heinrich Limbach *was born in 1943 in Brühl near Cologne, Germany. He studied Chemistry at the Universities of Bonn and Freiburg, where he obtained his Ph.D. in 1973 and his habilitation in Physical Chemistry in 1980. As a Heisenberg fellow he worked in 1984 with C. S. Yannoni at the IBM Research Laboratory, San Jose, USA and in 1984 and with Prof. C. B. Moore, UC Berkeley. In 1990 he joined the Free University of Berlin. Limbach's research interests are the study of hydrogen and deuterium transfer and bonding in organic liquids and solids, polymers, mesoporous systems, metallorganic compounds, nano-particles and enzymes. For this purpose he uses liquid and solid state Nuclear Magnetic Resonance techniques.*

Richard L. Schowen *was born in 1934 in West Virginia, USA. He was educated at the University of California at Berkeley (B.S. 1958), and the Massachusetts Institute of Technology (Ph.D. 1962). He joined the Chemistry faculty of the University of Kansas in 1963 and retired as Summerfield Professor in the chemical sciences in 2000. He has spent periods in Tokyo, Kyoto, Indiana (USA), Costa Rica, Sheffield (UK), Freiburg, the Scripps Research Institute (USA), the Free University of Berlin as a Humboldt awardee with Professor Limbach, and at the Martin Luther University in Halle as the Kurt Mothes Visiting Professor. Schowen's research addresses mechanisms of solution reactions, including enzyme catalysis, with the use of isotopic methods including solvent isotope effects.*

BICENTENNIAL 1807 WILEY 2007 BICENTENNIAL

www.wiley-vch.de

Volume 1 of 4

ISBN 978-3-527-30777-7

Hynes · Klinman
Limbach · Schowen (Eds.)

1

Hydrogen-Transfer Reactions

WILEY-VCH

Edited by J. T. Hynes, J. P. Klinman, H.-H. Limbach, R. L. Schowen

WILEY-VCH

Hydrogen-Transfer Reactions

Foreword by Ahmed Zewail

Volume 1

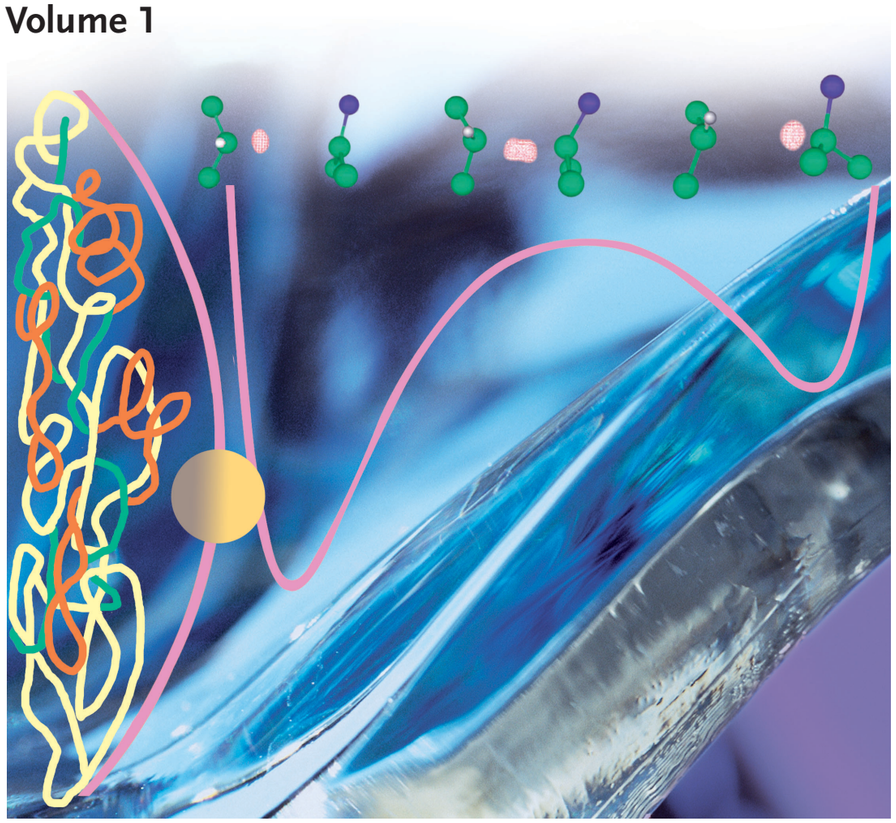

WILEY-VCH
Schowen
2. UK
N. Denzau

Kühn & Weyh Satz und Medien
Freiburg
l:/Vch/Schowen/3b2/c06.3d
6.9.2006

Part II
Hydrogen Transfer in Condensed Phases

Hydrogen-Transfer Reactions. Edited by R. L. Schowen, J. P. Klinman, J. T. Hynes, and H. H. Limbach

ISBN: 3-527-30777-7

WILEY-VCH
Schowen
2. UK
N. Denzau

Kühn & Weyh Satz und Medien
Freiburg
l:/Vch/Schowen/3b2/c06.3d
6.9.2006

WILEY-VCH
Schowen
2. UK
N. Denzau

Kühn & Weyh Satz und Medien
Freiburg
l:/Vch/Schowen/3b2/c06.3d
6.9.2006

6
Single and Multiple Hydrogen/Deuterium Transfer Reactions in Liquids and Solids

Hans-Heinrich Limbach

Overview

In this chapter, Arrhenius curves of selected single and multiple hydrogen transfer reactions for which kinetic data are available over a large temperature range are reviewed. The curves are described by a combination of formal kinetics of reaction networks and the one-dimensional Bell–Limbach tunneling model for each reaction step. The main parameters of this model are the barrier heights and barrier widths of the isotopic reactions, the tunneling masses, the pre-exponential factor and a minimum energy for tunneling to occur. This approach allows one to compare efficiently very different reactions studied in different environments and to prepare the kinetic data for higher-dimensional quantum-mechanical treatments. The first type of reactions discussed is concerned with those where the hydrogen bond geometries of the reacting molecules are well established and where kinetic data of the isotopic reactions are available over a large temperature range. Here, it is possible to study the relation between kinetic isotope effects and chemical structure. Examples are the tautomerism of porphyrin, of the porphyrin anion and related compounds exhibiting intramolecular hydrogen bonds of medium strength, and the solid state tautomerism of pyrazoles and of benzoic acid in cyclic associates. One main result is the finding of pre-exponential factors of the order of $kT/h \cong 10^{13}$ s^{-1}, as expected by transition state theory for vanishing activation entropies. The barriers of multiple H-transfers are found to be larger than those of single H-transfers.

The second type of reactions discussed refers mostly to liquid state solutions and involves major heavy atom reorganization. Here, equilibria between reactive and non- or less reactive molecular configurations may play a role. Several cases are discussed where the less reactive forms dominate at low or at high temperature, leading to unusual Arrhenius curves. These cases include examples from small molecule solution chemistry like the base-catalyzed intramolecular H-transfer in diaryltriazene, 2-(2′-hydroxyphenyl)-benzoxazole, 2-hydroxy-phenoxyl radicals as well as an enzymatic system, thermophilic alcohol dehydrogenase. In the latter case, temperature dependent kinetic isotope effects are interpreted in terms of a transition between two regimes with different temperature independent kinetic isotope effects.

Hydrogen-Transfer Reactions. Edited by R. L. Schowen, J. P. Klinman, J. T. Hynes, and H. H. Limbach

ISBN: 3-527-30777-7

WILEY-VCH
Schowen
2. UK
N. Denzau
Kühn & Weyh Satz und Medien
Freiburg
l:/Vch/Schowen/3b2/c06.3d
6.9.2006

6.1 Introduction

Since the introduction of modern spectroscopic and kinetic techniques, H-transfer reactions constitute an active field of research because of their importance in chemistry and physics [1]. As in electron transfer reactions, tunneling plays an important role. However, in contrast to the Marcus theory of electron transfer [2], there is no widely accepted theory of H-transfer available to date. This is because H-transfer can occur in a variety of forms. Proton and hydride transfer are coupled to charge transfer and are strongly affected by solvent phenomena [3]. In contrast, hydrogen atom transfer and multiple proton transfers often take place without net charge transfer. As the electron/heavy atom mass ratios are smaller than 10^{-4} the tunneling motion of the electron is well separated from heavy atom reorganization. This may not be the case in H-transfers, where heavy atom tunneling may play a role. In contrast to electron transfer, hydrogen bond formation strongly affects the way H is transferred. Only H-transfer in weak and moderately strong hydrogen bonds can be described in terms of rate processes, as for electron transfer; in strong hydrogen bonds protons may no longer experience a barrier of transfer but are localized in the hydrogen bond center [3]. Finally, the three isotopes of hydrogen add to the complexity of H-transfer but also constitute important mechanistic tools.

Many different spectroscopic and kinetic techniques have been applied to the study of H-transfer reactions. Among these are dynamic nuclear magnetic resonance techniques. In the past decades it has been shown that NMR is an especially powerful tool for the study of degenerate single and multiple hydrogen transfer reactions in model hydrogen bonded systems embedded in liquid and solids [4]. Traditionally, the dynamic range of NMR was limited to the millisecond timescale but, for H-transfers in the solid state, it has been possible to extend this scale to the micro- to nanosecond timescale. In addition, it has been possible to elucidate multiple kinetic hydrogen isotope effects over large temperature ranges which enables one to detect tunnel effects at low temperatures from the observation of concave Arrhenius curves of the isotopic reactions. These curves can serve as benchmarks in order to check quantum-mechanical theories of rate processes in condensed matter.

Kinetic isotope effects of single H-transfers in organic liquids have often been interpreted in terms of a combination of Eyring's transition state theory [5] and isotope fractionation theory as proposed by Bigeleisen [6]. In this theory, kinetic isotope effects arise mainly from the difference in zero-point energies between the transition and the initial state. However, as has been shown by Bell [7], in hydrogen transfer reactions one has to take into account tunneling through the barrier, as has been mentioned above. His one-dimensional semiclassical "Bell tunneling model" has been very successful for the interpretation of Arrhenius curves of single hydrogen transfers using empirical parameters. The model was developed in times when computers were not available, i.e. was designed for the case of slow proton transfer, mainly hydrogen abstraction from carbon. Typically,

WILEY-VCH
Schowen
2. UK
N. Denzau
Kühn & Weyh Satz und Medien
Freiburg
l:/Vch/Schowen/3b2/c06.3d
6.9.2006

reactions in solution were studied around room temperature over a limited range of temperatures. For these cases, the so-called "Bell tunneling correction" to the Arrhenius curves, elucidated in terms of classical transition state theory, was sufficient and has, therefore, often been taken as synonymous with the "Bell tunneling model". Full semiclassical tunneling calculations employing modified barriers have been performed by various other authors e.g. Ingold et al. [8], Limbach et al. [9], and Sutcliffe et al. [10]. Other semiclassical models of single proton abstractions have been proposed by Kuznetsov and Ulstrup [11, 12] and modified by Knapp et al. [13] for use in enzyme reactions. Siebrand et al. [14] have proposed a golden rule treatment of H-transfer between the eigenstates of the reactants and products where low-frequency vibrations play an important role varying the heavy atom distances.

Various quantum-mechanical theories have been proposed which allow one to calculate isotopic Arrhenius curves from first principles, where tunneling is included. These theories generally start with an *ab initio* calculation of the reaction surface and use either quantum or statistical rate theories in order to calculate rate constants and kinetic isotope effects. Among these are the "variational transition state theory" of Truhlar [15], the "instanton" approach of Smedarchina et al. [16], or a Redfield-relaxation-type theory as proposed by Meyer et al. [17]. However, these methods require extensive theoretical work and are, generally, not available for the experimentalist in the stage where he needs to simulate his Arrhenius curves. For this stage, empirical tunneling models are important.

This is especially true for the case of multiple hydrogen transfer reactions. In a number of papers, Limbach et al. have proposed to use formal kinetics in order to describe multiple kinetic isotope effects of intramolecular [18–23] and intermolecular HH-transfers [24]. This method has been extended to triple [25] and quadruple transfer reactions [26, 27]. In order to solve the problem of multiple particle transfer two limiting cases were considered. The "concerted" transfer refers to the case where several hydrogen and heavy atoms are transferred at the same time in such a way that they can be treated as a single particle. The "stepwise" transfer refers to the case where intermediates are involved. Here, the overall rate constants of the isotopic reactions studied are related using formal kinetics, to those of the individual reaction steps. Each reaction step, consisting of a single or concerted multiple H-transfer is treated in terms of a tunneling model based on Bell model [9]. In order to avoid possible confusion, this model will be denoted as the "Bell–Limbach" model. We note that the formal kinetic treatment of the stepwise transfer does not need to be combined with this model, but can also be combined with any theory treating a single step. For example, Smedarchina et al. [16] have used this approach in connection with their instanton approach.

The Bell–Limbach model is not designed to give definite interpretations of Arrhenius curves of hydrogen transfer reactions which have to come from more sophisticated methods. However, it provides an opportunity to check whether the number of parameters describing a given set of Arrhenius curves matches or exceeds the number of parameters necessary to describe the same set in terms of sums of single Arrhenius exponentials. This check also tells whether it is useful

WILEY-VCH
Schowen
2. UK
N. Denzau
Kühn & Weyh Satz und Medien
Freiburg
l:/Vch/Schowen/3b2/c06.3d
6.9.2006

to apply a more sophisticated tunnel model containing a larger number of parameters. Finally, the Bell–Limbach model provides a platform which allows one to compare different reactions with each other and to derive general trends important for the kineticist to guide future research.

The scope of this chapter is, therefore, (i) to review the Bell–Limbach tunneling model in comparison with other models and its use for describing single steps of multiple hydrogen transfer networks and (ii) to review applications of this approach in a number of cases which have been studied mainly by NMR. A description of the techniques used for the determination of rate constants of H-transfer will not be included in this chapter; readers interested in this problem are referred to a recent review [4].

6.2 Theoretical

In this section first different models of single H-transfer will be reviewed, including primary kinetic H/D isotope effects, where the focus is on the Bell–Limbach model. Then formal kinetics will be used to describe multiple hydrogen transfers and their kinetic isotope effects.

6.2.1 Coherent vs. Incoherent Tunneling

The simplest model proposed to accommodate a degenerate hydrogen transfer process has been derived [28] from the theory of the one-dimensional symmetric double oscillator [29]. As illustrated in Fig. 6.1(a), this model assumes a symmetric double well with delocalized vibrational hydrogen states which are given in approximation as the positive and the negative linear combinations of the corresponding harmonic oscillator states. The energy splitting is hJ, where J can be interpreted as the frequency of coherent hydrogen tunneling of a wave packet created at $t = 0$, oscillating between the two wells. This type of coherent H tunneling has been verified for small molecules such as malonaldehyde [30], tropolone [31] (Chapt. 1), or formic acid dimer [32] (Chapt. 2) in the gas phase. In contrast, when malonaldehyde is embedded in condensed matter, intermolecular interactions lift the gas phase symmetry of the double well, leading to localized protons [33]. The situation is depicted schematically in Fig. 6.1(b). Here, the one-dimensional double oscillator theory predicts vibrational states with more or less localized proton wavefunctions. In order to arrive at a rate process, more dimensions have to be taken into account. One way is to couple the double oscillator to a bath of harmonic oscillators which will result in vibrational relaxation (VR), taking place on the femtosecond timescale [34]. VR is responsible for the transfer of vibrational energy between the double oscillator and the bath. By VR the localized reactant ground state is converted to higher vibrational states producing a nuclear wave packet. The latter is transferred by tunneling to the product well and deactivated to the product ground

WILEY-VCH
Schowen
2. UK
N. Denzau
Kühn & Weyh Satz und Medien
Freiburg
l:/Vch/Schowen/3b2/c06.3d
6.9.2006

state. Usually, if VR is fast enough, the H tunneling process can be described in terms of rate constants for the forward and the backward H-transfer.

In the liquid state, the effective symmetry of the potential is restored by solvent relaxation (Fig. 6.1(c)). In principle, H-transfer is not restricted to symmetric configurations but can also take place in asymmetric configurations. Hynes et al. [35, see also Chapter 10] have proposed an alternative view which is sketched in Fig. 6.1(d). Here, localized states exhibiting asymmetric single or double wells are first converted by solvent relaxation to a strong symmetric low-barrier hydrogen bond in which the transfer takes place adiabatically before it is completed again by solvent relaxation. In conclusion, in condensed matter coherent tunneling generally becomes incoherent and can then be described by a rate constant instead of a tunnel frequency.

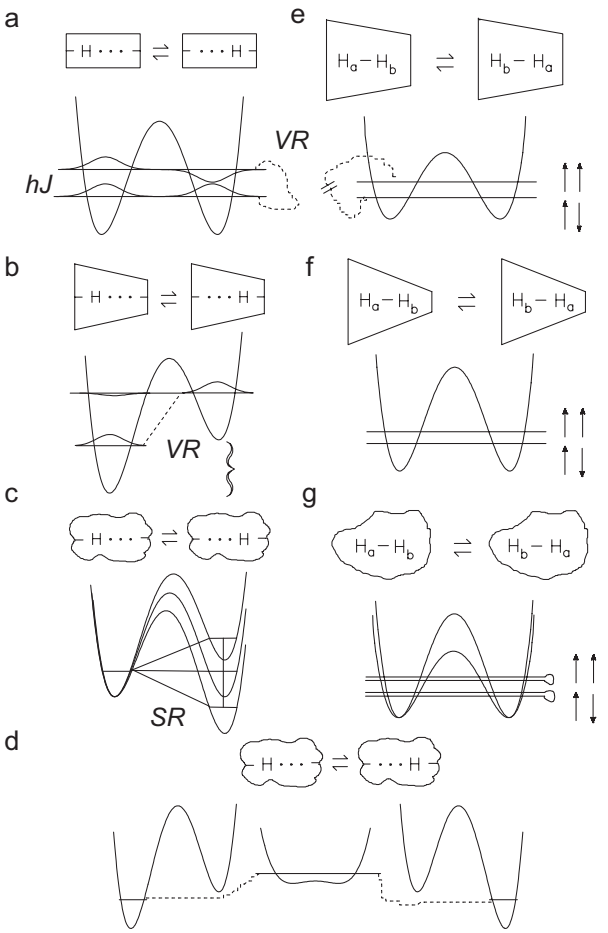

Figure 6.1 One-dimensional double oscillator models for hydrogen transfer and dihydrogen exchange under different conditions.

WILEY-VCH
Schowen
2. UK
N. Denzau
Kühn & Weyh Satz und Medien
Freiburg
l:/Vch/Schowen/3b2/c06.3d
6.9.2006

An exception to this rule is, however, the case of exchange of the nuclei of dihydrogen pairs bound to a transition metal center, where the exchange exhibits a barrier. This phenomenon will be sketched only briefly; for further information the reader is referred to Chapter 21 and to a recent minireview [36].

The situation is illustrated for the gas phase in Fig. 6.1(e). The nuclear spins – characterized by arrows – play a decisive role. The lower tunnel state is symmetric with respect to a permutation H_a–$H_b \leftrightarrow H_b$–H_a and the upper state is antisymmetric. Since hydrogen has a nuclear spin 1/2 the lower state has to be coupled with the antisymmetric nuclear spin function $\uparrow\downarrow$ (antiparallel spins) in order to fuIfill the Pauli exclusion principle. In contrast, the upper tunnel state is antisymmetric and has to be combined with the symmetric nuclear spin states $\uparrow\uparrow$ (parallel spins), as in the case of o-H_2 and p-H_2. Thus, interconversion of the delocalized dihydrogen states also involves a nuclear spin conversion which is much slower than VR. Thus, the tunnel splitting hJ can survive even in larger molecules, even on the NMR timescale. In the crystalline solid the barrier of interchange and the value of J may be altered but not the inherent symmetry of the process, Fig. 6.1(f). When placing the molecule in a multitude of different exchanging environments, i.e. in a liquid (Fig. 6.1(g)) solvent relaxation (SR) will lead to an average temperature dependent tunnel splitting as long as nuclear spin conversion is slow.

As this chapter focuses on hydrogen transfers in liquids and solids, it will be assumed that the transfer constitutes a rate process which can be described in terms of rate constants, for which the usual rate theories can be applied, in particular those derived from transition state theory.

6.2.2 The Bigeleisen Theory

In the theory of Bigeleisen [6], a combination of the theory of equilibrium isotope effects with Eyrings transition state theory [5], kinetic H/D isotope effects can be expressed by

$$\frac{k^{H}}{k^{D}} = \frac{Q^{D} Q^{H\ddagger}}{Q^{H} Q^{D\ddagger}} \tag{6.1}$$

Here, Q^{H} and Q^{D} represent the partition functions of the protonated and deuterated initial state and $Q^{H\ddagger}$ and $Q^{D\ddagger}$ those of the transition state. In order to evaluate Eq. (6.1) the vibrational frequencies of the initial and the transition states are needed. Generally, they are calculated using quantum-mechanical *ab initio* methods in harmonic approximation. The main source of kinetic isotope effects arises then from zero-point energy changes of the protons and deuterons in flight, as has been discussed by Bell [7, 37]. These effects are illustrated for a triatomic model system in Fig. 6.2. There is only a single stretching vibration of AH in the initial state. The transition state exhibits three normal vibrations, an imaginary antisymmetric stretch, a real symmetric stretch (not illustrated), and a real bending vibration. The antisymmetric stretch does not involve any zero-point energy, neither for H nor for D. The symmetric stretch is not isotope sensitive. However,

WILEY-VCH
Schowen
2. UK
N. Denzau
Kühn & Weyh Satz und Medien
Freiburg
l:/Vch/Schowen/3b2/c06.3d
6.9.2006

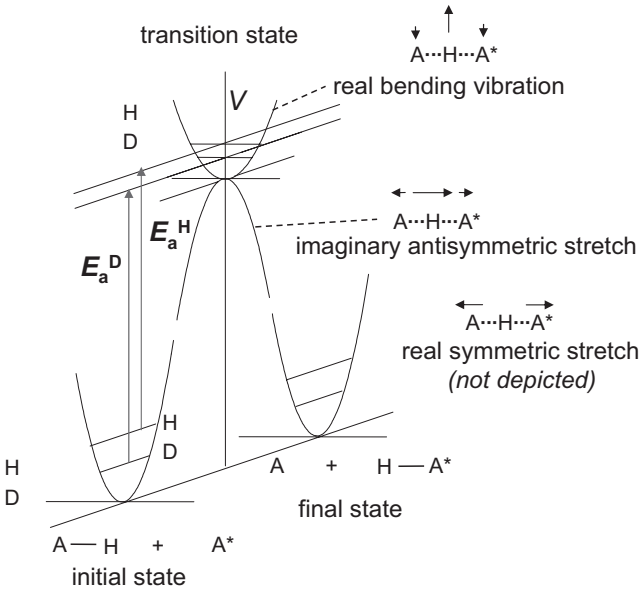

Figure 6.2 Triatomic model of H-transfer illustrating changes in zero-point energies of normal vibrations between the initial and transition states.

the bending vibration contains different zero-point energies for H and for D. Overall, the model predicts a different barrier for H and D transfer, and a kinetic H/D isotope effect of about 6 at room temperature.

6.2.3
Hydrogen Bond Compression Assisted H-transfer

Hydrogen bonding dominates H-transfers from and to oxygen, nitrogen, and fluorine. The barrier of the transfer depends strongly on the hydrogen bond geometry. Unfortunately, a general relation between both is not available to date. In fact, H-transfers in hydrogen bonds constitute a multidimensional problem where many different modes can contribute to the reaction coordinate. Experimentally, it is not easy to identify these modes and to take them into account in simple tunneling models. There is, however, one exception: from an empirical standpoint, hydrogen bond compression has been identified as one important mode which can be taken into account using empirical hydrogen bond correlations which will be described in this section.

With any hydrogen bond A–H···B one can normally associate two distances, the A–H distance $r_1 \equiv r_{AH}$ for the diatomic unit AH, and the H···B distance $r_2 \equiv r_{HB}$ for the diatomic unit HB. According to Pauling [38], one can associate with these distances so-called valence bond orders or bond valences, which correspond to the "exponential distances"

WILEY-VCH
Schowen
2. UK
N. Denzau

Kühn & Weyh Satz und Medien
Freiburg
l:/Vch/Schowen/3b2/c06.3d
6.9.2006

$$p_1 = \exp\{-(r_1 - r_1^\circ)/b_1\},\ p_2 = \exp\{-(r_2 - r_2^\circ)/b_2\},\ \text{with } p_1 + p_2 = 1 \tag{6.2}$$

b_1 and b_2 are parameters describing the decrease of the bond valences of the AH and the HB units with the corresponding distances. r_1° and r_2° are the equilibrium distances of the fictive non-hydrogen bonded diatomic molecules AH and HB. If one assumes that the total valence for hydrogen is unity, it follows that the two distances depend on each other, leading to an ensemble of allowed r_1 and r_2 values representing the "geometric hydrogen bond correlation". The hydrogen bond angle does not appear in Eq. (6.2). This correlation may be transformed into a correlation between the natural hydrogen bond coordinates $q_1 = {}^1/_2(r_1 - r_2)$ and $q_2 = r_1 + r_2$. For a linear hydrogen bond, q_1 represents the distance of H from the hydrogen bond center and q_2 the distance between atoms A and B. Experimentally, hydrogen bond correlations have been established using X-ray and neutron diffraction crystallography [39], as well as by NMR [40]. Note, however, that correlations of the type of Eq. (6.2) were also used a long time ago in the context of describing the "bond energy bond order conservation" reaction pathway of the $H_2 + H$ reaction [41].

A typical geometric hydrogen bond correlation according to Eq. (6.2) derived for NHN-hydrogen bonded systems [42] is depicted in Fig. 6.3. When H is transferred from one heavy atom to the other, q_1 increases from negative values to positive values, and q_2 goes through a minimum which is located at $q_1 = 0$ for hydrogen bonded systems of the AHA-type and near 0 for those of the AHB-type. This correlation implies that, as an approximation, both proton transfer and hydrogen bonding coordinates can be combined into a single coordinate.

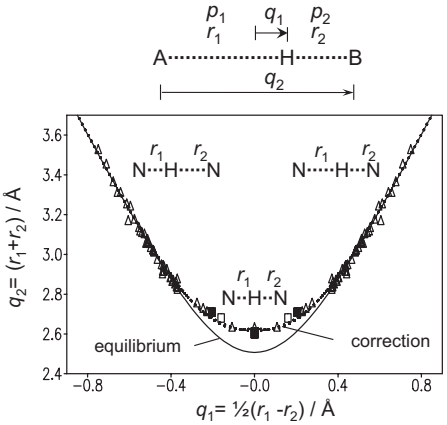

Figure 6.3 Correlation of the hydrogen bond length $q_2 = r_1 + r_2$ with the proton transfer coordinate $q_1 = {}^1/_2(r_1 - r_2)$. Solid line: correlation for equilibrium distances calculated with $b_1 = b_2 = 0.404$ Å and $r_1^\circ = r_2^\circ = 0.992$ Å. Dotted line: empirical correction for zero-point vibrations. Adapted from Ref. [42].

WILEY-VCH
Schowen
2. UK
N. Denzau
Kühn & Weyh Satz und Medien
Freiburg
l:/Vch/Schowen/3b2/c06.3d
6.9.2006

The solid correlation line in Fig. 6.3 is calculated by adapting the parameters of Eq. (6.2) to experimental hydrogen bond geometries established by low-temperature neutron diffraction and NMR data. A deviation has been observed between the experimental data and the solid correlation line in the region of strong hydrogen bonds around $q_1 = 0$. This effect has been associated with zero-point energy vibrations which are not taken into account in Eq. (6.2), which is valid only for equilibrium geometries. An empirical correction leading to the dotted line in Fig. 6.3 has been proposed [36]. A similar empirical correction has also been proposed for OHN-hydrogen bonds [43].

The shortest possible equilibrium heavy atom distance is given by [39b]

$$q_{2\min} = 2(r_o - b \ln {}^1/_2) \tag{6.3}$$

which leads to the values for symmetric hydrogen bonds listed in Table 6.1. These distances provide interesting references for characterizing transition states of H-transfers obtained by quantum-mechanical calculations. For example, hydride transfer distances between two carbon atoms at the transition state were calculated to be in the range 2.69–2.75 Å for various enzyme reactions [44].

Table 6.1 Shortest possible heavy atom distances of symmetric H-bonds predicted by the valence bond order model.

	r_o/Å	b/Å	q_{2min}/Å
OHO	0.95	0.37	2.41
NHN	0.99	0.404	2.53
CHC	1.1	~0.4	~2.75

6.2.4 Reduction of a Two-dimensional to a One-dimensional Tunneling Model

How do the H-bond geometries change during a typical H-transfer process? It is clear that at the minimum value of the heavy atom coordinate q_2 only a single geometry is realized, which is consistent with a single well potential for the H-motion. In contrast, at other geometries, the correlation curve indicates the possibility of double well situations, where the barrier height E_d increases with increasing value of the heavy atom coordinate q_2.

The situation is illustrated schematically in Fig. 6.4(a) for the case of degenerate H-transfers. One-dimensional cuts $V(q_1)$ at different values of q_2 through a two-dimensional potential surface of a degenerate H-transfer are displayed. The barrier height E_d of the double well describing the H-transfer decreases when q_2 is

WILEY-VCH
Schowen
2. UK
N. Denzau
Kühn & Weyh Satz und Medien
Freiburg
l:/Vch/Schowen/3b2/c06.3d
6.9.2006

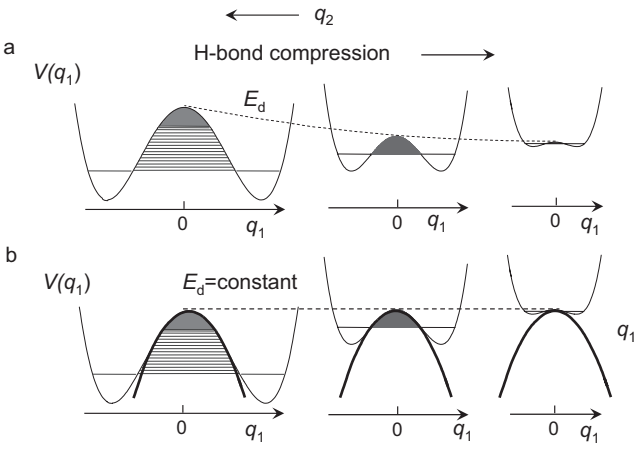

Figure 6.4 (a) One-dimensional cuts $V(q_1)$ through a two-dimensional potential energy surface of a degenerate H-transfer at different values of q_2. (b) Reduction of the two-dimensional double-well potential problem to a one-dimensional Bell model. Adapted from Refs. [9] and [26].

decreased, and eventually a single well configuration is reached. There are only a small number of AH vibrational states available; here, only the vibrational ground states are depicted.

As has been pointed out in Ref. [9], such a two-dimensional model can be reduced to a one-dimensional model by setting E_d = constant, as indicated in Fig. 6.4(b) and by assuming a continuous distribution of rapidly interconverting configurations with different values of q_2. Such a situation can be reached practically by excitation of low-frequency H-bond vibrations or phonons. The situation of Fig. 6.4(b) can practically be replaced by an inverted parabola as a barrier, with a continuous distribution of vibrational levels on both sides of the barrier.

A similar argument holds for non-degenerate H-transfers, as illustrated schematically in Fig. 6.5. Here, the asymmetry of the potential curve, i.e. the difference in the energy between the two wells will disappear in the region of the strongest H-bond compression.

In order to evaluate qualitatively the expected kinetic isotope effects one has to discuss (i) zero-point energy (ZPE) changes of H in the transition state as compared to the initial state and (ii) tunnel effects.

The expected changes in the zero-point energies of the H transferred are illustrated schematically in Fig. 6.6 for the degenerate case, as proposed by Westheimer [45]. The antisymmetric stretch in the initial state exhibits quite different ZPEs for H and for D as the force constants are large. This vibration becomes imaginary in the transition state, which is assumed here to be located in the minimum of q_2 , i.e. the ZPE of the antisymmetric stretch is lost in the transition state. The ZPE of the symmetric stretch in the transition state is small and exhibits little isotope dependence. We note that ZPE is built up in the bending vibration in the

WILEY-VCH
Schowen
2. UK
N. Denzau

Kühn & Weyh Satz und Medien
Freiburg
l:/Vch/Schowen/3b2/c06.3d
6.9.2006

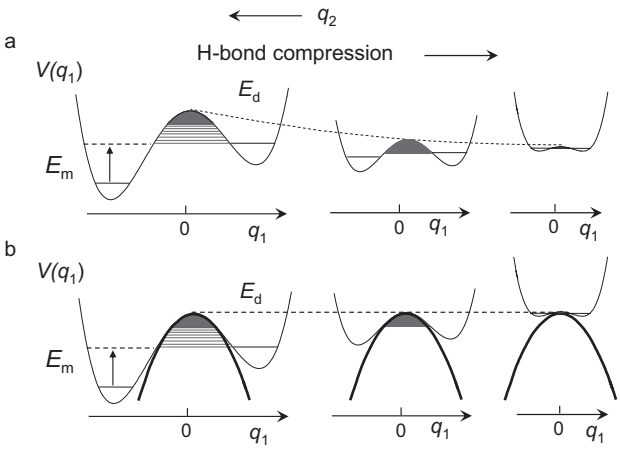

Figure 6.5 (a) One-dimensional cuts $V(q_1)$ through a two-dimensional potential energy surface of a *non-degenerate* H-transfer at different values of q_2. (b) Reduction of the two-dimensional double-well potential problem to a one-dimensional Bell model. E_m refers to a minimum energy for tunneling to occur.

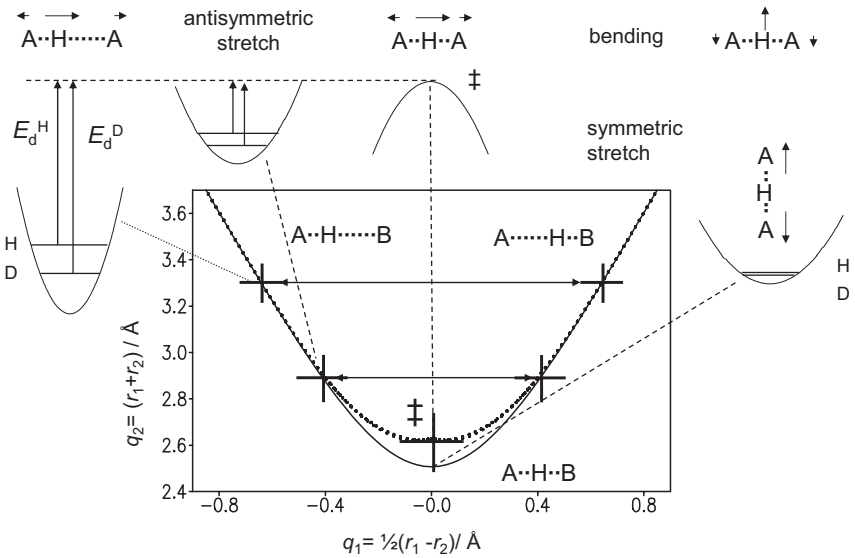

Figure 6.6 Hydrogen bond correlation and zero-point vibrations for a degenerate H-transfer.

transition state. Overall, a substantial difference in the effective barriers for the H-transfer and for the D-transfer is expected. Tunneling pathways can occur at larger values of q_2, which is expected to remain constant during the tunnel process. As only hydrogen isotopes move at constant q_2 the tunneling masses are then 1 for H and 2 for D.

WILEY-VCH
Schowen
2. UK
N. Denzau

Kühn & Weyh Satz und Medien
Freiburg
l:/Vch/Schowen/3b2/c06.3d
6.9.2006

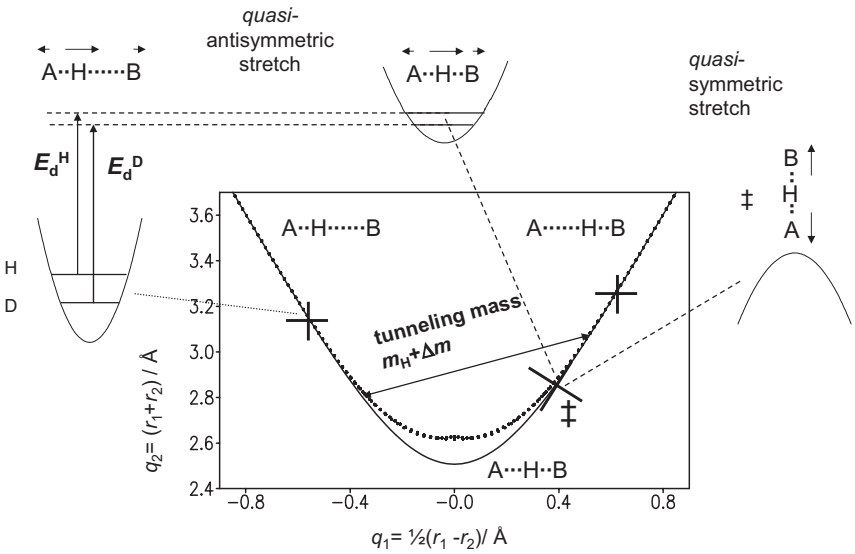

Figure 6.7 Hydrogen bond correlation and zero-point vibrations for a non-degenerate H-transfer.

In contrast, if the transfer is non-degenerate, a situation may occur as illustrated in Fig. 6.7. At the transition state there is remaining ZPE in the antisymmetric stretch. This will lead to a decrease in the difference between the effective barriers for H and for D, as has been proposed by Westheimer [45]. This decrease has also been called the "Westheimer-effect" [46]. Tunneling pathways may no longer involve only changes in q_1, but also a substantial heavy atom motion. This means that the effective tunneling masses will be increased by an additional mass Δm as illustrated schematically.

6.2.5
The Bell–Limbach Tunneling Model

The simplest tunnel model which allows one to calculate Arrhenius curves of H-transfer reactions is the Bell tunneling model [7] which has been modified in our laboratory [9]. The model has been reviewed recently by Limbach et al. [26]. It is visualized in Fig. 6.8 which will be explained in the following.

According to Bell, the probability of a particle passing through or crossing a barrier is given by [7]

$$G(W) = \frac{1}{1 + D(W)^{-1}} \tag{6.4}$$

where W represents the energy of the particle and $D(W)$ the transmission coefficient, given according to the Wentzel–Kramers–Brillouin approximation [47] by

$$D(W) = \exp\left(-\frac{2}{\hbar}\int_{-a'}^{a'} p\,\mathrm{d}x\right) = \exp\left(-\frac{2}{\hbar}\int_{-a'}^{a'} \sqrt{2m(V(x) - W)}\,\mathrm{d}x\right) \tag{6.5}$$

WILEY-VCH
Schowen
2. UK
N. Denzau

Kühn & Weyh Satz und Medien
Freiburg
l:/Vch/Schowen/3b2/c06.3d
6.9.2006

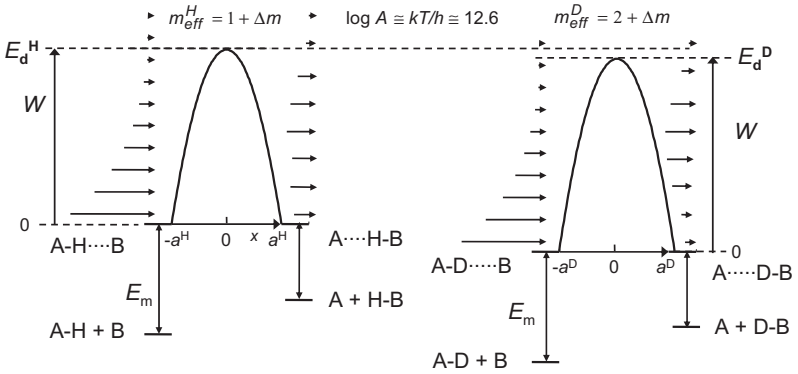

Figure 6.8 Modified Bell tunneling model for H and D transfer. Adapted from Refs. [9] and [26].

p represents the momentum and m the mass of the particle moving in the $q_1 \equiv x$-direction, and $V(x)$ the potential energy experienced by the particle. $|\alpha'|$ represents the position of the particle when it enters or leaves the barrier region at energy W. $V(0) = E_d$ represents the energy of the barrier i.e. the "barrier height" and $2a$ the width of the barrier at the lowest energy where tunneling can occur. Classically $G(W) = 0$ for $W < E_d$ and $G(W) = 1$ for $W > E_d$, but quantum-mechanically $G(W) > 0$ for $W \leq E_d$ and $G(W) < 1$ for $W \geq E_d$. Note here that D is related to the energy splitting of a symmetric double oscillator by [28]

$$\Delta E = \frac{h\nu}{\pi} D^{1/2} \tag{6.6}$$

Assuming that the barrier region can be approximated by an inverted parabola it follows that

$$V(x) = E_d\left(1 - \frac{x^2}{a^2}\right) \quad \text{and that} \quad W = E_d\left(1 - \frac{a'^2}{a^2}\right) \tag{6.7}$$

It has been shown by Bell [48] that

$$D(W) = \exp\left(-\frac{2\pi(E_d - W)}{h\nu_t}\right), \quad \nu_t = \frac{1}{\pi a}\sqrt{\frac{E_d}{2m}} \tag{6.8}$$

where ν_t represents a "tunnel frequency". The fraction of particles in the energy interval dW is given by the Boltzmann law

$$\frac{dN}{N} = \frac{\exp(-W/kT)dW}{\int_0^\infty \exp(-W/kT)dW} = \frac{1}{kT}\exp(-W/kT)dW \tag{6.9}$$

The classical integrated reaction probability is then given by

$$\left(\frac{\Delta N}{N}\right)_{\text{class}} = \frac{1}{kT}\int_{E_d}^{\infty} \exp(-W/kT)dW = \exp(-E_d/kT) \tag{6.10}$$

WILEY-VCH
Schowen
2. UK
N. Denzau

Kühn & Weyh Satz und Medien
Freiburg
l:/Vch/Schowen/3b2/c06.3d
6.9.2006

the quantum mechanical integrated reaction probability by

$$\left(\frac{\Delta N}{N}\right)_{\mathrm{QM}} = \frac{1}{kT}\int_0^\infty G(W)\exp(-W/kT)\mathrm{d}W \tag{6.11}$$

and the ratio of both quantities by

$$Q_t = \frac{\left(\frac{\Delta N}{N}\right)_{\mathrm{QM}}}{\left(\frac{\Delta N}{N}\right)_{\mathrm{class}}}$$

$$= \frac{\frac{1}{kT}\int_0^\infty G(W)\exp(-W/kT)\mathrm{d}W}{\exp(-E_\mathrm{d}/kT)} = \int_0^\infty \frac{G(W)}{kT}\exp((E_\mathrm{d}-W)/kT)\mathrm{d}W \tag{6.12}$$

Using an Arrhenius law for the classical temperature dependence it follows that

$$k = k_{\mathrm{class}}Q_t = A\exp(-E_\mathrm{d}/kT)\int_0^\infty \frac{G(W)}{kT}\exp((E_\mathrm{d}-W)/kT)\mathrm{d}W \tag{6.13}$$

Replacing the Boltzmann constant by the gas constant, and introducing a superscript as label for the isotope L = H, D it follows that

$$k^\mathrm{L} = A^\mathrm{L}\exp(-E_\mathrm{d}^\mathrm{L}/RT)\int_0^\infty \frac{G^\mathrm{L}(W)}{RT}\exp\left(\left(E_\mathrm{d}^\mathrm{L}-W\right)/RT\right)\mathrm{d}W, \mathrm{L} = \mathrm{H}, \mathrm{D} \tag{6.14}$$

At very high temperatures, the integral becomes unity and one obtains the classical expression

$$k^\mathrm{L} = A^\mathrm{L}\exp(-E_\mathrm{d}^\mathrm{L}/RT), \mathrm{L} = \mathrm{H}, \mathrm{D} \tag{6.15}$$

From Eq. (6.14) one obtains the following expression for the "primary" kinetic isotope effect for the H-transfer as a function of temperature

$$P = \frac{k^\mathrm{H}}{k^\mathrm{D}} = \frac{A^\mathrm{H}Q^\mathrm{H}\exp(-E_\mathrm{d}^\mathrm{H}/RT)}{A^\mathrm{D}Q^\mathrm{D}\exp(-E_\mathrm{d}^\mathrm{D}/RT)} \tag{6.16}$$

where Q^L has been called the "tunnel correction". This equation has been introduced by Bell [7]. The energy difference $\Delta\varepsilon = E_\mathrm{d}^\mathrm{D} - E_\mathrm{d}^\mathrm{H}$ describing the losses of zero-point energy between the reactant and the transition state can be calculated using Bigeleisen theory [6].

In the low temperature regime for $W = 0$ it follows from Eq. (6.8) that

$$G(0) \cong D(0) = \exp\left(-\frac{2\pi^2 a}{h}\sqrt{2mE_\mathrm{d}}\right) \tag{6.17}$$

Therefore,

$$k_o^\mathrm{L} = A^\mathrm{L}D^\mathrm{L}(0) = A^\mathrm{L}\exp\left(-\frac{2\pi^2 a^\mathrm{L}}{h}\sqrt{2m^\mathrm{L}E_\mathrm{d}^\mathrm{L}}\right) \tag{6.18}$$

The width of the barrier for the D-transfer can be calculated from Eq. (6.7) and is given by

WILEY-VCH
Schowen
2. UK
N. Denzau
Kühn & Weyh Satz und Medien
Freiburg
l:/Vch/Schowen/3b2/c06.3d
6.9.2006

$$2a^{\mathrm{D}} = 2a^{\mathrm{H}}\sqrt{\frac{E_{\mathrm{d}}^{\mathrm{D}}}{E_{\mathrm{d}}^{\mathrm{H}}}} \tag{6.19}$$

With $m^{\mathrm{H}} = 1$ and $m^{\mathrm{D}} = 2$, the low-temperature rate constant k_0^H is then determined mainly by a^{H} for a given value of E_{d}^H. The low-temperature and temperature independent kinetic isotope effect k_0^H/k_0^D is, therefore, determined by E_{d}^D which is obtained experimentally at high temperatures. In other words, k_0^H/k_0^D and the high-temperature kinetic isotope effects cannot be varied independently of each other, which is not in agreement with experimental data. This effect can be associated with heavy atom tunneling during the H-transfer. The tunneling mass is increased and the low-temperature H/D isotope effect decreased.

In order to take heavy atom tunneling into account, the expansion

$$(a\sqrt{m})^{\mathrm{L}} = \sqrt{\sum_i a_i^2 m_i} = \left((a^{\mathrm{L}})^2 m_{\mathrm{L}} + \sum_k a_k^2 m_k\right)^{1/2} = a^{\mathrm{L}}\sqrt{m^{\mathrm{L}} + \Delta m} \tag{6.20}$$

is used [9], where

$$\Delta m = \sum_k \left(\frac{a_k}{a^{\mathrm{L}}}\right)^2 m_k,\ \mathrm{L} = \mathrm{H},\ \mathrm{D}\ \text{and}\ k = \text{heavy atoms} \tag{6.21}$$

The heavy atom contribution reduces generally the value of k_0^H/k_0^D. For example, if during H-tunneling in an OHO-hydrogen bond over $2a^{\mathrm{H}} = 0.5$ Å both oxygen atoms are displaced, each by $2a^{\circ} = 0.05$ Å, it follows that $\Delta m = 0.32$, and the total tunneling mass is 1.32 instead of 1.

Equation (6.14) is visualized in Fig. 6.8. Particles of different kinetic energies W, given by a Boltzmann distribution, hit the barrier from the left side, where the probabilities of finding given energies are symbolized by arrows of different length. The arrows on the right side represent the particles which came through the barrier by tunneling. As the tunneling mass of H is smaller than that of D, at a given temperature, the energy for the maximum number of H tunneling through the barrier is smaller than for D.

As Limbach et al. have proposed, Eq. (6.14) needs to be modified in a minor way for application in multiple proton transfer reactions [9, 18, 21, 25, 49]. The most important change is to replace the lower integration limit in Eq. (6.13) by a minimum energy E_{m} for tunneling to occur as indicated in Fig. 6.8, i.e.

$$k^{\mathrm{L}} = A^{\mathrm{L}}\exp(-E_{\mathrm{d}}^{\mathrm{L}}/RT)\int_{E_m}^{\infty}\frac{G^{\mathrm{L}}(W)}{RT}\exp\left(\left(E_{\mathrm{d}}^{\mathrm{L}} - W\right)/RT\right)\mathrm{d}W,\ \mathrm{L} = \mathrm{H},\mathrm{D} \tag{6.22}$$

This modification is necessary for example, when the reaction pathway involves an intermediate. Tunneling can then take place only at an energy which corresponds to the energy of the intermediate. Then, one can identify E_{m} with the energy E_{i} of this intermediate. However, E_{m} may also represent a reorganization energy E_{r} necessary for a heavy atom rearrangement preceding the tunneling process. Thus, E_{m} includes the "work term" in Marcus theory of electron transfer [2]. In addition, E_{m} may include the reaction enthalpy ΔH of a pre-equilibrium to H-transfer as discussed above.

WILEY-VCH
Schowen
2. UK
N. Denzau
Kühn & Weyh Satz und Medien
Freiburg
l:/Vch/Schowen/3b2/c06.3d
6.9.2006

A set of Arrhenius curves calculated using Eq. (6.22) depends then on the following parameters:

1. A single pre-exponential factor A in s^{-1} is used for all isotopic reactions, i.e. a possible mass dependence [7] is neglected within the margin of error. If solvent reorganization and pre-equilibria are absent, A is expected to be about 10^{13} s^{-1}. According to transition state theory, pre-exponential factors are given by $kT/h = 10^{12.6}$ s^{-1} for $T = 298$ K.
2. $E_m = \Delta H + E_r + E_i$ represents the minimum energy for tunneling to occur as described above and is assumed to be isotope independent. Note that a similar effect on the Arrhenius curves may be obtained by using more complex barrier shapes [10].
3. E_d^H is the barrier height for the H-transfer step of interest. Therefore, the sum $E_m + E_d^H$ represents the total barrier height for the H-transfer.
4. $2a^H$ is the barrier width of the inverted parabola used to describe the barrier of the H-transfer at the energy E_m. This parameter indicates the tunnel distance of H. $2a^D$ can be approximated by Eq.(6.19).
5. $\Delta\varepsilon = E_d^D - E_d^H$ represents the increase in the barrier height when H is replaced by D.
6. The tunneling masses are given by $m_{eff}^L = m^L + \Delta m$, L = H, D with $m^H = 1$ and $m^D = 2$.

Δm corresponds to the contribution of heavy atom displacements during the tunneling process.

In order to illustrate the formalism typical Arrhenius curves of H and D transfer using arbitrary parameters are plotted in Fig. 6.9. From the slope of the curves at high temperature one can obtain the quantities $E_m + E_d^H$ and $E_m + E_d^D$ which were the same in all graphs of Fig. 6.9. Because of the different slopes of the H and the D curve, temperature dependent kinetic H/D isotope effects occur in the high-temperature range, as illustrated by the dotted lines. At low temperatures, parallel Arrhenius curves are expected, exhibiting a slope given by E_m. The low-temperature branches are also illustrated by dotted lines. By extrapolation of the low-temperature branches to high temperatures, the values of k_0^H and of k_0^D are obtained. According to Eq. (6.18), they provide information about the barrier width $2a^H$ and the heavy atom tunneling extra mass Δm.

Let us discuss the effects of $2a^H$ and Δm on the Arrhenius curves. In Fig. 6.9(a) and (b) the H curves are identical, as the product $2a^H(1+\Delta m)^{1/2}$ is the same. However, the introduction of an extra tunneling mass of 3 in Fig. 6.9(b) reduces the kinetic isotope effects in the low-temperature regime but not in the high-temperature regime. On the other hand, by comparison of Fig. 6.9(a) with Fig. 6.9(c), or of Fig. 6.9(b) with Fig. 6.9(d), it follows that when a barrier of constant height becomes narrower, the regime of temperature independent kinetic isotope effects is reached at higher temperatures.

WILEY-VCH
Schowen
2. UK
N. Denzau

Kühn & Weyh Satz und Medien
Freiburg
l:/Vch/Schowen/3b2/c06.3d
6.9.2006

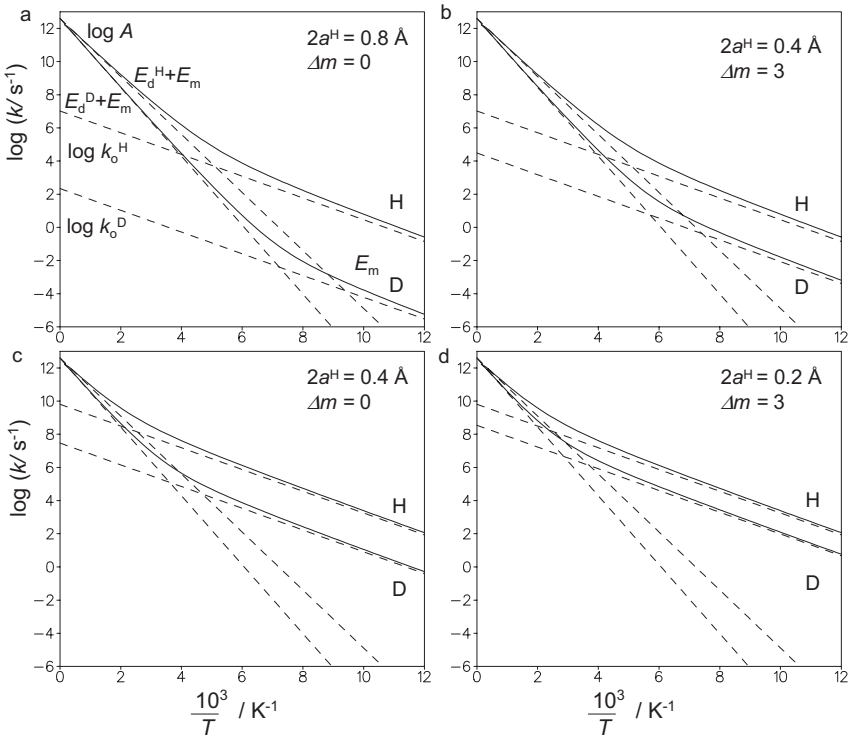

Figure 6.9 Arrhenius curves of H and D transfer calculated according to the Bell–Limbach tunneling model. Minimum energy for tunneling to occur $E_d^H = 12.55$ kJ mol^{-1}, barrier heights $E_d^H = 20.9$ kJ mol^{-1}, $E_d^D = 27.2$ kJ mol^{-1}, tunneling masses m^H=1+ Δm , m^D= 2+ Δm . Barrier width $2a^D = 2a^H(E_d^D / E_d^H)^{1/2}$ according to Eq. (6.19). k_o^H and k_o^D are the extrapolated ground state tunneling rates as defined in Eq. (6.18).

6.2.6
Concerted Multiple Hydrogen Transfer

Equation (6.22) may not only be used in the case of a single proton transfer but also in the case of concerted multiple proton transfers, according to Fig. 6.10, characterized by a single barrier. Only some minor changes are necessary.

1. $\Delta\varepsilon = E_d^D - E_d^H$ continues to represent the increase in the barrier height when a given H is replaced by D. For successive replacements of H by D, generally, the so-called "Rule of the Geometric Mean" (RGM) derived for equilibrium isotope effects [6b] is applied, i.e. it is assumed that replacement of each H by D leads to the same increase $\Delta\varepsilon$ of the barrier height

$$E_d^{HD} = E_d^{HH} + \Delta\varepsilon,\ E_d^{DD} = E_d^{HH} + 2\Delta\varepsilon, \ldots . E_d^{DDDD} = E_d^{HHHH} + 4\Delta\varepsilon \qquad (6.23)$$

WILEY-VCH
Schowen
2. UK
N. Denzau

Kühn & Weyh Satz und Medien
Freiburg
l:/Vch/Schowen/3b2/c06.3d
6.9.2006

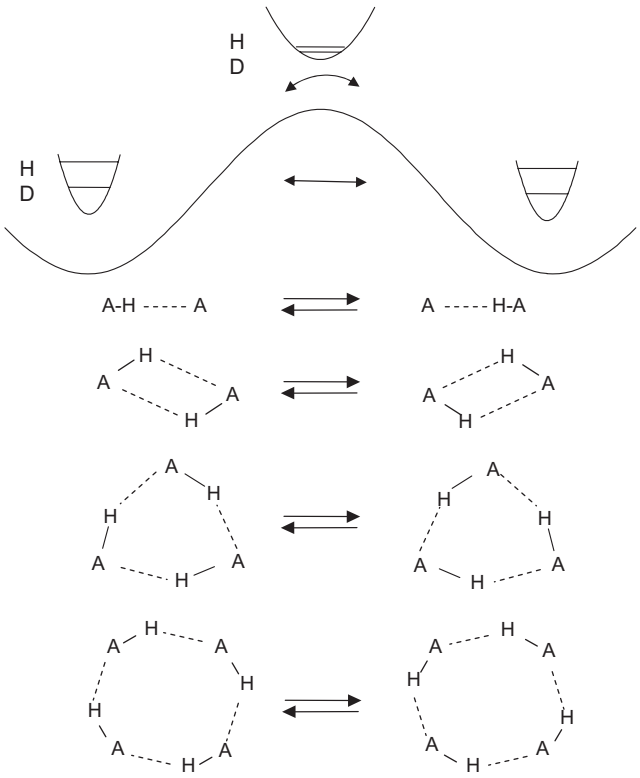

Figure 6.10 Schematic one-dimensional energy profile of degenerate single-barrier hydron (H, D , T) transfers in coupled networks of 1 to 4 cyclic hydrogen bonds. The hydron transfer can be an over-barrier process or a tunneling process, as indicated by the double arrows in the energy profile. The over-barrier process leads to kinetic isotope effects because of the loss of zero-point energy at the top of the barrier for each proton transferred, as indicated schematically. The tunneling process leads to kinetic isotope effects because of different tunneling masses for the hydrogen isotopes. Reproduced with permission from Ref. [26].

$\Delta\varepsilon$ is symbolized schematically in Fig. 6.10 by the different spacings of H and D levels in the ground state and the transition states.

2. The tunneling mass of a given isotopic reaction is written as $m_{\text{eff}} = \sum_i m_i^{\text{L}} + \Delta m$

6.2.7 Multiple Stepwise Hydrogen Transfer

In a number of papers, Limbach et al. have proposed to use formal kinetics in order to describe the case of stepwise HH-transfer [18, 24]. This method has been

WILEY-VCH
Schowen
2. UK
N. Denzau

Kühn & Weyh Satz und Medien
Freiburg
l:/Vch/Schowen/3b2/c06.3d
6.9.2006

extended to the stepwise triple [25] and quadruple transfer cases [26]. In these papers the Bell–Limbach model was employed for the treatment of each reaction step. We note again that the same equations developed can also be used when each reaction step is described in terms of a first-principle theory. In this section the main results of this research are reviewed only briefly. For a more detailed description the reader is referred to Ref. [26].

6.2.7.1 **HH-transfer**

In Fig. 6.11 is depicted a general scheme of a stepwise HH-transfer reaction between the initial state A and the final state D. B and C are intermediates whose concentration is small. In each reaction step a single H is transferred, the other H is bound. Let us denote the formation of the intermediate as "dissociation" and the backward reaction as "neutralization". The corresponding free energy reaction profile is illustrated in Fig. 6.11(b).

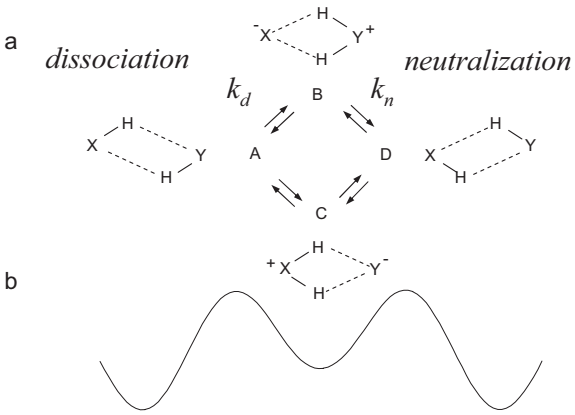

Figure 6.11 Degenerate stepwise HH-transfer involving metastable intermediates. (a) Chemical reaction network as base for a description in terms of formal kinetics. (b) Corresponding free energy diagram. Reproduced with permission from Ref. [26].

Using the steady-state approximation it can easily be shown that the rate constant of the interconversion between A and D is given by

$$k_{AD} = \frac{k_{AB}k_{BD}}{k_{BA} + k_{BD}} + \frac{k_{AC}k_{CD}}{k_{CA} + k_{CD}} \tag{6.24}$$

For the isotopic rate constants it follows that

WILEY-VCH
Schowen
2. UK
N. Denzau

Kühn & Weyh Satz und Medien
Freiburg
l:/Vch/Schowen/3b2/c06.3d
6.9.2006

$$k_{AD}^{HH} = \frac{k_{AB}^{HH} k_{BD}^{HH}}{k_{BA}^{HH} + k_{BD}^{HH}} + \frac{k_{AC}^{HH} k_{CD}^{HH}}{k_{CA}^{HH} + k_{CD}^{HH}}, \; k_{AD}^{HD} = \frac{k_{AB}^{HD} k_{BD}^{DH}}{k_{BA}^{HD} + k_{BD}^{DH}} + \frac{k_{AC}^{DH} k_{CD}^{HD}}{k_{CA}^{DH} + k_{CD}^{HD}}$$

$$k_{AD}^{DH} = \frac{k_{AB}^{DH} k_{BD}^{HD}}{k_{BA}^{DH} + k_{BD}^{HD}} + \frac{k_{AC}^{HD} k_{CD}^{DH}}{k_{CA}^{HD} + k_{CD}^{DH}}, \; k_{AD}^{DD} = \frac{k_{AB}^{DD} k_{BD}^{DD}}{k_{BA}^{DD} + k_{BD}^{DD}} + \frac{k_{AC}^{DD} k_{CD}^{DD}}{k_{CA}^{DD} + k_{CD}^{DD}} \tag{6.25}$$

The primary and secondary kinetic isotope effects of a given reaction step *ij* can be written in the form

$$P_{ij} = \frac{k_{ij}^{H(L)}}{k_{ij}^{D(L)}} \quad \text{and} \quad S_{ij} = \frac{k_{ij}^{L(H)}}{k_{ij}^{L(D)}} \tag{6.26}$$

where the brackets indicate the bound hydrogen. The corresponding isotopic fractionation factor is given by

$$\phi_{ij} = \frac{P_{ji}}{P_{ij}} \frac{S_{ji}}{S_{ij}} \tag{6.27}$$

For the case of degenerate HH-transfers, the following isotopic reaction rate constants have been derived [18a–c, 26]

$$\begin{aligned} k_{AD}^{HH} &= k_{d}^{HH} \\ k_{AD}^{HD} &= k^{DH} = k_{d}^{HH} P_{d}^{-1} \left[\frac{\phi_d S_n^{-1} + S_d^{-1}}{\phi_d S_n^{-1} + P_d^{-1}} \right] \\ k_{AD}^{DD} &= k_{d}^{DD} = k_{d}^{HH} P_{d}^{-1} S_{d}^{-1} \end{aligned} \tag{6.28}$$

The subscript d refers to the dissociation and the subscript n to the neutralization step in Fig. 6.11(a). In the absence of isotopic fractionation $\phi_d = 1$, $S_n = S_d = S$, $P_n = P_d = P$, and Eq. (6.28) simplifies to

$$\begin{aligned} k_{AD}^{HH} &= k_{d}^{HH} \\ k_{AD}^{HD} &= k_{AD}^{DH} = k_{AD}^{HH} \left[\frac{2}{S + P} \right] = k_{AD}^{DD} \left[\frac{2}{P^{-1} + S^{-1}} \right] \\ k_{AD}^{DD} &= k_{d}^{DD} = k_{AD}^{HH} P^{-1} S^{-1} = k_{d}^{HH} P^{-1} S^{-1} \end{aligned} \tag{6.29}$$

and in the absence of secondary isotope effects to

$$\begin{aligned} k_{AD}^{HH} &= k_{d}^{HH} \\ k_{AD}^{HD} &= k_{AD}^{DH} = k_{AD}^{HH} \left[\frac{2}{1 + P} \right] = k_{AD}^{DD} \left[\frac{2}{P^{-1} + 1} \right] = k_{d}^{DD} \left[\frac{2}{P^{-1} + 1} \right] \\ k_{AD}^{DD} &= k_{d}^{DD} = k_{AD}^{HH} P^{-1} = k_{d}^{HH} P^{-1} \end{aligned} \tag{6.30}$$

As the bound H does not contribute, the notation can be simplified by setting $k_{d}^{LL} = k_{d}^{L}$, by dropping the labels for the tautomeric states and by keeping in mind that according to Eq. (6.26)

$$P = k^{H}/k^{D} = k^{HH}/k^{DD}$$

Thus, it follows that

$$\begin{aligned} k^{HH} &= k^{H} \\ k^{HD} &= k^{DH} = \frac{2k^{H}}{1 + k^{H}/k^{D}} = \frac{2k^{D}}{k^{D}/k^{H} + 1} \\ k^{DD} &= k^{D} = k^{HH}P^{-1} = k^{H}P^{-1} \end{aligned} \tag{6.31}$$

This means that at low temperature where P is large the HD reaction is ca. twice as fast as the DD reaction. Equation (6.31) has been used in connection with the Bell–Limbach tunneling model to describe the stepwise double proton transfer in porphyrins, azophenine, and oxalamidines, as will be discussed in Section 6.3. Smedarchina et al. [16] used the same equations for their quantum-mechanical treatment of the porphyrin tautomerism.

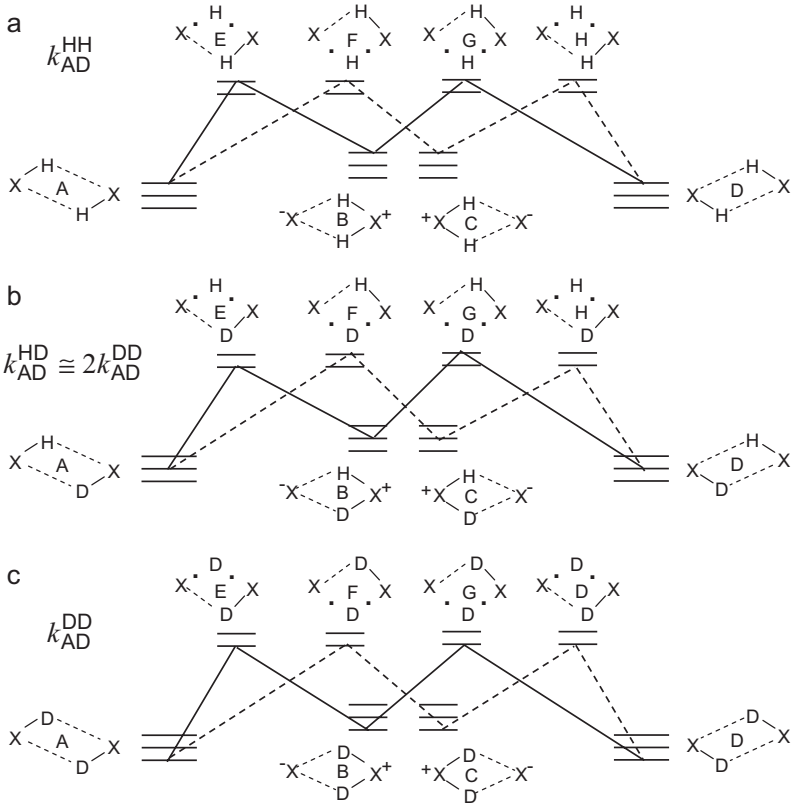

Figure 6.12 Free energy correlation (shown schematically) for the H and D zero-point vibrations for a degenerate stepwise double hydrogen transfer reaction according to Eq. (6.31), where secondary kinetic isotope effects and isotopic fractionation between the initial and the intermediate state were neglected. Adapted from Ref. [18c].

WILEY-VCH
Schowen
2. UK
N. Denzau
Kühn & Weyh Satz und Medien
Freiburg
l:/Vch/Schowen/3b2/c06.3d
6.9.2006

Equation (6.30) can be visualized in the free energy diagrams shown in Fig. 6.12. Different free energies for different isotopic reactions arise either from zero-point energy differences or from tunneling contributions. In all isotopic processes there are equivalent pathways via either intermediate B or C. The initial and final states A and D as well as the two intermediates B and C have two bound hydrogen isotopes, leading to three isotopic states of different free energy, containing either mobile HH, HD, or DD isotopes. In contrast, the states where one hydrogen isotope is in flight are characterized by only two isotopic states of different free energy because there is only one bound hydrogen isotope. Note that the term "state with a hydrogen isotope in flight" can be either a conventional transition state or a state where the isotope tunnels from a thermally activated state through the reaction energy barrier. Let us first compare the HH and the DD reaction profiles in Fig. 6.12(a) and (c). Both profiles are symmetric. Therefore, internal return causes the intermediate to react to the product D only with a probability of $^1/_2$; it returns with the same probability to A. The factor of $^1/_2$ entering the expression for k_{AD}^{HH} and k_{AD}^{DD} is, however, canceled in Eq. (6.30) because there are two equivalent pathways via B and via C for all isotopic reactions. The DD reaction is slower than the HH reaction because of the loss of zero point energy of the XH/XD stretching vibration in the transition states or because of tunneling. In contrast, the reaction profile of the HD process is asymmetric and the transition states E and G (and F and H) are now no longer equivalent. Therefore, the problem of internal return is absent. If one neglects secondary kinetic isotope effects, the energy necessary to reach the H transition states is similar to that in the HH process and the energy necessary to reach the D transition states is similar to that in the DD case. The D transfer step constitutes, therefore, the rate-limiting step of the reaction. The HD reaction has then the same free energy of activation as the DD reaction; however, since in the HD reaction all molecules that have passed the transition state react to products in contrast to the DD reaction, it follows that $k_{AD}^{HD} \cong 2k_{AD}^{DD}$ (Eq. (6.30)).

In contrast, for the case of a non-degenerate reaction where A represents the dominant form and B the dominant intermediate it has been shown [19b] that

$$k_{AD}^{HD} \cong k_{AD}^{DD} \quad \text{and} \quad k_{AD}^{DH} = k_{AD}^{HH} \tag{6.32}$$

These results can again be visualized in a free energy diagram as shown in Fig. 6.13. Since the transition states H are higher in energy than G, the pathways symbolized by the dashed lines do not contribute to the reaction rates. These pathways are, therefore, no longer discussed; only the favored pathways characterized by the solid lines that involve the transition states E and G are considered in the following. The true transition state of all isotopic reactions is G. In the latter, the loss of zero-point energy of XD is larger than of XH and hence the DD reaction is slower than the HH reaction. Thus, neglecting secondary kinetic isotope effects, it follows that the DH reaction is as fast as the HH reaction as H is transferred in the rate-limiting step. By contrast, the D isotope is transferred in the rate-limiting step of the HD reaction which exhibits, therefore, similar rate constants to those of the DD reaction.

WILEY-VCH
Schowen
2. UK
N. Denzau
Kühn & Weyh Satz und Medien
Freiburg
l:/Vch/Schowen/3b2/c06.3d
6.9.2006

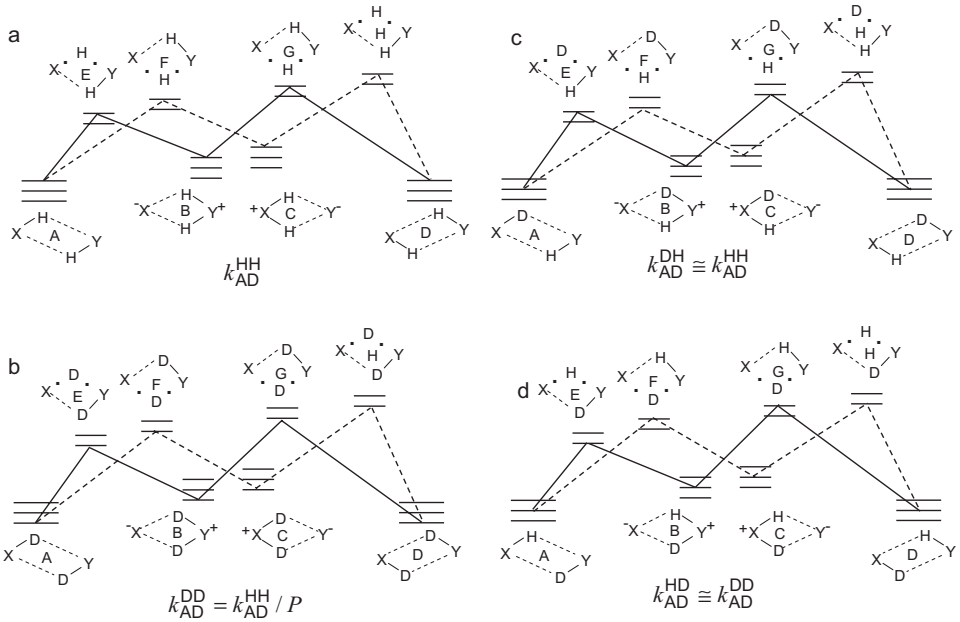

Figure 6.13 Free energy correlation (shown schematically) for the H and D zero-point vibrations for a non-degenerate stepwise HH-transfer reaction. The secondary kinetic isotope effect *S* was set to unity. Adapted from Ref. [18c].

Some calculated kinetic isotope effects are illustrated in the Arrhenius diagrams of Fig. 6.14. If the secondary isotope effects were equal to the primary ones, this would mean that both protons are in flight in the rate-limiting step and the double barrier case would reduce to the single barrier case. Then, one would obtain the rule of the geometric mean (RGM) with $k^{HH}/k^{HD} = k^{HD}/k^{DD} = P$, and the overall isotope effect is $k^{HH}/k^{DD} = P^2$. This result represents in fact a derivation of the RGM for the single barrier case. In the Arrhenius plot of Fig. 6.14(a) the validity of this rule was assumed. However, this rule is valid only in the absence of tunneling and if both proton sites are equivalent. In the presence of tunneling $k^{HH}/k^{HD} > k^{HD}/k^{DD}$ as has been verified previously.

In Fig. 6.14(b) the two-barrier or stepwise transfer Arrhenius diagrams are plotted, where it was assumed that the secondary isotope effects of dissociation and neutralization are small, i.e. equal to 1. In addition, absence of isotopic fractionation is assumed, i.e. $\phi_d = 1$. In this case, k^{DD}/k^{HH} is equal to the kinetic isotope effects $P_d = P_n$ of the dissociation and neutralization steps. When these isotope effects are large, which is the case at low temperatures, k^{HD}/k^{DD} is equal to 2. The statistical factor arises from the fact that in the DD reaction D is transferred in both steps. Therefore, when the intermediate is reached, return to the reactant as well as reaction to the product occurs with equal probability. By contrast, there is no internal return in the HD reaction which exhibits only a single rate-limiting

WILEY-VCH
Schowen
2. UK
N. Denzau

Kühn & Weyh Satz und Medien
Freiburg
l:/Vch/Schowen/3b2/c06.3d
6.9.2006

step, i.e. the one in which D is transferred. Note that Eq. (6.30) is valid even in the presence of tunneling.

When isotopic fractionation takes place, for example through a strenghtening of the H-bond in the intermediate leading to reduced zero-point energies [50], the factor will be larger than 2, leading to an increase of k^{HD}/k^{DD} as illustrated in Fig. 6.14c.

The effect of an increasing reaction asymmetry is illustrated in Fig. 6.14(d)–(f). When the asymmetry is small, the HD and DH processes are almost equally fast, and again characterized by approximately twice the rate constant of the DD process. When the asymmetry becomes larger, the HD curve merges rapidly with the DD curve, and eventually the DH curve with the HH curve.

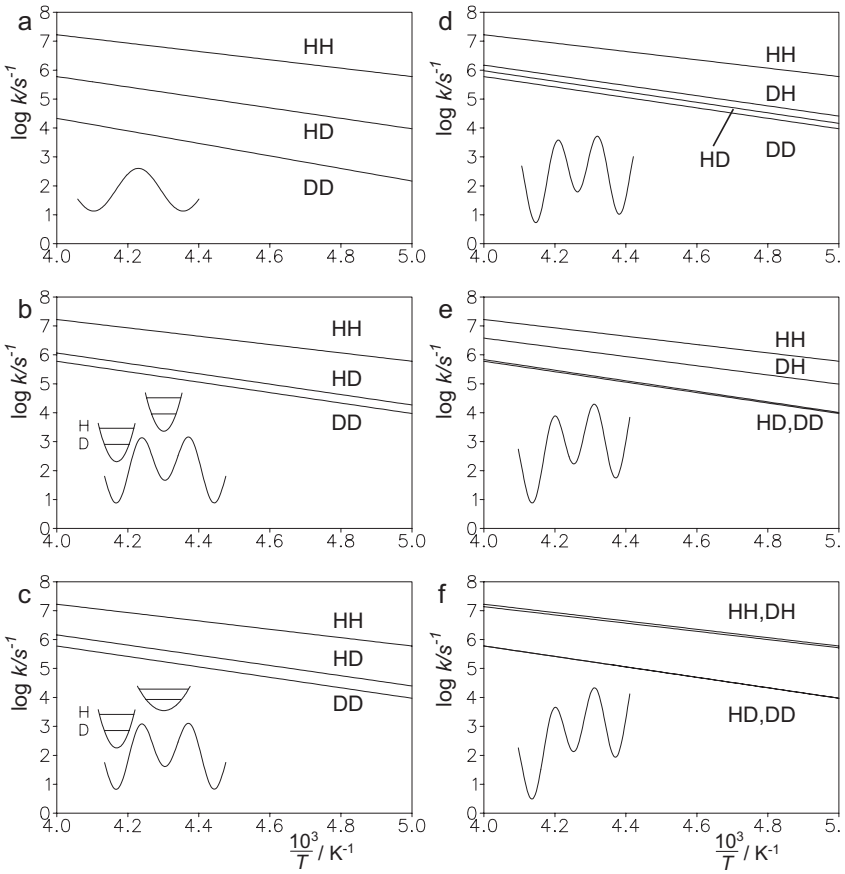

Figure 6.14 Arrhenius diagrams of a degenerate double hydron transfer using the following arbitrary parameters:
$k^{HH} = 10^{13}\exp(-27.6\ \text{kJ mol}^{-1}/\text{RT})$,
$P = P_d = P_f = \exp(-7\ \text{kJ mol}^{-1}/\text{RT})$. (a) Single barrier case. (b) Double barrier case with the H/D fractionation factor of dissociation $\phi_d = 1$. (c) As (b) but with an arbitrary value of $\phi_d = \phi_f = \exp(-0.92\ \text{kJ mol}^{-1}/\text{RT})$;. Adapted from Ref. [26]. (d) to (f) Effect of increasing asymmetry on the kinetic HH/HD/DH/DD isotope effects.

WILEY-VCH
Schowen
2. UK
N. Denzau

Kühn & Weyh Satz und Medien
Freiburg
l:/Vch/Schowen/3b2/c06.3d
6.9.2006

Finally, note that the concerted and the stepwise HH-transfer constitute limiting cases and that various intermediate cases are possible. Rauhut et al. [51] have studied "plateau" reactions which are realized when the energy of the intermediate is raised, producing a very wide flat single barrier region which cannot be described in terms of an inverted parabola.

Meschede and Limbach [24c] have pointed out that compression of both hydrogen bonds of a double proton transfer system leads eventually to a single barrier situation, even if at large H-bond distances a stepwise reaction mechanism is realized.

6.2.7.2 **Degenerate Stepwise HHH-transfer**

The case of a stepwise triple proton transfer [25] is illustrated in Fig. 6.15. It can take place along different pathways via at least two metastable intermediates. For example, if hydrons {1}, {2} and {3} are transferred one after the other the reac-

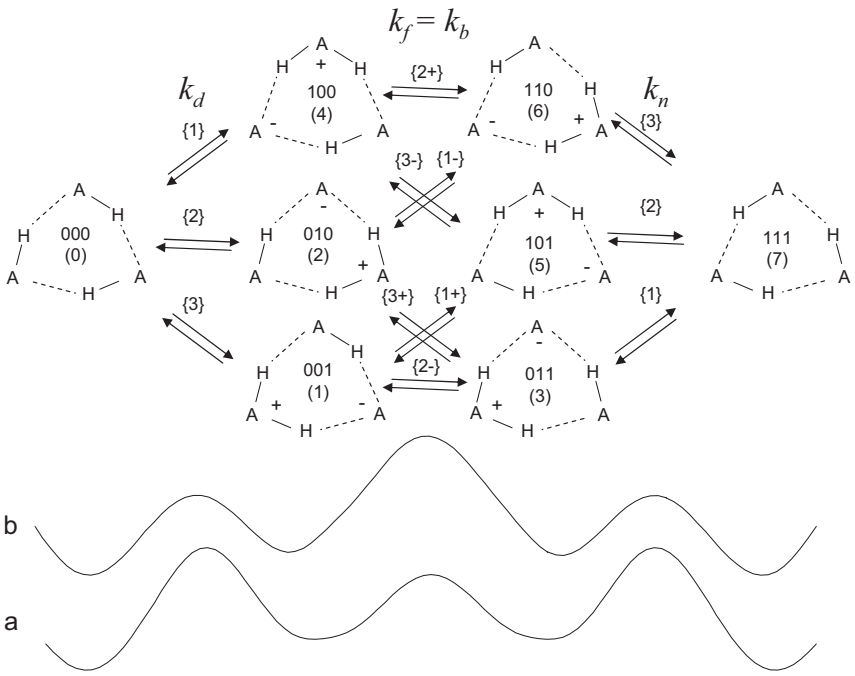

Figure 6.15 Degenerate triple-barrier triple hydron transfer involving two zwitterionic intermediates. A complete transfer consists of a dissociation step, one or more cation or anion "propagation" steps, characterized by the forward and backward rate constants $k_f = k_b$, and a neutralization step. These isotope dependent rate constants depend on whether a cation or an anion is propagated. Cation and anion propagation are included in the brackets indicating the hydron number transferred as a plus or minus sign in the brackets. The rate-limiting step may correspond to the propagation (a) or the dissociation (b). In each step only a single hydron loses zero-point energy at the configuration at the top of the barrier. Adapted from Ref. [26].

WILEY-VCH
Schowen
2. UK
N. Denzau

Kühn & Weyh Satz und Medien
Freiburg
l:/Vch/Schowen/3b2/c06.3d
6.9.2006

Table 6.2 Kinetic isotope effects of degenerate triple proton transfers according to Ref. [9].

			
KIE	$P_1 = P_2 = P_3 = P$	–	$\phi_d < 1,\ P_f^{-1} << 1$
$\frac{k^{HHD}}{k^{HHH}}$	P^{-1}	$1/3(2 + P_d^{-1})$	$1/3(1 + \phi_d)$
$\frac{k^{HDD}}{k^{HHH}}$	P^{-2}	$1/3(1 + 2P_d^{-1})$	$\phi_d/3$
$\frac{k^{DDD}}{k^{HHH}}$	P^{-3}	P_d^{-1}	$P_f^{-1}\phi_d$

tion pathway is 000→100→110→111. As a degenerate reaction is considered the reaction energy profile must be symmetric, leaving only two cases: in the first case the central reaction step is rate-limiting and in the second case the first and third steps, as indicated schematically at the top of Fig. 6.15.

The derivation of expressions for the multiple kinetic isotope effects of the triple hydrogen transfer case is analogous to the HH-transfer but more tedious. Therefore, the reader is referrred to refs. [25] and [26]. The main results are included in Table 6.2. As in the case of the HH-transfer, the kinetic isotope effects derived for the stepwise transfers are valid in the presence of tunneling and are independent of the tunneling model used. By contrast, the kinetic isotope effects of the single barrier reaction are affected by tunneling.

The Arrhenius curves calculated for a small temperature range without tunneling contributions are illustrated in Fig. 6.16. For the single barrier case (Fig. 6.16(a)) Table 6.2 again predicts the rule of the geometric mean. Now, the overall isotope effect is larger than in the HH case, i.e. $k^{HHH}/k^{DDD} = P^3$, however the individual isotope effects are the same if P is kept constant.

In the stepwise triple barrier case with the central propagation as the rate-limiting step the overall isotope effect is given by $k^{HHH}/k^{DDD} = P_d$. It seems astonishing that the individual isotope effects $k^{HHH}/k^{HHD} = 3/2$ and $k^{HHH}/k^{HDD} = 3$ are given only by statistical values when P_d is large (Table 6.2). Thus, the Arrhenius curves of the HHH, HHD and HDD reaction are grouped closely together as illustrated in Fig. 6.16(b). This result can be explained as follows. When the central step is rate-limiting either H is transferred in this step with the probability 1/3 or D with the probability 2/3. The latter D-transfer does not contribute substantially to the overall rate constant, as H is transferred in the central step as fast as in the HHH reaction. Therefore, the HHH/HHD and the HHD/HDD isotope effects are given only by statistical factors.

When the propagation is the rate-limiting step (Fig. 6.16(c)) a similar phenomenon occurs. In the HDD reaction there are pathways where H is transferred both in the first and the final rate-limiting steps, e.g. the sequence 000 → 100 → 101

WILEY-VCH
Schowen
2. UK
N. Denzau

Kühn & Weyh Satz und Medien
Freiburg
l:/Vch/Schowen/3b2/c06.3d
6.9.2006

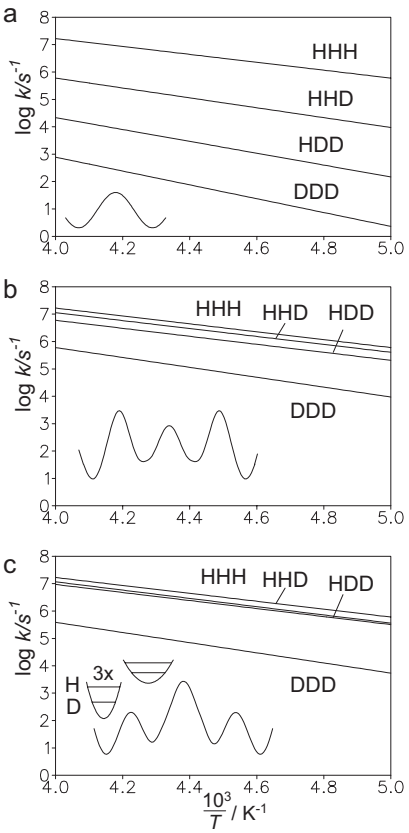

Figure 6.16 Arrhenius diagrams of a degenerate triple hydron transfer. For the HHH-transfer an arbitrary Arrhenius law $k^{HHH} = 10^{13}\exp(-27.6\ \text{kJ mol}^{-1}/\text{RT})$ in s^{-1} was assumed, involving the single proton kinetic isotope effects $P = P_d = P_f = \exp(-7\ \text{kJ mol}^{-1}/\text{RT})$. (a) Single barrier case. (b) Triple barrier case with the dissociation as rate-limiting step. The rate constants are independent of the fractionation factor ϕ_d of the dissociation. (c) Triple barrier case with $\phi_d = \exp(-0.92\ \text{kJ mol}^{-1}/RT)$ and equal rate constants $k_f = k_b$ for the cation and anion propagation, i.e. $\alpha = 1$. Reproduced with permission from Ref. [26].

$\rightarrow$ 001 $\rightarrow$ 011 $\rightarrow$ 111. Therefore, also in this case only replacement of the last proton by a deuteron exhibits a non-statistical kinetic isotope effect. However, the HDD process will experience isotopic fractionation of the dissociation process. Moreover, the DDD process is additionally affected by isotopic fractionation.

6.2.7.3 **Degenerate Stepwise HHHH-transfer**

In Ref. [26] three limiting cases were considered, i.e. a single barrier (Fig. 6.10), a double barrier (Fig. 6.17) and a quadruple-barrier reaction pathway (Fig. 6.18). The first process does not involve any intermediate. The second process consists essentially of consecutive double proton transfer steps, where each step involves a single barrier. There are two possibilities, either protons {1, 2} are transferred first, followed by protons {3, 4}, or vice versa, proceeding via the zwitterionic intermediates 1100 or 0011. It is again assumed that the intermediates can be treated as separate species, i.e. that there are no delocalized states involving different potential wells. This assumption will be realized when the barriers are large. Each reaction step is then characterized by an individual rate constant. The process con-

WILEY-VCH
Schowen
2. UK
N. Denzau

Kühn & Weyh Satz und Medien
Freiburg
l:/Vch/Schowen/3b2/c06.3d
6.9.2006

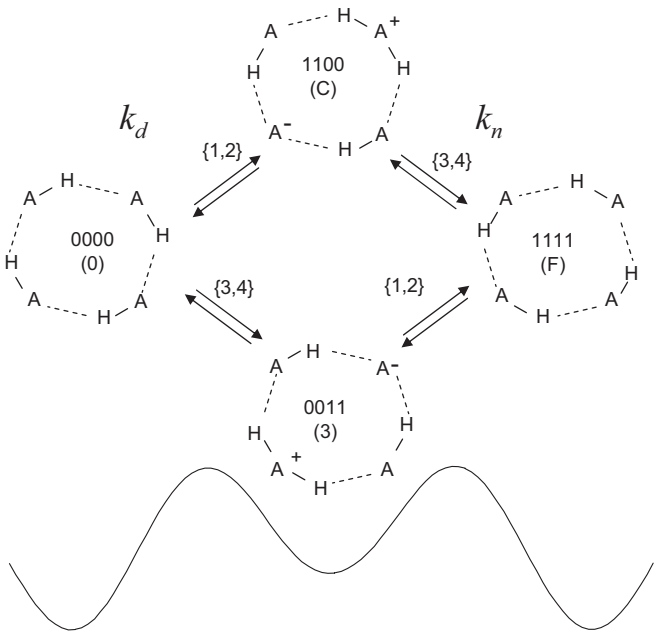

Figure 6.17 Degenerate two-barrier quadruple hydron transfer involving a single zwitterionic intermediate. Two hydrons lose zero-point energy in the configuration corresponding to the top of the barrier. Isotopic fractionation ϕ_d can occur for the dissociation. Reproduced with permission from Ref. [26].

sists of consecutive single proton transfer steps, corresponding to dissociation (k_d), two propagation steps (k_f and k_b), and a neutralization step (k_n). In the propagation steps one of the four protons is transferred and coupled to the transfer of either a positive or a negative charge (cation or anion propagation), indicated by + or – signs. Two possible intermediates, 0101 and 1010 are double zwitterions involving very high energies and are, therefore, neglected.

The expected kinetic isotope effects obtained by neglecting secondary kinetic isotope effects are summarized in Table 6.3. The results are visualized in Fig. 6.19, where again a simple Arrhenius law was assumed for the HHHH reaction with the same arbitrary parameters as for the HH and the HHH reactions in Fig. 6.14 and 6.16.

In the case of the single-barrier mechanism, all four hydrons are in flight in the transition state. Subsequent replacement of H by D involves similar primary kinetic isotope effects P, leading to equally spaced Arrhenius curves of the isotopic reactions in Fig. 6.19(a), with an overall kinetic isotope effect of $k^{HHHH}/k^{DDDD} \approx P^4$. This result is analogous to the single-barrier HH and the HHH-transfer cases discussed above. Note that, generally, the transfer of n hydrons is expected to give rise to an overall kinetic isotope effect of P^n [26].

For the two-barrier HHHH case it was assumed that the first and second primary kinetic isotope effects of the double proton transfer in the dissociation steps

WILEY-VCH
Schowen
2. UK
N. Denzau

Kühn & Weyh Satz und Medien
Freiburg
l:/Vch/Schowen/3b2/c06.3d
6.9.2006

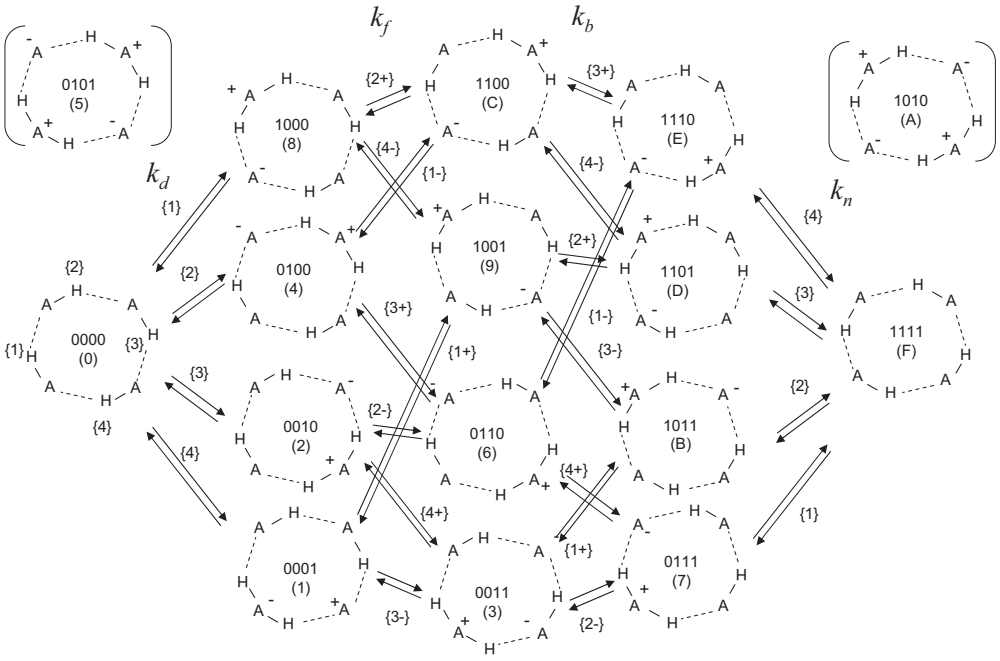

Figure 6.18 Degenerate quadruple-barrier quadruple hydron transfer. A complete transfer consists of a dissociation step, two or more propagation steps and a neutralization step. The double-cation–double-anion intermediates 0101 and 1010 are not further taken into account because of their high Couloumb energy. Reproduced with permission from Ref. [26].

$P_{d1}$and P_{d2} are equal. ϕ_d represents the single H/D fractionation factor of the dissociation step, corresponding to the equilibrium constant of the formal reaction

initial state (D) + intermediate state (H) $\rightleftharpoons$ initial state (H) + intermediate state (D). (6.33)

The results are depicted in Fig. 6.19(b) and (c). Whereas in Fig. 6.19(b) ϕ_d=1, in Fig. 6.19(c) it was assumed that $\phi_d = \exp(-0.92\ \text{kJ mol}^{-1}/RT) < 1$. This fractionation factor takes into account the fact that the zero-point energies of each proton in the intermediate may be reduced due to low-frequency shifts of the proton vibrations, as expected for an increase in the H-bond strength in the intermediate.

One observes three groups of Arrhenius curves, i.e. the HHHH curve, the group of the HHHD and the HDHD curves, and the group of the HHDD, HDDD and DDDD curves. Within each group the differences are small. They are further attenuated by isotope fractionation (Fig. 6.19c). The overall kinetic isotope effect, given by $k^{HHHH}/k^{DDDD} = P_d{}^2$, is typical for a concerted double proton transfer reaction. It is interesting to note that replacement of the first H by D already leads to a

WILEY-VCH
Schowen
2. UK
N. Denzau

Kühn & Weyh Satz und Medien
Freiburg
l:/Vch/Schowen/3b2/c06.3d
6.9.2006

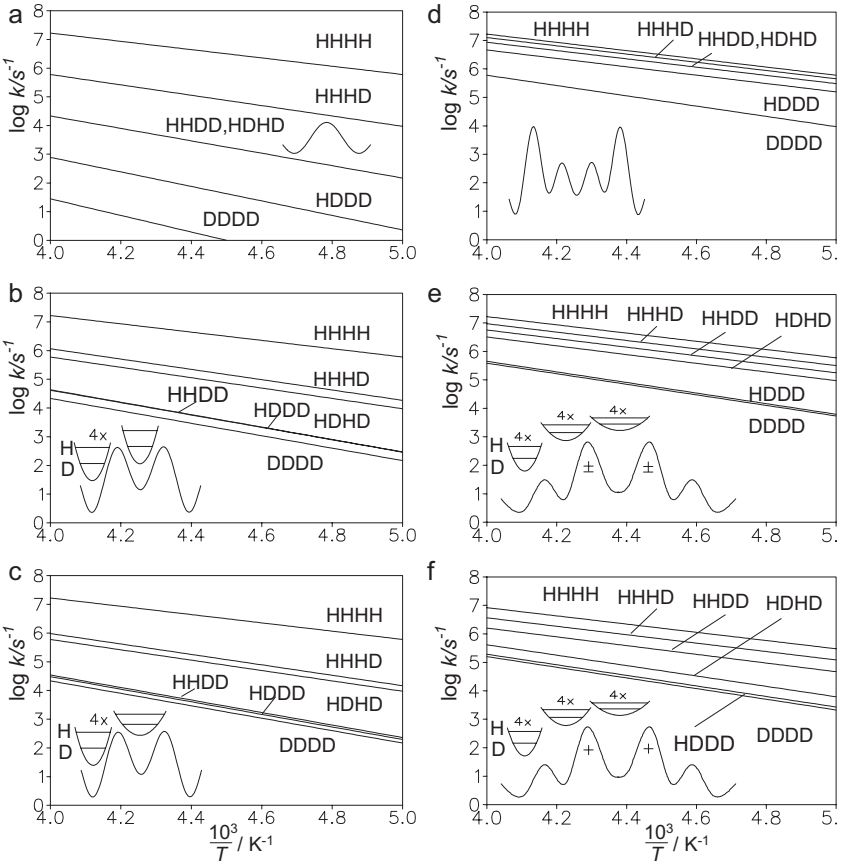

Figure 6.19 Simulated Arrhenius diagrams of a degenerate quadruple hydron transfer. Arrhenius laws are assumed for the HHHH-transfer. (a) Single-barrier case. (b) Double-barrier case with $\phi_d = 1$. (c) Double-barrier case with $\phi_d = \exp(-0.92\ \text{kJ mol}^{-1}/RT)$. (d) Quadruple-barrier case with dissociation as rate-limiting step. (e) Quadruple-barrier case with propagation as rate-limiting step, equal cation and anion propagation $\alpha = 1$ (as indicated by the ± signs), $\phi_d = \phi_f = \exp(-0.92\ \text{kJ mol}^{-1}/RT)$. (f) Quadruple-barrier case with propagation as rate-limiting step, only cation propagation α=0 (as indicated by the + signs), $\phi_d = \phi_f = \exp(-0.92\ \text{kJ mol}^{-1}/RT)$. Adapted from Ref. [26].

substantial isotope effect of $k^{\text{HHHH}}/k^{\text{HHHD}} = P_d/2$ when isotopic fractionation is absent.

In the quadruple-barrier case one needs to distinguish whether dissociation/neutralization or propagation are the rate-limiting steps. Furthermore, a parameter α is needed describing the ratio of the forward reaction rate constants of the anion and the cation propagation, i.e.

$$\alpha = \frac{k_f^{i-}}{k_f^{i+}} \cong \frac{k_b^{i-}}{k_b^{i+}} \tag{6.34}$$

WILEY-VCH
Schowen
2. UK
N. Denzau

Kühn & Weyh Satz und Medien
Freiburg
l:/Vch/Schowen/3b2/c06.3d
6.9.2006

Table 6.3 Kinetic isotope effects of degenerate quadruple proton transfers according to Ref. [26].

KIE	$P_1 = P_2 = P_3 = P$	$P_{d1}^{-1} = P_{d2}^{-1} = P_d^{-1} << 1$	$P_d^{-1} << 1$	$\phi_d < 1, \phi_f < 1,$ $P_f^{-1} << 1, \alpha = 1$	$\phi_d < 1, \phi_f < 1,$ $P_f^{-1} << 1, \alpha = 0$
$\frac{k^{HHHD}}{k^{HHHH}}$	P^{-1}	$P_d^{-1}(1+\phi_d^{-1})$	$\frac{3}{4}$	$\frac{1+\phi_d}{3}$	$\frac{1+\phi_d}{4}$
$\frac{k^{HHDD}}{k^{HHHH}}$	P^{-2}	$P_d^{-2}(1+\phi_d^{-2})$	$\frac{1}{2}$	$\frac{\phi_d}{4}$	$\frac{\phi_d}{4}$
$\frac{k^{HDHD}}{k^{HHHH}}$	P^{-2}	P_d^{-1}	$\frac{1}{2}$	$\frac{\phi_d}{2}$	$P_f^{-1}(1+\phi_d\phi_f)$
$\frac{k^{HDDD}}{k^{HHHH}}$	P^{-3}	$P_d^{-2}(1+\phi_d^{-1})$	$\frac{1}{4}$	$P_f^{-1}\phi_d(1+\phi_f)$	$\frac{P_f^{-1}(1+3\phi_d+2\phi_d\phi_f)}{4}$
$\frac{k^{DDDD}}{k^{HHHH}}$	P^{-4}	P_d^{-2}	P_d^{-1}	$P_f^{-1}\phi_d$	$P_f^{-1}\phi_d$

where *i*– and *i*+ indicate the transfer of hydron *i* coupled to the transfer of a negative or positive charge. In Table 6.3 P_f and P_b constitute the kinetic isotope effects of the two propagation steps; ϕ_d corresponds to the fractionation factor of the dissociation.

When dissociation and neutralization are the rate-limiting steps (Fig. 6.19(d)), an overall kinetic isotope effect of $k^{HHHH}/k^{DDDD} = P_d$ is expected, again typical for a single H-transfer. Surprisingly, only replacement of the last H by D is affected by P_d. As in the stepwise HHH case, this effect arises again from the possibility of reaction pathways involving transfer of H in the rate-limiting steps, even in the HDDD reaction.

In the case of the propagation as rate-limiting step, an overall isotope effect of $k^{HHHH}/k^{DDDD} = P_f\phi_d$ is expected. The rate constants of the other isotopic reactions are between the values of k^{HHHH} and k^{DDDD}. In Fig. 6.19(e) it is assumed that both cation and anion propagation exhibit the same rate constants, and in Fig. 6.19(f) it is assumed that anion propagation does not contribute fundamentally to the rate constants. This effect leads to a reduction in k^{HDHD}.

6.2.8
Hydrogen Transfers Involving Pre-equilibria

According to Eigen's scheme of H-transfer [52] in solution the reaction partners have first to meet in order to react. For an intermolecular H-transfer from AH to B one can write

WILEY-VCH
Schowen
2. UK
N. Denzau

Kühn & Weyh Satz und Medien
Freiburg
l:/Vch/Schowen/3b2/c06.3d
6.9.2006

$$A\text{–}H + B \overset{K}{\rightleftharpoons} A\text{–}H\cdots B \overset{k}{\rightleftharpoons} A\cdots H\text{–}B \rightleftharpoons A + HB \tag{6.35}$$

In Eq. (6.35) electrical charges are omitted. k represents the intrinsic forward rate constant. The pre-equilibrium constant is given by

$$K = \frac{c_{AB}}{c_A c_B} \tag{6.36}$$

where c_A and c_B represent the concentrations of the reactants AH and B, and c_{AB} the concentration of the reactive complex AHB. The total concentrations are then given by $C_A = c_A + c_{AB}$ and $C_B = c_B + c_{AB}$. The experimentally accessible forward pseudo-first order rate constant is then given by [53]

$$\begin{aligned} k_{obs} &= -\frac{dC_A}{C_A dt} = -\frac{d(c_A + c_{AB})}{C_A dt} = -\frac{dc_{AB}}{C_A dt} = \frac{kc_{AB}}{C_A} \\ &= \frac{k}{2KC_A}\left[-\sqrt{(C_A - C_B)^2K^2 + 1 + 2K(C_A + C_B)} + 1 + K(C_A + C_B)\right] \end{aligned} \tag{6.37}$$

Equation (6.37) predicts changes in the apparent reaction order as a function of C_A and C_B. It can easily be shown that

$$k_{obs} = kKC_B \text{ for } K \ll 1 \text{ and } k_{obs} = k \text{ for } K \gg 1 \tag{6.38}$$

For the case of two proton donors AH of the same kind which exchange two protons in a cyclic dimer $(AH)_2$ the following equation has been derived

$$k_{AA} = \frac{k}{4KC_A}\left[-\sqrt{1 + 8KC_A} + 1 + 4KC_A\right] \tag{6.39}$$

which can also be obtained from Eq. (6.37) by setting $C_A = C_B$ and replacing K by $2K$ [24]. Again,

$$k_{obs} = 2kKC_B \text{ for } K \ll 1 \text{ and } k_{obs} = k \text{ for } K \gg 1 \tag{6.40}$$

Finally, the intramolecular case is interesting, where AH and B are functional groups of the same molecule. The equilibrium constant between the non-reactive form AH + B and the reactive form AHB is given by

$$K = \frac{c_R}{c_{NR}} \tag{6.41}$$

With the total concentration $C = c_{NR} + c_R$ it follows that

$$c_R = \frac{KC}{1 + K} \tag{6.42}$$

Often, only the sum of the concentrations of NR and R is measured, i.e. the kinetics cannot distinguish between NR and R. As the interconversion between

WILEY-VCH
Schowen
2. UK
N. Denzau
Kühn & Weyh Satz und Medien
Freiburg
l:/Vch/Schowen/3b2/c06.3d
6.9.2006

NR and R is assumed to be fast, the observed first order or pseudo-first order rate constant is then given by

$$k_{obs} = -\frac{1}{C}\frac{dc_R}{dt} = \frac{kc_R}{C} = \frac{kK}{1+K} \tag{6.43}$$

In the case where $K \gg 1$ it follows that

$$k_{obs} = k \tag{6.44}$$

By contrast, if $K \ll 1$ it follows that

$$k_{obs} = kK \tag{6.45}$$

In other words, the observed rate constants depend in a similar way on the equilibrium constants in the three cases discussed. In order to have an impression of the effects on the Arrhenius curves let us discuss the intramolecular case given by Eq. (6.43).

The temperature dependence of the pre-equilibrium constant is given by

$$K = \exp(-\Delta H/RT + \Delta S/R) \tag{6.46}$$

where ΔH and ΔS represent the enthalpy and entropy of the pre-equilibrium. Let us assume a simple Arrhenius law for the intrinsic H-transfer step

$$k = A\exp(-E_a/RT) \tag{6.47}$$

with the arbitrary parameters $A = 10^{13}$ s^{-1} and $E_a = 30$ kJ mol^{-1}, represented by the dashed lines in the Arrhenius diagrams of Fig. 6.20. The effective Arrhenius curves calculated using Eq. (6.43) are represented by the solid lines.

Figure 6.20(a) depicts the case where the formation of the reactive state involves a negative enthalpy and a negative entropy, as expected for a hydrogen bond association between the reaction partners AH and B. Thus, the reacting state predominates at low temperatures where $k_{obs} = k$. The true Arrhenius curve is then measured, with normal pre-exponential factors. At high temperatures, however, non-reactive state dominates and $k_{obs} = kK$. As $K \ll 1$ in this region, the observed Arrhenius curves exhibits a convex curvature and unusually small pre-exponential factors. The effective activation energy is given by $E_a - |\Delta H|$.

Figure 6.20(b) depicts the case where the formation of the reactive state involves a positive entropy and enthalpy. Such a case could happen if the reaction partners AH and B are involved in strong interactions with other species. For example, AH could be hydrogen bonded to any proton acceptor, or B to any proton donor, which requires this interaction to be broken before the partners can react. Now, the reacting state predominates at high temperatures and the non-reactive state at low temperatures. Only at high temperatures is the true Arrhenius curve measured, exhibiting a normal pre-exponential factor of about 13. At low temperatures, the

WILEY-VCH
Schowen
2. UK
N. Denzau

Kühn & Weyh Satz und Medien
Freiburg
l:/Vch/Schowen/3b2/c06.3d
6.9.2006

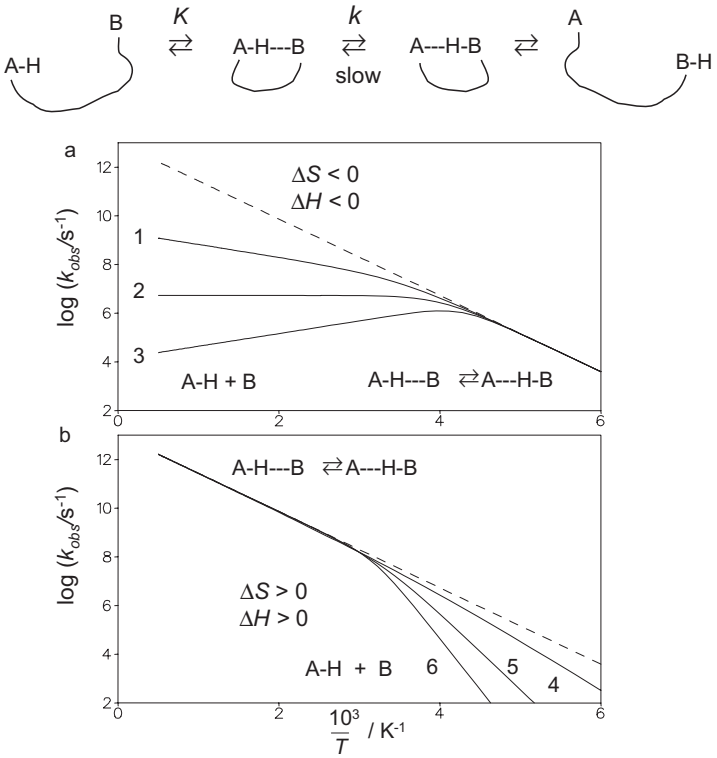

Figure 6.20 Arrhenius curves of a H-transfer in the presence of a pre-equilibrium. Arbitrary parameters of the Arrhenius curves in the reactive complex: log$A$ = 13, and E_a = 30 kJ mol^{-1}. Parameters of the formation of the active complex: (1) ΔH = – 20 kJ mol^{-1}, ΔS = – 70 J K^{-1} mol^{-1}; (2) ΔH = – 30 kJ mol^{-1}, ΔS = – 120 J K^{-1} mol^{-1}; (3) ΔH = –40 kJ mol^{-1}, ΔS = – 170 J K^{-1} mol^{-1} ; (4) ΔH = 10 kJ mol^{-1}, ΔS = 40 J K^{-1} mol^{-1}; (5) ΔH = 30 kJ mol^{-1}, ΔS = 100 J K^{-1} mol^{-1}; (6) ΔH = 50 kJ mol^{-1}, ΔS = 160 J K^{-1} mol^{-1}. Adapted from Ref. [53].

observed rate constants are slower than the intrinsic ones, the effective activation energy is given by E_a + |ΔH|. In addition, the observed pre-exponential factor is unusually large.

6.3 Applications

In this section various hydrogen transfer systems are reviewed for which Arrhenius curves of the different isotopic reactions are available over a large temperature range. Mainly the systems are discussed exhibiting degenerate hydrogen transfers which could be studied by dynamic NMR. The main question is how the reaction properties are related to the molecular structure.

Table 6.4 Bell–Limbach tunneling model parameters of various H-transfers[1)]

System	Ref	k_{298K} / s^{-1}	KIE_{298K}	E_m / kJ mol^{-1}	ΔH / kJ mol^{-1}	ΔS / J K^{-1} mol^{-1}	log (A/s^{-1})	E_d / kJ mol^{-1}	Δm / a.m.u.	$2a$ / Å	$\Delta\varepsilon$ / kJ mol^{-1}
tetraphenylporphyrin organic solvents/solid state	18b	5600	HH/HD 16 HH/DH 4 HH/DD	26.8	–	–	12.9	29.3	1.5	0.48	HD 5.0
porphyrin organic solvents/solid state	18d, 18e	16000	HH/DD 11.5 HH/HD 6.5 HD/DD 1.9 H/D 11.4 D/T 3.4 H/T 39	22.7	–	–	12.6	28.7	2.5 [1.5]	0.48 [0.68]	HD 4.9 [4.95] DT 3.0 [2.2]
porphyrin anion organic solvent/solid phosphazene matrix	23b	10^5	H/D 16.5 D/T 3 H/T 49.6	10.0	–	–	12.6	34.3	0 [1.5]	0.87 [0.78]	HD 6.5 [7.74] DT 4.2 [3.8]
phthalocyanine α-form solid	66b	1.1×10^5	–	29.3	–	–	12.9	17.6	1.5	0.48	HD 5.9
phthalocyanine β-form solid	66b	4.3×10^5	–	24.7	–	–	12.6	15.5	1.5	0.48	HD 5.9

1) Square brackets indicate values published previously.

System	Ref	k_{298K} / s^{-1}	KIE_{298K}	E_m / kJ mol^{-1}	ΔH / kJ mol^{-1}	ΔS / J K^{-1} mol^{-1}	log (A/s^{-1})	E_d / kJ mol^{-1}	Δm / a.m.u.	2a / Å	$\Delta\varepsilon$ / kJ mol^{-1}
acetyl-porphyrin AC → AD organic solvents	20b	2870	HH/HD 16 HH/DH 4 HD/DD 1.2 DH/DD 4.5	24.3	–	–	12.6	31.0	1.5	0.48	HD 5.9
trans-cis BD and cis-trans step AD				23.0	–	–	12.6	22.6	1.5	0.48	HD 5.9
tetraphenyl-chlorin organic solvents	19b	15	HH/HD 2.6	33.5	–	–	12.6	36.8	1.5	0.48	HD 5.9
tetraphenyliso-bacterio-chlorin organic solvents k_1	19a	4×10^5	–	16.7	–	–	12.6	26.4	1.5	0.48	HD 5.9
tetraphenyliso-bacterio-chlorin organic solvents k_2	19a	350	–	29.3	–	–	12.6	29.3	1.5	0.6	HD 5.9
indigodiimin HH-transfer organic solvent	68	4×10^8	–	17.6	–	–	12.6	29.7	1.5	0.4	HD 5.9

System	Ref	k_{298K} / s^{-1}	KIE_{298K}	E_m / kJ mol^{-1}	ΔH / kJ mol^{-1}	ΔS / J K^{-1} mol^{-1}	log (A/s^{-1})	E_d / kJ mol^{-1}	Δm / a.m.u.	2a / Å	$\Delta\varepsilon$ / kJ mol^{-1}
indigodiimin NH_2 rotation organic solvent	68	2.6×10^{9}	–	16.7	–	–	12.6	16.3	1.5	0.48	HD 5.9
porphycene solid state	70	5×10^{7}	–	5.9	–	–	12.6	24.7	1.5	0.48	HD 5.9
DTAA solid state		2.5×10^{6}	–	20.5	–	–	12.6	17.6	3	0.34	HD 1.05
TTAA solid state	49	3×10^{9}	1.8	3.4 [2.9]	–	–	12.6 [12.4]	15.1 [14.2]	3 [3]	0.17 [0.50]	1.05 [3.0]
$(PhCOOH)_2$ solid state	74	9×10^{10}		0.84			11.6	5.4	1.8	0.48	
(PhCOOH/ PhCOOD) solid state	74		HH/HD ≈2.4 (298 K) HH/HD 24 (15 K)	0.84			11.6	7.5	1.8	0.52	
$(PhCOOD)_2$ solid state	74		HH/HD ≈ 6 (298 K) HD/DD 21 (15 K)	1.0			11.6	12.1	1.8	0.44	
DPBrP crystal	27	6500	HH/HD 5 HD/DD 5 HH/DD 25	5.6	–	–	12.65	47.5	2.3	0.55	HH/HD HD/DD

System	Ref	k_{298K} / s^{-1}	KIE_{298K}	E_m / kJ mol^{-1}	ΔH / kJ mol^{-1}	ΔS / J K^{-1} mol^{-1}	log (A/s^{-1})	E_d / kJ mol^{-1}	Δm / a.m.u.	2a / Å	$\Delta\varepsilon$ / kJ mol^{-1}
DMP crystal	25, 27	990	HHH/HHD 3.8 HHD/HDD 3.7 HDD/DDD 3.4 HHH/DDD 47	8.4	–	–	12.3	48.1	2.8	0.43	HHH/HHD 2.7 HHD/HDD 2.7 HDD/DDD 2.7
DPP crystal	27	10000	HHHH/HDLL 3, HDLL/DDLL 4 HDLL/DDLL 4 HHHH/DDDD 12	19	–	–	12.6	32.5	4	0.384	HHLL/HDLL 2.7 HDLL/ DDLL 2.7
azophenine in organic solvents	21	720	HH/HD 4.1 HD/DD 1.4	27.2	–	–	12.6	30.1	1.5	0.6	HD 3.8
tetraphenyl-oxalamidine in CD_2Cl_2	22a	1500	HH/HD 3	44.4	–	–	12.6	24	1.5	0.42	HD 2.5
oxalamidine OA7 in methyl-cyclohexane	22b	14	HH/HD 3.1 HD/DD 1.5	52.7	–	–	12.6	27.2	1.5	0.2	HD 2.9
oxalamidine OA7 in acetonitrile	22b	75	HH/HD 3.2 HD/DD 1.6	52.7	–	–	12.6	16.7	1.5	0.2	HD 3.8
F-amidine in THF	24	10^7	HH/HD 4.1 HD/DD 3.5 HH/DD 14.3	5.4			12.2	26.4	1.05	0.55	HH/HD 3.0 HD/DD 3.0

System	Ref	k_{298K} / s^{-1}	KIE_{298K}	E_m / kJ mol^{-1}	ΔH / kJ mol^{-1}	ΔS / J K^{-1} mol^{-1}	log (A/s^{-1})	E_d / kJ mol^{-1}	Δm / a.m.u.	$2a$ / Å	$\Delta\varepsilon$ / kJ mol^{-1}
Me-BO	83	2×10^9	H/D 14.5	0.293	-9	-60	12.6	19.7	2.1	0.29	5.44
Ingold radical	8	$\approx 10^4$	H/D 18	4.2	-19	-85	12.6	50.2	1.9	0.34	6.7
2-hydroxyphenoxyl radical CCl_4+ dioxane	86	2×10^7	H/D 56	0.0	21	38	12.6	27.2	0	0.3	6.7
di-tertbutyl-2-hydroxyphenoxyl radical in heptane	85	4×10^9	H/D 9.8	1.26	–	–	12.6	23.9	1	0.17	3.3
CH_3COOH+ CH_3OH in THF	9b	750	HH/HD 5.1 HD/DD 3.1 HH/DD15.5	16.5	16.5	-42	12.6 (10.4)	36	0	0.44	HH/HD 0.64 HD/DD 0.64
2 CH_3COOH+ CH_3OH in THF	9b	3200	HHH/DDD 11.5 HHH/DHH 2.1	27.2	27.2	-34	12.6 (11)	33.5	0	0.2	0.25
Thermophilic Dehydrogenase	91	90	H/D 4.8	0.0	96	326	12.6	67.0	0	0.515	0.0
pure methanol and calix[4]arene	93, 74	10^{11}	–	0.13	–	–	12.4	8.8	2.8	0.49	–

WILEY-VCH
Schowen
2. UK
N. Denzau
Kühn & Weyh Satz und Medien
Freiburg
l:/Vch/Schowen/3b2/c06.3d
6.9.2006

According to Eigen's scheme of H-transfer (Eq. (6.35)) it can be divided into two steps, i.e. a diffusion step and an intrinsic H-transfer step in a hydrogen bonded complex. This picture can be specified further, for example by introduction of heavy atom reorganization in the intrinsic H-transfer step, either before or during the actual H-transfer.

Therefore, in the first part of this section, intramolecular hydrogen transfers or intermolecular hydrogen transfers in preformed hydrogen bonded complexes in the solid state which are coupled only to minor heavy atom motions are discussed. H-transfers coupled to major heavy atom motions will then be treated in the second part; they include pre-equilibria, hydrogen bond switches, conformational changes, solvent motions etc.

For a better comparison, the Arrhenius curves of all hydrogen transfers discussed in this section have been recalculated for this review using the Bell–Limbach tunneling model described in the theoretical section. Some systems have already been presented recently in a mini-review [54]. The parameters used are assembled in Table 6.4. Finally, note that in all cases where hydrogen isotopes are transferred from and to nitrogen the compounds had to be enriched for NMR measurements with the ^{15}N isotope.

6.3.1
H-transfers Coupled to Minor Heavy Atom Motions

6.3.1.1 Symmetric Porphyrins and Porphyrin Analogs

The tautomerism of porphyrin and of its analogs is illustrated in Fig. 6.21. Experimental aspects have been reviewed recently by Elguero et al. [55] and theoretical aspects by Maity et al. [56].

The thermal tautomerism of *meso*-tetraphenylporphyrin (TPP) – which is more soluble than the parent compound porphyrin – was discovered by Storm and Teklu [57] using liquid state ^1H NMR. A large kinetic HH/DD isotope effect was observed which was interpreted in terms of a concerted double proton transfer. Hennig et al. [18a, 58] established in the late 70s and early 80s of the last century the intramolecular pathway of the reaction, measured the HH and DD reaction rates and later also the HD rates of TPP over a wide temperature range. The data were interpreted in terms of tunneling. As NMR methods to obtain rate constants were still developing, the low-temperature rate constants were overestimated by Hennig et al. [58] as criticized by Stilbs and Moseley [59]. As a consequence, the methods used were improved and led to a novel NMR pulse sequence based on "magnetization transfer in the rotating frame" [60], referred to later as "CAMELSPIN" [61] and then as "ROESY" [62], one of the most used NMR pulse sequences nowadays.

In the late 70s and early 80s, tunneling theories indicated a preference for tunneling in symmetric double wells vs. asymmetric wells, supporting the concerted double proton transfer [63]. Thus, it seemed at that time that tunneling observed experimentally was only compatible with a concerted reaction pathway, supported

WILEY-VCH
Schowen
2. UK
N. Denzau

Kühn & Weyh Satz und Medien
Freiburg
l:/Vch/Schowen/3b2/c06.3d
6.9.2006

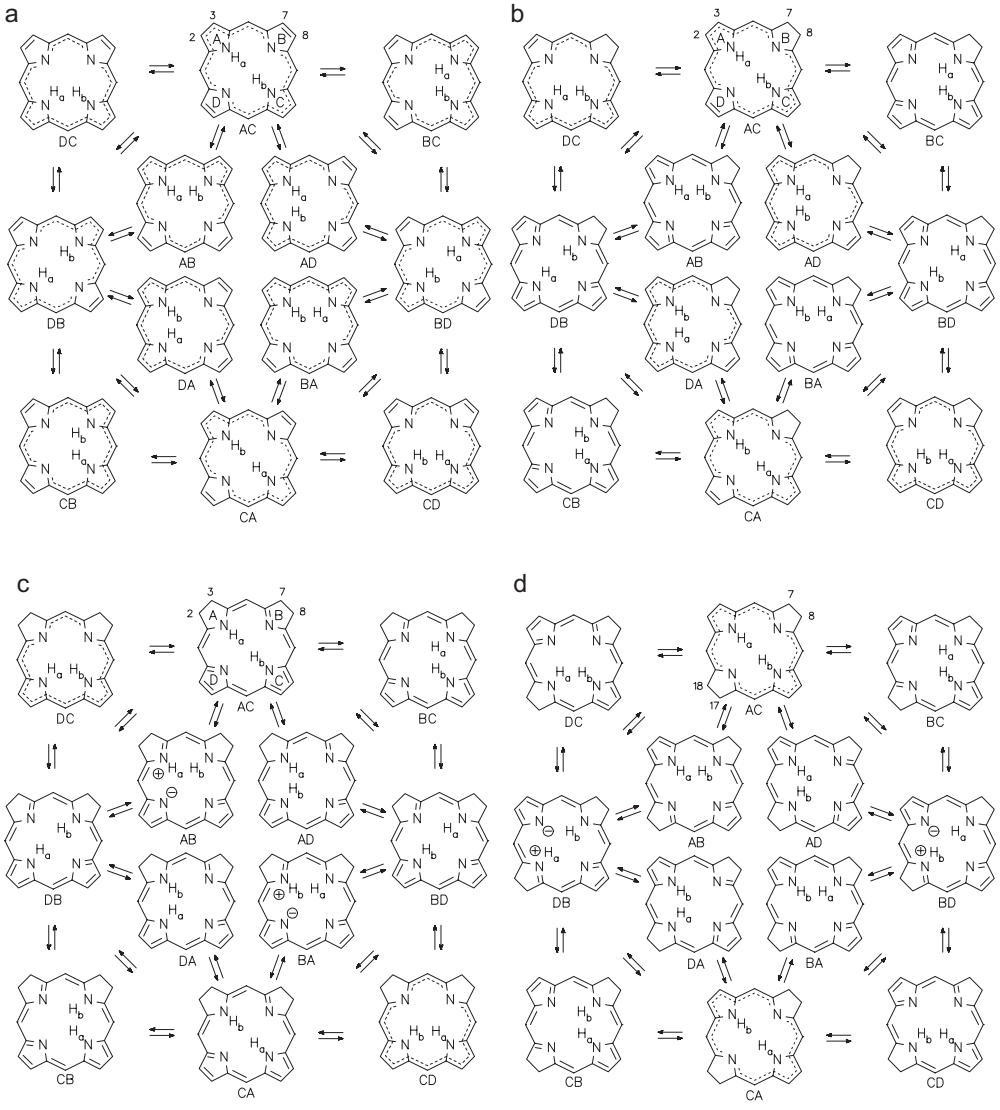

Figure 6.21 Tautomerism of (a) porphyrin, (b) chlorin, (c) isobacteriochlorin and (d) bacteriochlorin. Adapted from Ref. [19a].

by the finding that the two NH-stretches in the ground state of porphyrins are coupled [63]. In a number of papers, a stepwise transfer was proposed by Sarai [64], promoted by specific vibrations of the porphyrin skeleton which lower the N···N distance for H-transfer. In parallel, quantum-mechanical calculations indicated that cis-tautomers represent metastable intermediates, as indicated in Fig. 6.21(a). To our knowledge, the most recent *ab initio* calculation was published by Maity et al. [65]. Further theoretical progress will be discussed later.

WILEY-VCH
Schowen
2. UK
N. Denzau

Kühn & Weyh Satz und Medien
Freiburg
l:/Vch/Schowen/3b2/c06.3d
6.9.2006

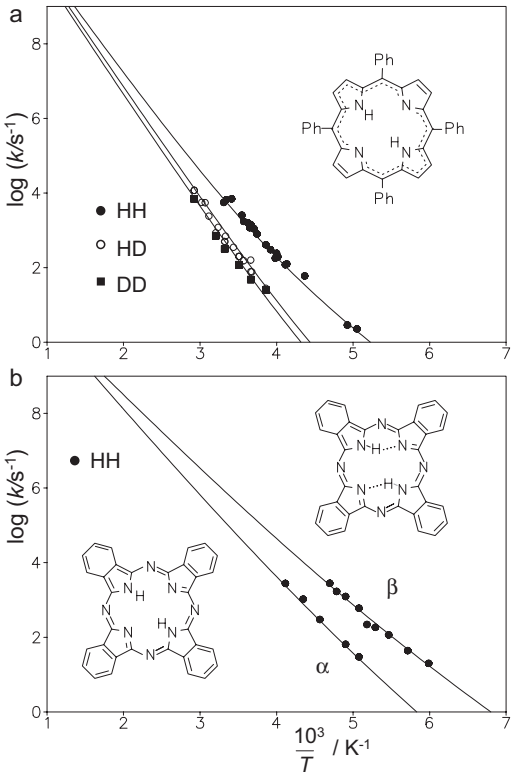

Figure 6.22 Arrhenius curves of the tautomerism of (a) tetraphenylporphyrin in the liquid and solid state [18b] and (b) of the *α*- and *β*-forms of solid phthalocyanin [66b]. The Arrhenius curves were calculated using the parameters listed in Table 6.4.

In the meantime, Limbach et al. [58b] showed, for *meso*-tetraarylporphyrins, that the transfer also takes place in the solid state [58c], but it was found that the degeneracy of the reaction can be lifted by solid state interactions. Thus, the tautomerism of *meso*-tetratolylporphyrin was found to be degenerate in the solid state, but the tautomerism of triclinic TPP was perturbed in the sense that the trans-tautomers BD and DB exhibited a larger energy than the trans-tautomers AC and CA (Fig. 6.21(a)). However, by co-crystallization with a small amount of Ni-TPP a tetragonal structure was obtained in which the degeneracy of the tautomerism was restored, as shown by Schlabach et al. [18b]. No difference between the rate constants of the degenerate reactions in the liquid and the solid state could then be observed. Schlabach et al. also published the final set of rate constants for the HH, HD, and the DD tautomerism of TPP depicted in Fig. 6.22(a). The kinetic isotope effects were interpreted in terms of Eq. (6.31) for degenerate stepwise HH-transfers in the absence of isotopic fractionation between initial and intermediate state and of secondary isotope effects, re-written as

WILEY-VCH
Schowen
2. UK
N. Denzau
Kühn & Weyh Satz und Medien
Freiburg
l:/Vch/Schowen/3b2/c06.3d
6.9.2006

$$k^{HH} = k^{H}, k^{HD} = \left[\frac{2k^{D}}{1 + k^{D}/k^{H}}\right], k^{DD} = k^{D} \tag{6.48}$$

Here k^{H} and k^{D} represent the single H-transfer rate constants of the formation of the individual intermediates in Fig. 6.21(a). Equations (6.31) and (6.48) had already been discussed by Limbach et al. [58] but used only after independent confirmation in the cases of azophenine and oxalamidines [21, 22], discussed below. Equation (6.48) was visualized in Fig. 6.12 and 6.14(b). The reaction energy profile of the HH-transfer involves two transition states of equal height. Thus, the product side is reached only with probability $^1/_2$ as the internal return to the initial state also exhibits the same probability. The same is true for the DD reaction, only the effective barriers are larger. However, the symmetry is destroyed in the HD reaction. The rate-limiting step is the D-transfer which involves the same barrier as the corresponding process of the DD reaction. But as there is only a single barrier of this type in contrast to the DD reaction the HD reaction is about 2 times faster than the DD reaction.

The fit of the experimental data to Eq. (6.48) is very satisfactory, as illustrated in Fig. 6.22(a), where the solid lines were recalculated here using the Bell–Limbach model, with the parameters included in Table 6.4. This result also means that there is no substantial decrease in the zero-point energies of the two protons in the cis-intermediate states as compared to the initial and final trans-states, as this would increase the HD/DD isotope effect beyond the value of 2 as was illustrated in Fig. 6.14(c).

The solid state tautomerism of solid phthalocyanine was discovered [66a] and studied by Limbach et al. [66b]. As illustrated in Fig. 6.22(b), there are two forms which differ in the arrangement of the central nitrogen atoms. They are arranged in a square in the α- form but in a rectangular way in the β-form [66b]. Thus, the latter contains two weak inner NHN-hydrogen bonds.

The reaction rates observed are substantially increased as compared to TPP; the increase is larger for the β-form as compared to the α- form (Fig. 6.22(b)). Kinetic H/D isotope effects have not yet been studied. The difference in the reaction kinetics of the two forms has been explained as follows. The observed tautomerism in the α- form was interpreted with a circular tautomerism as illustrated in Fig. 6.21(a), with similar transfer rates for the formation of all intermediates. However, the observed transfer in the β-form was assigned to a local HH-transfer within the two intramolecular hydrogen bonds which led to an extra increase in the rate constants.

The thermal tautomerism of the unsubstituted solid parent compound porphyrin was discovered by Wehrle et al. [18c]. Again, the degeneracy of the tautomerism was not lifted. The HH, HD, DD rate constants in the liquid and the solid state were determined by Braun et al. [18d] leading to the Arrhenius diagram of Fig. 6.23(b). Again, no kinetic liquid–solid state effects could be observed. The motivation of these studies was to elucidate the influence of substituents on the tautomerism and to facilitate the comparison with theoretical studies which are generally performed on the non-substituted parent compound. In fact, although the observed isotopic pattern is similar to that of TPP, it is found that the reaction

WILEY-VCH
Schowen
2. UK
N. Denzau

Kühn & Weyh Satz und Medien
Freiburg
l:/Vch/Schowen/3b2/c06.3d
6.9.2006

in the parent compound is considerably faster than in TPP, but slower than in phthalocyanine (Table 6.4). These findings indicate that NHN-hydrogen bond compression is necessary for the HH-transfer in porphyrins and its analogs to occur, and that this compression is hindered by substituents in the *meso*-positions but facilitated by replacement of *meso*-carbon by *meso*-nitrogen atoms.

As matrix effects on the tautomerism of porphyrin are absent, it is justified to combine the data obtained by NMR with those obtained at low temperatures using optical methods for porphyrin embedded in solid hexane [67], leading to the full Arrhenius diagram depicted in Fig. 6.23(a) [18d]. In contrast, rate constants obtained for substituted and unsubstituted porphyrins should not be included in a single Arrhenius diagram.

Before the full Arrhenius diagram is discussed in detail, let us first include the results of a subsequent study of Braun et al. [18e] who measured also the rate constants k^{HT} and k^{TT} using liquid state ^{3}H NMR of tritiated porphyrin dissolved in toluene. In order to discuss the new data it is convenient to convert the rate constants k^{LL} into the rate constants k^{L} using Eq. (6.31) which is naturally valid also

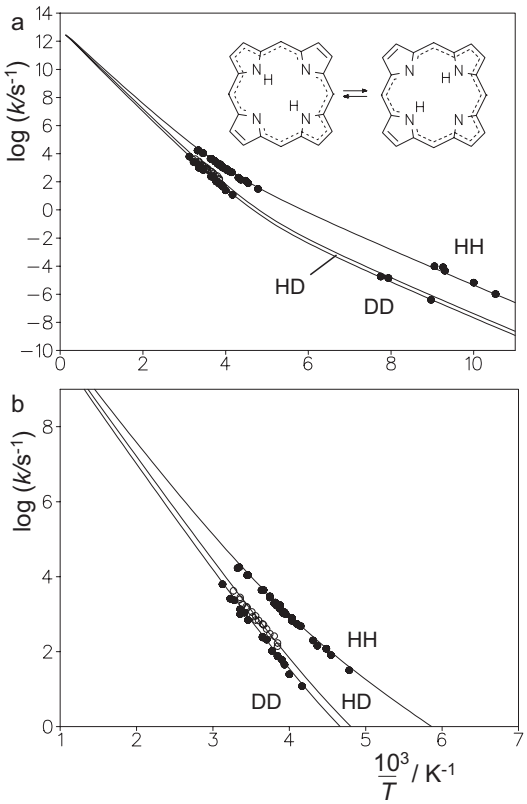

Figure 6.23 Mixed liquid and solid state Arrhenius diagrams of the HH-transfer of porphyrin, adapted from Ref. [18d].

WILEY-VCH
Schowen
2. UK
N. Denzau

Kühn & Weyh Satz und Medien
Freiburg
l:/Vch/Schowen/3b2/c06.3d
6.9.2006

for L = T. The resulting single H/D/T Arrhenius diagram of the porphyrin trans-cis reaction is depicted in Fig. 6.24. This representation allows comparison with the Arrhenius diagram of the tautomerism of the deprotonated unsubstituted porphyrin anion depicted in Fig. 6.25. The tautomerism of the latter was discovered by Braun et al. [23a], and the rate constants k^H were measured for the liquid and the solid state, as well as k^D and k^T for the liquid state [23b]. Whereas the reaction profile for the anion is symmetric, it is asymmetric for the parent compound, as illustrated schematically in Fig. 6.26.

For the parent compound porphyrin, an Arrhenius curve pattern of the type discussed in Fig. 6.9 is observed. Noteworthy is the same low-temperature slope E_m of the Arrhenius curves of the HH and DD reaction in Fig. 6.23, i.e. of the H- and D- reaction in Fig. 6.24. E_m will be mainly caused by the asymmetry of the reaction profile because at least the energy of the cis-intermediate is required for tunneling to occur, but also the reorganization energy of the ring skeleton will contribute. Note also that the low-temperature kinetic H/D isotope effect is smaller

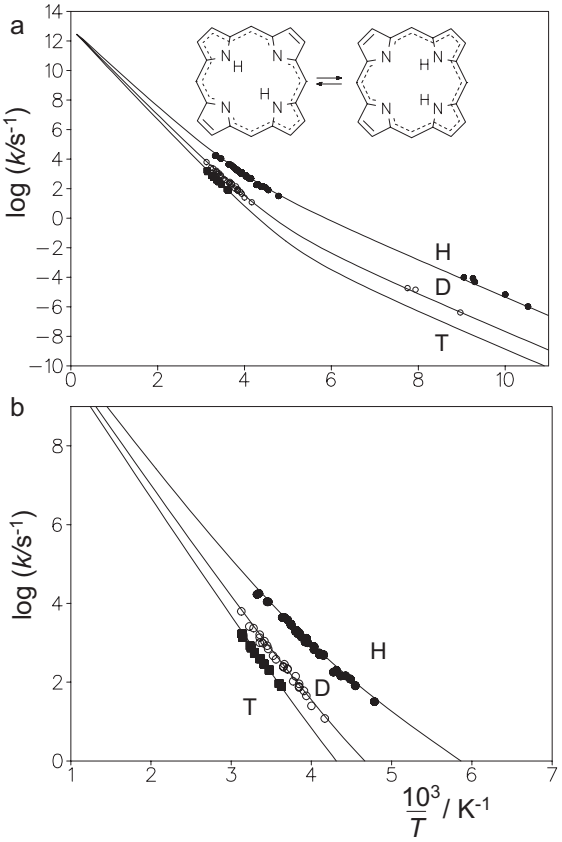

Figure 6.24 Mixed liquid and solid state Arrhenius diagram of the uphill trans–cis H/D/T-transfer of porphyrin. Data from Ref. [18e].

WILEY-VCH
Schowen
2. UK
N. Denzau

Kühn & Weyh Satz und Medien
Freiburg
l:/Vch/Schowen/3b2/c06.3d
6.9.2006

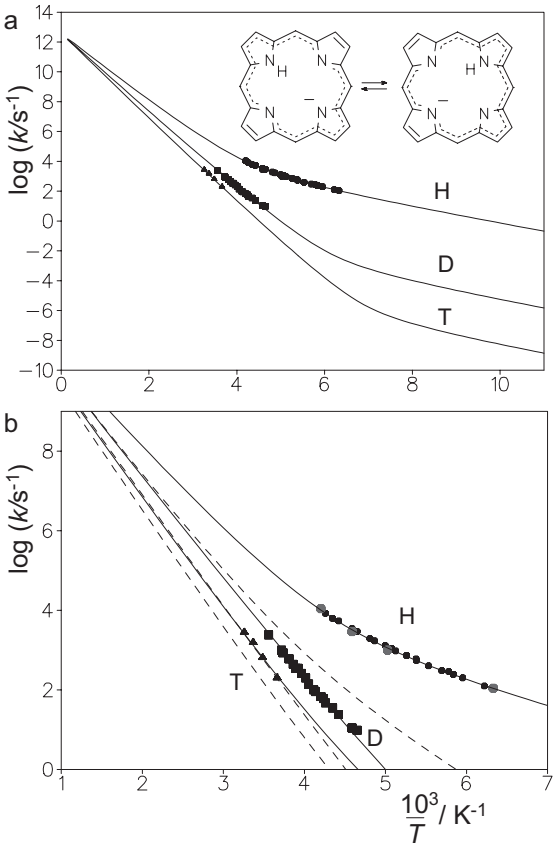

Figure 6.25 Mixed liquid and solid state Arrhenius diagram of the tautomerism of the porphyrin anion. Adapted from Ref. [23b].

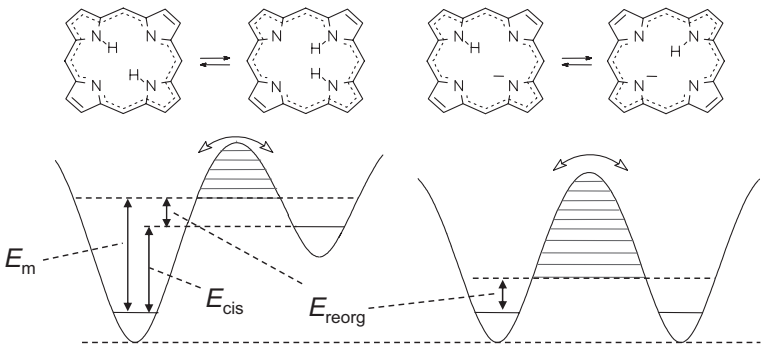

Figure 6.26 Potential curves (shown schematically) of the tautomerism of porphyrin and its mono-deprotonated anion. Adapted from Ref. [18e].

WILEY-VCH
Schowen
2. UK
N. Denzau
Kühn & Weyh Satz und Medien
Freiburg
l:/Vch/Schowen/3b2/c06.3d
6.9.2006

than predicted from the relatively large barrier difference for H and D evaluated at high temperatures. In order to match this effect a relatively high value of Δm for the heavy atom tunneling contribution had to be used in order to reduce the low-temperature isotope effect.

In contrast, this was not necessary in the case of the porphyrin anion where the transfer is degenerate and where the low-temperature kinetic isotope effects are substantially larger than in the parent compound. Therefore, the much smaller value of E_m in the anion is assigned to the reorganization of the porphyrin skeleton preceeding the transfer. As compared to the parent compound, both larger values for the tunneling distance as well as for the differences of the barrier heights of the isotopic reactions are obtained. These findings can be associated with the lack of the reaction asymmetry in the anion, as discussed in the previous section.

6.3.1.2 **Unsymmetrically Substituted Porphyrins**

In subsequent studies the question arose as to how the kinetics of the tautomerism of porphyrins and porphyrin analogs are affected by a reduction in the molecular symmetry arising from the introduction of single substituents. From a theoretical viewpoint, this question was especially interesting as formal kinetics of the stepwise transfers in Fig. 6.21 predict an evolution of the Arrhenius curves as discussed in Fig. 6.14(d)–(f). When the symmetry of the reaction is perturbed, one of the two barriers of the stepwise transfer is increased and the other decreased, as was illustrated in Fig. 6.13. In the HD reaction the D transfer exhibits the larger barrier and becomes rate-limiting, whereas in the DH reaction H is transferred in the rate-limiting step. Therefore, the HD reaction becomes slower and the DH reaction faster until they coincide with the DD and with the HH rates, as illustrated in Fig. 6.14(f).

This effect was observed by Schlabach et al. [20] for an unsymmetrically substituted acetylporphyrin (ACP, Fig. 6.27, X=CH_3CO) dissolved in CD_2Cl_2. The thermodynamics and the kinetics of the HH, HD, DH and DD reactions could be studied by NMR. It was observed that the acetyl substituted pyrrole ring exhibits a smaller proton affinity as compared to the other pyrrole rings which are substituted with aliphatic substituents (Fig. 6.28(a)). The equilibrium constant was given by

$$K_{AC\rightarrow BD} = 1.14 \times \exp(-5.82 \text{ kJ mol}^{-1}/RT) \tag{6.49}$$

Therefore, reaction pathways involving transition states and intermediates with hydrogen isotopes located on the non-substituted pyrrole rings are favored.

The Arrhenius curve pattern of Fig. 6.28(a) corresponds to the intermediate case between those of Fig. 6.14(d) and (e). It was calculated as follows. It was assumed that only the pathway AC→AD→BD contributes to the reaction rate constants but not AC→BC→BD (Fig. 6.21). Thus, only the first terms in Eq. (6.25) needed to be retained. Neglecting secondary isotope effects, the second hydron in the superscripts of the rate constants could be omitted. Using the substitution A→AC, B→AC and D→BD it was shown that

WILEY-VCH
Schowen
2. UK
N. Denzau

Kühn & Weyh Satz und Medien
Freiburg
l:/Vch/Schowen/3b2/c06.3d
6.9.2006

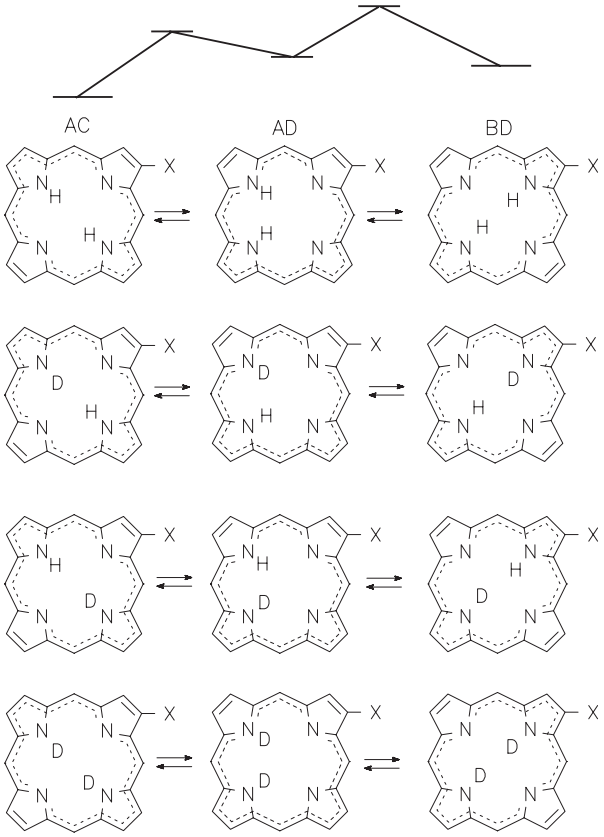

Figure 6.27 Stepwise HH, HD, DH and DD transfer in monosubstituted porphyrins.

$$k^{HH}_{AC\to BD} = \frac{k^{H}_{AC\to AD} K_{AC\to BD} k^{H}_{BD\to AC}}{k^{H}_{AC\to AD} + K_{AC\to BD} k^{H}_{BD\to AC}}, k^{DD}_{AC\to BD} = \frac{k^{D}_{AC\to AD} K_{AC\to BD} k^{D}_{BD\to AC}}{k^{D}_{AC\to AD} + K_{AC\to BD} k^{D}_{BD\to AC}}$$
$$k^{HD}_{AC\to BD} = \frac{k^{H}_{AC\to AD} K_{AC\to BD} k^{D}_{BD\to AC}}{k^{H}_{AC\to AD} + K_{AC\to BD} k^{D}_{BD\to AC}}, k^{DH}_{AC\to BD} = \frac{k^{D}_{AC\to AD} K_{AC\to BD} k^{H}_{BD\to AC}}{k^{D}_{AC\to AD} + K_{AC\to BD} k^{H}_{BD\to AC}} \quad (6.50)$$

Equation (6.50) expresses the experimental rate constants as a function of the single H-transfer forward and backward rate constants $k^{H}_{AC\to AD}$ and $k^{H}_{BD\to AC}$ of the steps defined in Fig. 6.27. Both reaction steps are now characterized by different tunnel parameters listed in Table 6.4, used to calculate the Arrhenius curves of Fig. 6.28(a). The step AC→AD involves a slightly larger barrier energy E_d and a slightly larger minimum energy E_m for tunneling to occur as compared to step BD→AD because of the asymmetry of the reaction. From a quantitative standpoint, the tunnel parameters may be subject to changes if data could be observed over a wider temperature range.

WILEY-VCH
Schowen
2. UK
N. Denzau

Kühn & Weyh Satz und Medien
Freiburg
l:/Vch/Schowen/3b2/c06.3d
6.9.2006

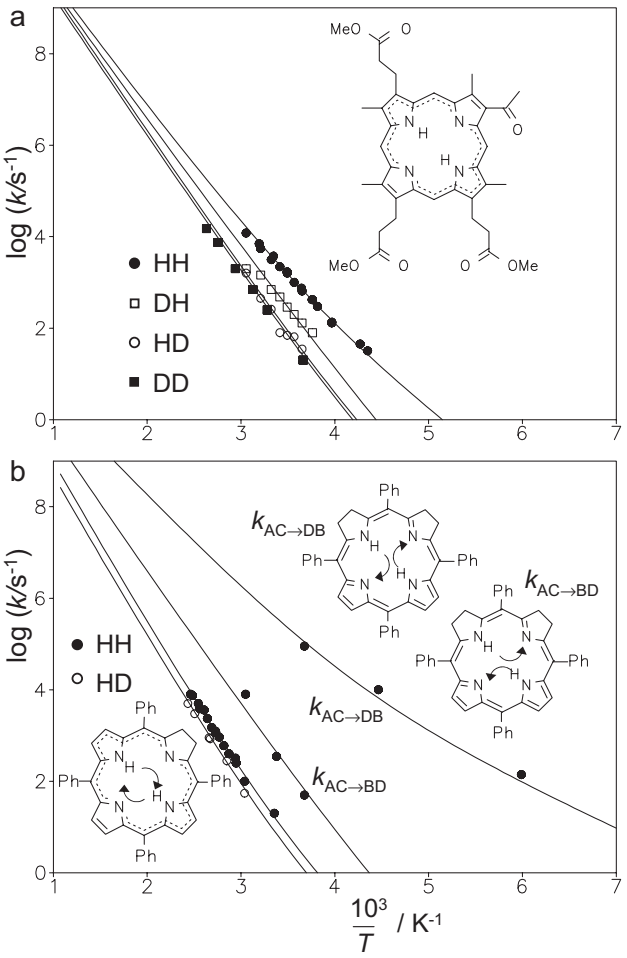

Figure 6.28 Arrhenius diagrams of the HH-transfer (a) in a substituted acetylporphyrin according to Ref. [20] and (b) in *meso*- tetraphenylisobacteriochlorin (upper curves) [19a] and in *meso*-tetraphenylchlorin (lower curves) dissolved in organic solvents [19d].

In conclusion, the theory of formal kinetics developed in the theoretical section for the description of stepwise multiple hydrogen transfers is supported by these experiments, at least for cases with weak hydrogen bonds. Thus, in these systems the assumption that each reaction step can be described in terms of a rate process characterized by rate constants is valid. The hydrogen bonds involved are not strong enough and the barriers not small enough that coherent tunneling states with delocalized protons or hydrogen atoms play an important role in this class of compounds.

WILEY-VCH
Schowen
2. UK
N. Denzau
Kühn & Weyh Satz und Medien
Freiburg
l:/Vch/Schowen/3b2/c06.3d
6.9.2006

6.3.1.3 Hydroporphyrins

Hydroporphyrins consist of porphyrins where one or more pyrrole rings are hydrogenated. The inner hydrogen atoms of porphyrins and substituted porphyrins resonate around –2 ppm which is typical for a Hückel aromatic $4n+2$ electronic π-system. The same was found for the AC and CA tautomers of *meso*-tetraphenylchlorin (TPC, Fig. 6.28(b)) where a single pyrrole ring is hydrogenated, and for *meso*-tetraphenylbacteriochlorin (TPBC, Fig. 6.28(b)) exhibiting two hydrogenated rings in trans-arrangement [19a]. Therefore, is was concluded that the two peripheral double bonds of porphyrin and the peripheral double bond of chlorin are not essential for the aromatic electron delocalization pathway, as illustrated in Fig. 6.21. In other words, porphyrin, chlorin and bacteriochlorin represent Hückel systems with 18 π-electrons in the aromatic pathways depicted in Fig. 6.21. In contrast, the chemical shifts of the inner hydrogen atoms of *meso*-tetraphenylisobacteriochlorin (TPiBC, Fig. 6.21(d)) were shifted substantially to low field, leading to the conclusion that all trans-forms of TPiBC do not represent aromatic 18 π electron systems.

The analysis is different for the intermediate states. TPiBC is predicted to form aromatic cis-intermediates CD and DC which are then lowered in energy as compared to the zwitterionic intermediates AB and BA. Thus, Fig. 6.21c predicts the reactions of iso-bacteriochlorin to be faster than those of porphyrin. On the other hand, the aromatic character of bacteriochlorin is lost in the intermediate states, moreover the trans-tautomers BD and DB of bacteriochlorin exhibit a zwitterionic structure. Thus, one should expect a substantial increase in the barrier height of the exchange between AC and CA in bacteriochlorin as compared to porphyrin.

These predictions were indeed confirmed experimentally. Schlabach et al. [19b] showed that in the case of TPC the trans-tautomers BD and DB cannot be observed directly by NMR; however, rate constants of the HH and the HD reaction could be obtained for the interconversion between AC and CA. According to an analysis similar to that leading to Eq. (6.25) it was shown that in the case of the HH reaction the observed rate constants are given by

$$k^{HH}_{AC\rightarrow CA} = k^{HH}_{AC\rightarrow BD} = k^{H}_{AC\rightarrow AD} >> k^{DD}_{AC\rightarrow CA} = k^{DD}_{AC\rightarrow BD} = k^{D}_{AC\rightarrow AD} \tag{6.51}$$

It has been shown [19b] that for the HD reaction two pathways are possible exhibiting reaction profiles similar to those of Fig. 6.13(c) and (d). The rate constants of the HD reaction are given by

$$k^{HD}_{AC\rightarrow CA} = k^{HD}_{AC\rightarrow BD} = \tfrac{1}{2}k^{H}_{AC\rightarrow AD} + \tfrac{1}{2}k^{D}_{AC\rightarrow AD} \approx \tfrac{1}{2}k^{H}_{AC\rightarrow AD} \tag{6.52}$$

This result can also be directly obtained by inspection of Fig. 6.21(b), setting H_a = H and H_b = D: the pathways of the HD reaction are dominated by the steps where D is transferred from ring C to D to A, so that H is transferred from A to B to C. The latter pathway is rate-limiting and exhibits the same rate constant as the corresponding HH reaction. The factor of $^1/_2$ in Eq. (6.52) arises from the fact that the alternative pathway where D is transferred via ring B is much slower.

WILEY-VCH
Schowen
2. UK
N. Denzau
Kühn & Weyh Satz und Medien
Freiburg
l:/Vch/Schowen/3b2/c06.3d
6.9.2006

The corresponding Arrhenius curves obtained are included in the lower part of Fig. 6.28(b). Within the margin of error, the kinetic HH/HD isotope effect of about 2 predicted by Eq. (6.52) was confirmed experimentally. Table 6.4 indicates that both E_m and E_d are increased as compared to porphyrin, as expected. The total increase as compared to TPP is about 11 kJ mol^{-1}, an effect which can be attributed to the loss of the aromaticity of TPP in TPC when the tautomerism occurs.

For TPBC no intramolecular tautomerism could be observed up to 140 °C, indicating that the sum of E_m+E_d is larger than about 86 kJ mol^{-1}, assuming a rate constant smaller than 100 s^{-1} at 140 °C as estimated from the linewidths of the ^{1}H signal of the inner protons.

Finally, for TPiBC the rate constants of the processes AD ↔ DB and AD ↔ BD (Fig. 6.21(c)) could be measured [19b]. The results are included in the Arrhenius curves of Fig. 6.28(b). The AD ↔ BD reaction is slower than in TPP which is not surprising, as the molecule is not aromatic. By contrast, the AD ↔ DB reaction is substantially faster than in TPP, an effect which has been associated with the formation of the aromatic cis-intermediate. The reaction rates are similar to those of the porphyrin anion. Although only a few rate constants were measured, one can anticipate with the accepted pre-exponential factor of $10^{12.6}$ s^{-1} a substantial concave curvature of the Arrhenius curves, i.e. a tunneling process occurring at much lower energies as compared to TPP. This is again the consequence of a more symmetric reaction profile as compared to TPP because the energy gap between the non-aromatic initial state AC and the aromatic cis-intermediate DC is substantially reduced.

6.3.1.4 Intramolecular Single and Stepwise Double Hydrogen Transfer in H-bonds of Medium Strength

When the hydrogen bonds become stronger the hydrogen transfer rates increase as the barriers are lowered. This is the case in a series of compounds discussed in this section.

The first system is indigodiimine which exhibits an intramolecular double proton transfer [68] as illustrated in Fig. 6.29(a), together with the corresponding Arrhenius curve (lower line). This process renders the two halves of the molecule equivalent. An even faster NH_2 rotation renders all NH protons equivalent. The rate constants were obtained by performing measurements at low temperatures, using a deuterated liquefied freon mixture $CDCl_3$/$CDFCl_2$/ CDF_2Cl as NMR solvent [68]. The parameters of the calculated Arrhenius curves are included in Table 6.4 but are not further discussed as kinetic isotope effects were not obtained.

The reaction rates are similar in the polycrystalline porphyrin analog dimethyldibenzo-tetraaza[14]annulene (DTAA) [69] representing a 6-membered H-chelate. They are even faster in the porphyrin isomer porphycene (Fig. 6.29(b)) [70] representing a 7-membered H-chelate with an even stronger intramolecular hydrogen bond. Both molecules form two trans-tautomers which are degenerate in the isolated molecules. However, solid state interactions lift this degeneracy. The rate constants of the forward uphill reactions could be measured in the case of DTAA

WILEY-VCH
Schowen
2. UK
N. Denzau

Kühn & Weyh Satz und Medien
Freiburg
l:/Vch/Schowen/3b2/c06.3d
6.9.2006

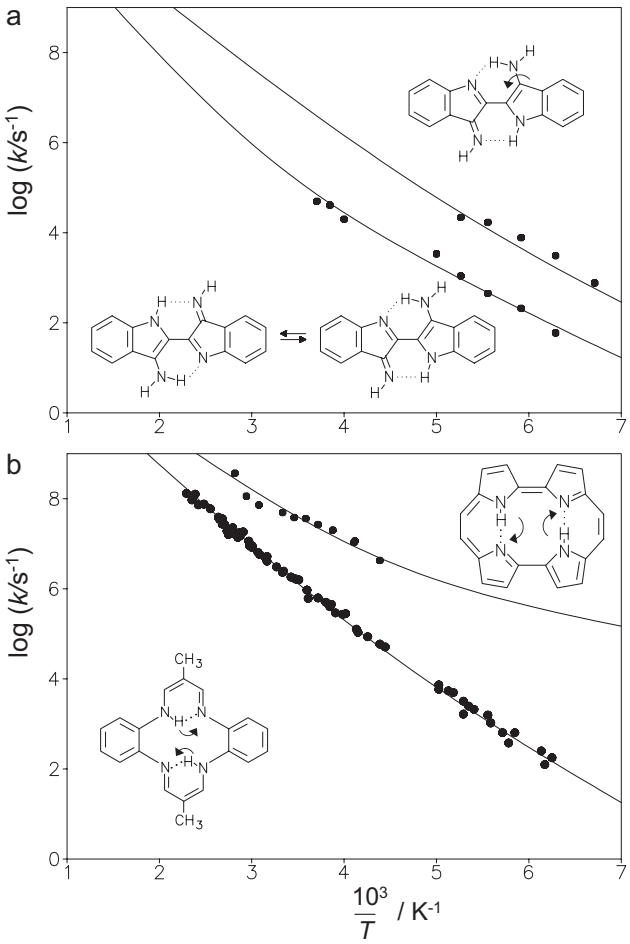

Figure 6.29 Arrhenius diagrams of the tautomerism of (a) indigodiimine [68] dissolved in a $CDCl_3/CDFCl_2/CDF_2Cl$ mixture and of (b) polycrystalline dimethyldibenzotetraaza[14]annulene (DTAA) [69] and of polycrystalline porphycene [70].

using high resolution ^{15}N solid state NMR by a combination of line shape analysis and ^{15}N-T_1 longitudinal relaxation time measurements. In the case of porphycene only the latter method could be used, which allows one to obtain rate constants on the micro- to nanosecond timescale. As kinetic isotope effects could not yet be obtained a detailed analysis of the reaction mechanisms was not yet possible. However, the present data seem to be compatible with stepwise HH tunneling processes where the energies of the cis-intermediates govern the Arrhenius curves at low temperatures.

In polycrystalline tetramethyldibenzotetraaza[14]annulene (TTAA, Fig. 6.30) a related tautomerism was observed [49]. By a combination of solid state ^{15}N and ^{2}H

WILEY-VCH
Schowen
2. UK
N. Denzau
Kühn & Weyh Satz und Medien
Freiburg
l:/Vch/Schowen/3b2/c06.3d
6.9.2006

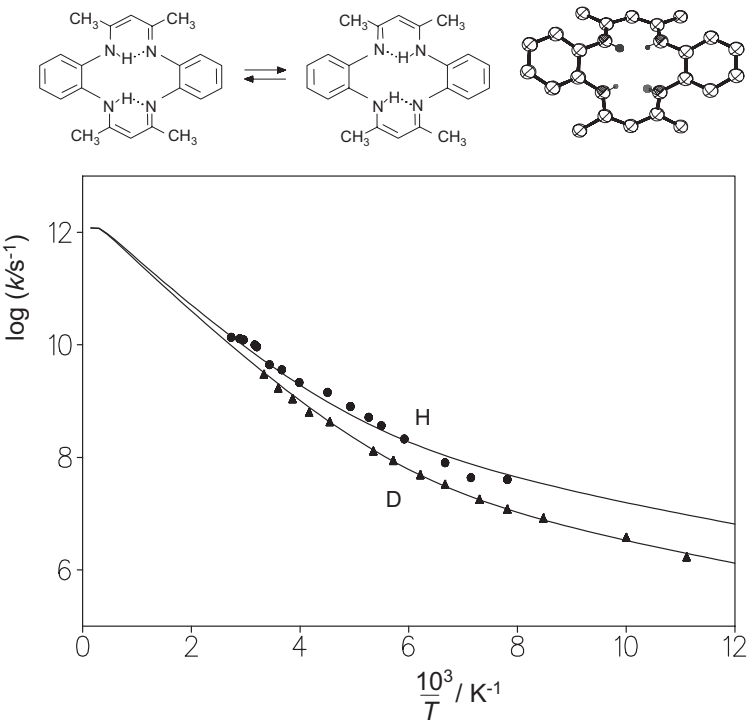

Figure 6.30 Arrhenius diagram of single H-transfer in polycrystalline tetramethyldibenzotetraaza[14]annulene (TTAA) according to Ref. [49].

NMR relaxometry rate constants and kinetic H/D isotope effects of the single H-transfer indicated in Fig. 6.30 could be measured. Evidence was found that the transfer is near-degenerate. Concave Arrhenius curves for the H- and the D-reactions were observed over a large temperature range, exhibiting surprisingly small kinetic H/D isotope effects, which were explained in terms of a relatively large heavy atom contribution to tunneling and a small barrier width. The latter arises from the substantially stronger H-bond in TTAA as compared to porphyrin.

6.3.1.5 **Dependence on the Environment**

The question of how intermolecular interactions perturb the symmetry of a degenerate H-transfer was studied as a function of temperature by Wehrle et al. [71] using TTAA dissolved in glassy polystyrene. In all cases, the transfer was found to be faster than the dynamic range of solid state ^{15}N NMR. The latter gave information about the distribution of the equilibrium constants of H-transfer. The results were rationalized in terms of the scenario of Fig. 6.31.

WILEY-VCH
Schowen
2. UK
N. Denzau

Kühn & Weyh Satz und Medien
Freiburg
l:/Vch/Schowen/3b2/c06.3d
6.9.2006

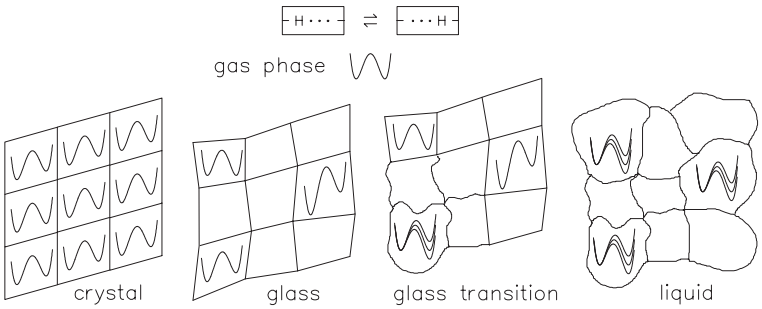

Figure 6.31 Model for the dependence of the proton transfer potential on the environment arising from experimental observations. Adapted from Wehrle et al. [71].

When a molecule exhibiting a symmetric double well for the proton motion in the gas phase is placed in a molecular crystalline environment, the crystal field will induce an energy difference ΔE between the tautomers. Whereas ΔE will be the same for all molecules in a crystal, ΔE will depend, in a disordered system such as a glass, on the local environment, leading to a distribution of ΔE-values. At the glass point, some environments may become mobile leading to an average value of $\Delta E_{av} = 0$, whereas other environments still experience non-zero values. Only well above the glass transition is a situation typical for the liquid reached where all molecules exhibit an average value $\Delta E_{av} = 0$.

6.3.1.6 Intermolecular Multiple Hydrogen Transfer in H-bonds of Medium Strength

The double proton transfer in cyclic dimers of crystalline benzoic acid has been studied by various authors using NMR relaxation techniques [72, 73]. For a recent account of this work the reader is referred to the study of Horsewill et al. [74] who published the correlation times of the HH, HD and DD reactions given by

$$\frac{1}{\tau_c} = k_{12} + k_{21}, \text{where} \quad K = \frac{x_2}{x_1} = \frac{k_{12}}{k_{21}} = \exp(-\Delta E/RT),$$

$$\Delta E = 85 \text{ K} = 0.36 \text{ kJ mol}^{-1} \tag{6.53}$$

Here, ΔE represents the energy difference between the two tautomers whose gas-phase degeneracy is lifted by solid-state interactions. x_1 and x_2 represent the mole-fractions.

The resulting Arrhenius diagram where the forward rate constants k_{12} of Horsewill et al. [74] are plotted as a function of the inverse temperature is depicted in Fig. 6.32. The Arrhenius curves exhibit large concave curvatures as expected for tunneling. Both τ_c as well as the backward reaction k_{21} (not plotted) are almost independent of temperature in this regime. The tunnel parameters used to calculate the Arrhenius curves are included in Table 6.4. The values of the minimum energy for tunneling to occur, E_m, are slightly larger than the energy difference ΔE between the two tautomers.

WILEY-VCH
Schowen
2. UK
N. Denzau
Kühn & Weyh Satz und Medien
Freiburg
l:/Vch/Schowen/3b2/c06.3d
6.9.2006

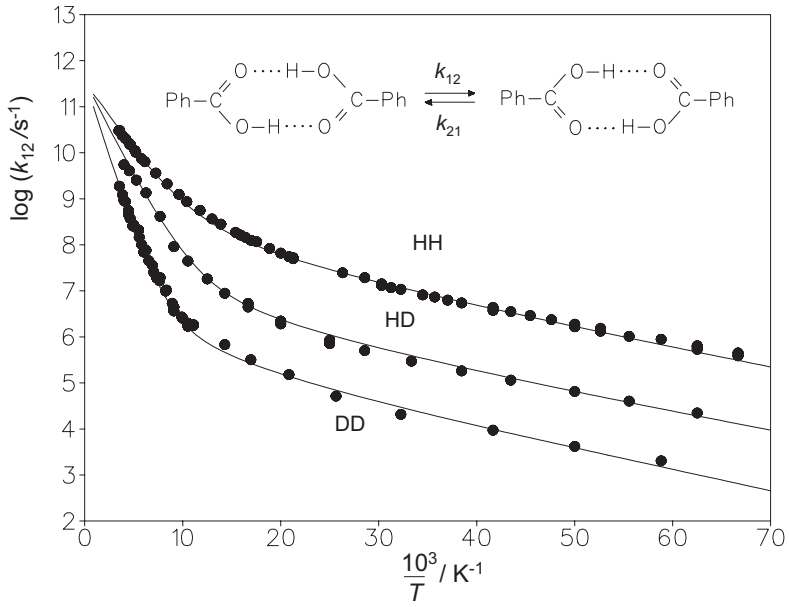

Figure 6.32 Arrhenius curves of the solid state tautomerism of benzoic acid dimers. Data for the HH and HD reactions taken from Ref. [74], and for the DD reaction from Ref. [72c]. The solid lines were calculated using the Bell–Limbach tunneling model with the parameters listed in Table 6.4.

In contrast to the intramolecular HH-transfers discussed above, replacement of each H by D leads to a significant isotope effect. At low temperatures, the HH/HD and the HD/DD isotope effects are 24 and 21, i.e. quite similar. In contrast, the extrapolated values at room temperature are about 3 and 6. As compared to other systems discussed below, usually, either similar values are obtained as was illustrated in Fig. 6.14(a) or the kinetic HH/HD isotope effects are larger than the HD/DD isotope effects, an effect arising from tunneling. Whereas the HH and the HD curves in Fig. 6.32 calculated for this review could be simulated assuming only the usual slight changes in the tunneling mass, barrier height and of the barrier width, a substantially larger barrier height and also a larger value of the minimum energy for tunneling to occur had to be assumed for the DD reaction. At present, it is tempting to associate this finding with the fact that something special has happened with the deuterated crystals. For this discussion remember that deuteration generally leads to a different position of D with respect to the hydrogen bond center as compared to H, and to an increase in the heavy atom distance. Such differences have been observed recently for acetic acid dimer [75] and other hydrogen bonded systems [40]. This would lead to an additional term which increases the barrier height of the DD transfer.

The tautomerism of crystalline pyrazoles which is discussed in the following, is particularly interesting because of the variety of hydrogen bonded complexes

WILEY-VCH
Schowen
2. UK
N. Denzau

Kühn & Weyh Satz und Medien
Freiburg
l:/Vch/Schowen/3b2/c06.3d
6.9.2006

formed by this type of compounds in the solid state. Depending on the substituents, one finds non-reactive chains or reactive cyclic dimers, trimers or even tetramers in which degenerate HH, HHH, or HHHH-transfers can take place [76, 77] as depicted in Fig. 6.33 to 6.37. In this series, the influence of crystal fields which can lift the gas phase degeneracy of the transfer processes was not observed within the margin of experimental error.

The Arrhenius diagram of the degenerate HH/HD/DD transfer in the cyclic dimer of crystalline 3,5-diphenyl-4-bromopyrazole (DPBrP) [27] is depicted in Fig. 6.33. The kinetic HH/HD and HD/DD isotope effects are about 5 at room temperature and are similar, i.e. follow the rule of the geometric mean (RGM) as predicted by Fig. 6.14(a). The total HH/DD isotope effect is about 25. Concave Arrhenius curves indicate tunneling at low temperatures. This finding has been interpreted in terms of a single barrier reaction where all H loose zero-point energy in the transition state.

The RGM is also fulfilled in the case of the degenerate HHH-transfer in the cyclic trimer of crystalline state 3,5-dimethylpyrazole (DMP) (Fig. 6.34) [25a]. The individual isotope effects are about 4 at room temperature, and the total isotope effect is around 47, which is typical again for a single-barrier reaction. The barrier height can be varied substantially by removing the bulky methyl groups and by introducing various substituents in the 4-positions as indicated in Fig. 6.35 [25b]. In the next section, the discussion of this effect will be pursued.

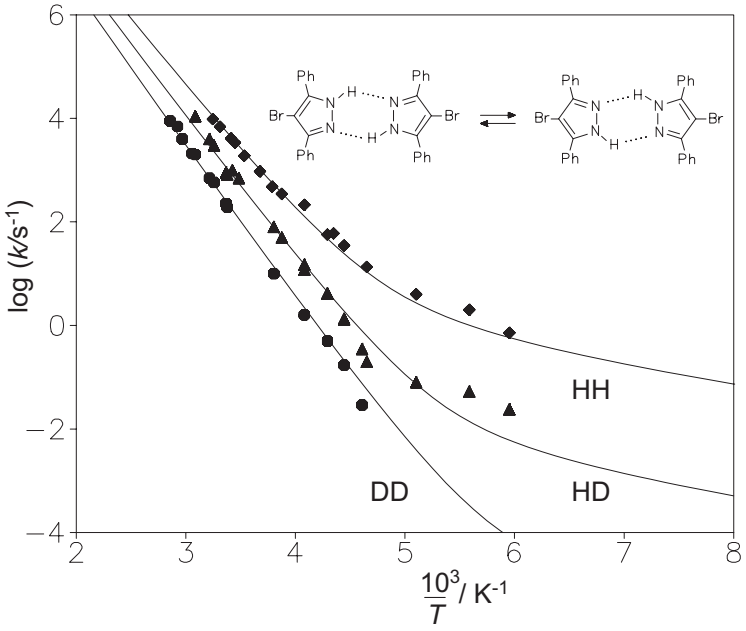

Figure 6.33 Arrhenius diagram for the double proton and deuteron transfer in solid DPBrP. Adapted from Ref. [27].

WILEY-VCH
Schowen
2. UK
N. Denzau

Kühn & Weyh Satz und Medien
Freiburg
l:/Vch/Schowen/3b2/c06.3d
6.9.2006

The kinetics of the HHHH-transfer in the cyclic tetramer of 3,5-diphenyl-4-pyrazole (DPP) has been evaluated recently [27]. The overall kinetic HHHH/DDDD isotope effects were found to be only around 12. This value indicated absence of a single barrier HHHH process where one would expect a larger overall effect. Instead, the Arrhenius pattern depicted in Fig. 6.36 could be explained in terms of a stepwise HH+HH process according to the profile of Fig. 6.17, where two hydrons are transferred in each step, leading to the expected isotope effects depicted in Fig. 6.19(b) and (c). This means that the rate constants of the HHHD and the HDHD reaction are very similar, and also those of the DDHH, DDHD, DDDD reactions. This leads to a very special dependence of the rate constants observed on the deuterium fraction x_D in the mobile proton sites. The mole fractions of all isotopologs according to a statistical distribution are depicted in Fig. 6.37(a), and the sums of mole fractions of the relevant species exhibiting similar rate constants in Fig. 6.37(b). It is clear, that practically only three different species and rate constants are observed in this case.

Ab initio calculations performed on pyrazole clusters reproduced these findings [78] and indicated a switch from concerted double and triple proton transfers in the cyclic dimer and trimer of pyrazole to a stepwise HH+HH mechanism for the

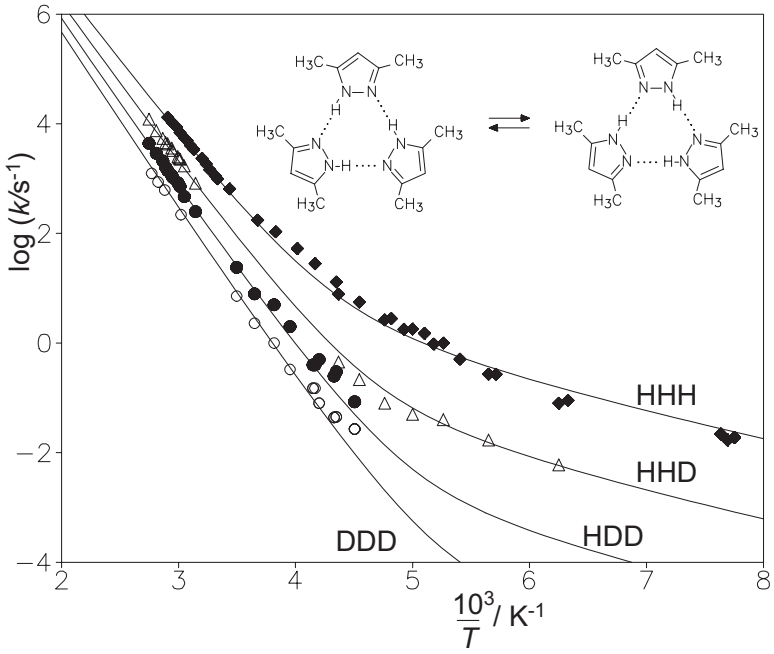

Figure 6.34 Arrhenius diagram for the double proton and deuteron transfer in the cyclic trimers of solid DMP. Adapted from Ref. [25a]. The solid curves were calculated using the Bell–Limbach tunneling model as described in the text.

WILEY-VCH
Schowen
2. UK
N. Denzau

Kühn & Weyh Satz und Medien
Freiburg
l:/Vch/Schowen/3b2/c06.3d
6.9.2006

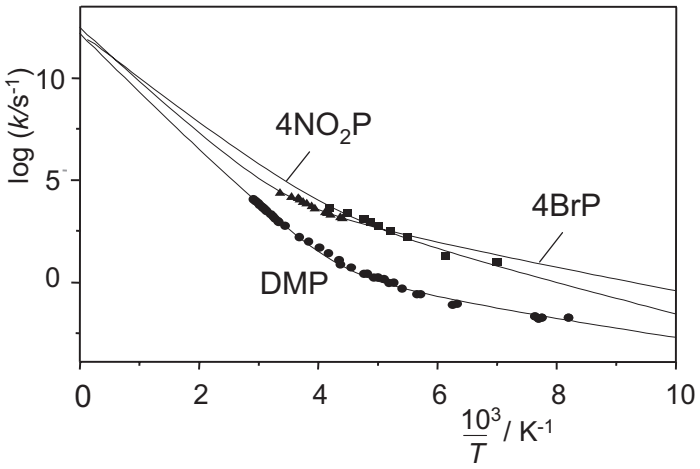

Figure 6.35 Arrhenius diagram for the triple proton transfers in cyclic trimers solid DMP, 4-nitropyrazole and 4-Br-pyrazole. Adapted from Ref. [25b].

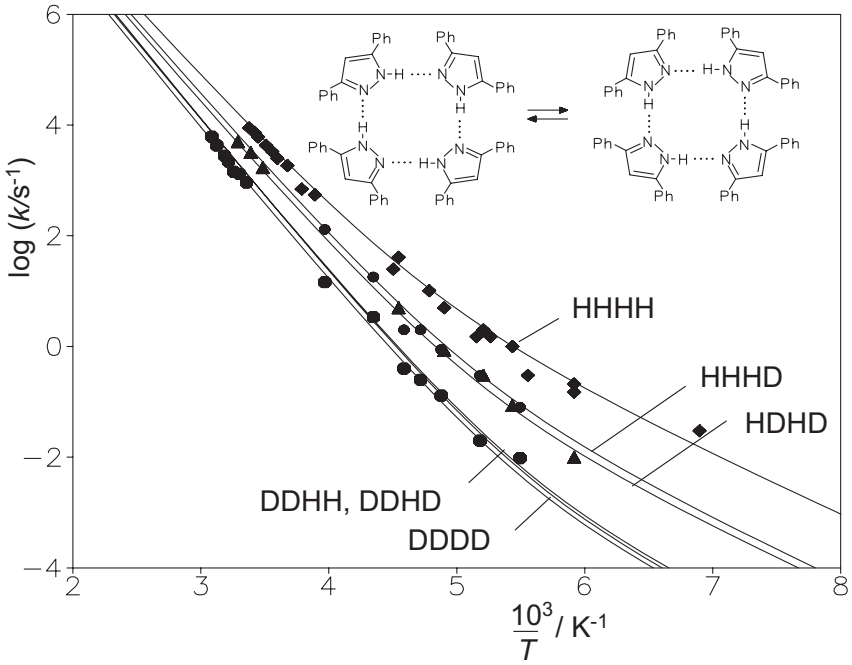

Figure 6.36 Arrhenius diagram for the quadruple proton and deuteron transfer in solid DPP. Adapted from Ref. [27]. The solid curves were calculated using the Bell–Limbach tunneling model.

WILEY-VCH
Schowen
2. UK
N. Denzau
Kühn & Weyh Satz und Medien
Freiburg
l:/Vch/Schowen/3b2/c06.3d
6.9.2006

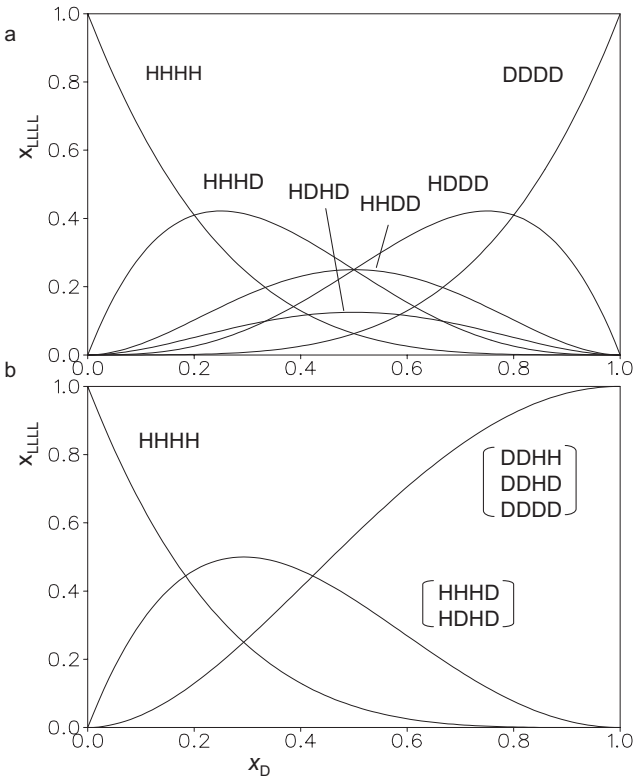

Figure 6.37 Statistical mole fractions of isotopologs (a) and ensembles of isotopologs (b) of the tetrameric DPP. Adapted from Ref. [27].

tetramer, consisting of two consecutive concerted double proton transfers. The concerted mechanism for the dimer was recently confirmed by Rauhut et al. [79].

Finally, note that Horsewill et al. [80] have reported an intramolecular quasi-degenerate quadruple HHHH tunneling process between the OH-groups of solid calix[4]arene, exhibiting temperature-independent rate constants. In a later section the discussion of this process will be pursued.

6.3.1.7 **Dependence of the Barrier on Molecular Structure**

In Fig. 6.38(a) are depicted the correlated NHN-hydrogen bond coordinates (Table 6.5) of porphyrin, of TTAA, porphycene, of the pyrazoles discussed in the previous section, as well as the calculated values of the transition states of porphyrin [65] and of its mono-deprotonated anion [81]. Also the data point of the double proton transfer in the cyclic *N,N'*-di-(*p*-F-phenyl)amidine dimer was added, which is discussed in the next section as it involves a hydrogen bond pre-equilibrium and a coupling to the reorientation of the aryl groups.

WILEY-VCH
Schowen
2. UK
N. Denzau

Kühn & Weyh Satz und Medien
Freiburg
l:/Vch/Schowen/3b2/c06.3d
6.9.2006

Note that all geometries are located on the NHN-hydrogen bond correlation curve of Fig. 6.3, especially the coordinates of the transition states of porphyrin and of its anion, exhibiting values of 2.60 and 2.66 Å. This means that hydrogen bond compression is the most important heavy atom motion which enables H-transfer; the transition state structures correspond to those expected for the strongest possible NHN-hydrogen bonds, whereas the initial states do not show any sign of hydrogen bonding.

The question arises how the intrinsic barrier of the symmetric H-transfer depends on the hydrogen bond geometries. In Fig. 6.38(b), therefore, the experimental values of the total barrier $E_d + E_m$ are plotted as a function of q_2 (Table 6.5). As a reference, the values of zero for the transition states calculated for porphyrin [65] and for the anion [81] are included. The dotted lines were calculated using the expression

$$E_d + E_m = C(q_2 - q_{2min}) \tag{6.54}$$

with $q_{2min} = 2.60$ Å, $C = 60$, 240, and 155 kJ mol^{-1} Å^{-1}. The calculated curve with the smallest slope reproduces well the experimental data of the H-transfers. The

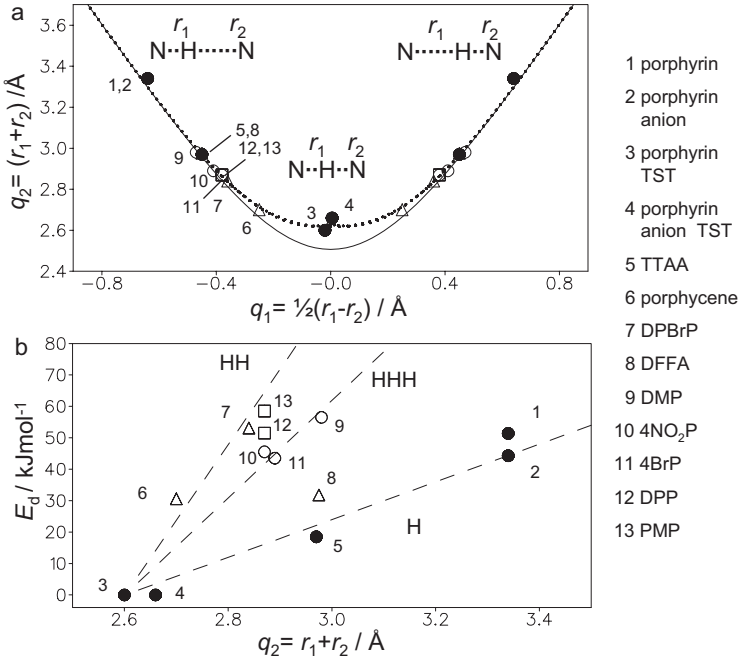

Figure 6.38 (a) Hydrogen bond geometries of various molecular systems containing NHN-hydrogen bonds. (b) Barrier heights of the H-transfers calculated from the Arrhenius curves of the species in (a). The barrier heights of the transition states are set to zero. Values taken from Table 6.5.

Table 6.5 Selected distances in systems with intra- and intermolecular H-transfers.

System		Ref	r_{NN}/Å	r_1/Å	r_2/Å	q_1/Å	q_2/Å	E_d/kJ mol^{-1}	E_m /kJ mol^{-1}
porphyrin	1	81, 18d, 18e	2.89	1.03	2.31	0.64	3.34	28.7	22.7
porphyrin TST[a]	2	56		1.28	1.32	0.02	2.60	0	0
porphyrin anion	3	81		1.03	2.31	0.64	3.34	34.3	10.0
porphyrin anion TST[a]	4	81		1.33	1.33	0.005	2.66	0	0
tetramethyltetraaza-[14]annulene TTAA	5	49	2.97	1.03	1.94	0.45	2.97	15.1	3.4
porphycene	6	70	2.63	1.10	1.60	0.25	2.70	24.7	5.9
diphenyl-p-bromopyrazole DPBrP	7	27	2.84	1.06	1.78	0.45	2.84	47.5	5.6
N,N′-di-(p-F-phenyl)amidine DFFA	12	24c, 82b	2.975	1.03	1.94	0.45	2.975	26.4	5.4
dimethylpyrazole DMP	8	25a,25b,27	2.98	1.02	1,96	0.48	2.98	48.1	8.4
4-nitropyrazole 4NO_2P	9	25b	2.87	1.03	1,96	0.42	2.89	36.0	7.52
4-bromopyrazole 4BrP	10	25b	2.89	1.05	1.82	0.41	2.87	38.0	7.53
diphenylpyrazole DPP	11	27	2.874	1.05	1.82	0.42	2.87	32.5	19.0

a calculated using ab initio methods.

WILEY-VCH
Schowen
2. UK
N. Denzau
Kühn & Weyh Satz und Medien
Freiburg
l:/Vch/Schowen/3b2/c06.3d
6.9.2006

calculated curve assigned to the HH-transfer is tentative, as there is only a single point (7, DPBrP) which is well established. Its slope is substantially larger than the slope of the H-transfer curve. This may arise from the fact that two bonds instead of one have to be broken and reformed. Point 6 (porphycene) is located on this curve; it is tempting to conclude that the tautomerism of this molecule represents a more or less concerted HH-transfer process. However, point 8 refers to the HH-transfer in cyclic dimers of a diarylamidine (Fig. 6.44–6.46) discussed later. This point is located very far from the HH curve. This might indicate that something unusual happens here, for example a mechanism somewhere in between a concerted and a stepwise HH-transfer. It is interesting to note that for a given hydrogen bond geometry, the total barrier increases substantially from the H to the HH reaction, but that the barrier decreases again for a HHH reaction. Points 12 and 13 representing the HHHH reaction in pyrazole tetramers are located close to the HH curve; this is in agreement with the interpretation of consecutive HH+HH reaction.

Let us at this point draw some conclusions based on the systems which have been discussed so far. All systems were "simple" in the sense that heavy atom motions were restricted to changes in bond lengths and angles of the molecular skeletons in which the hydrogen bonds are embedded. Major conformational changes or coupling to solvent molecules were not present. Figure 6.39 summarizes the findings schematically.

Figure 6.39(a) illustrates hydrogen bond compression during a single H-transfer process according to the hydrogen bond correlation of Fig. 6.3. In the initial and final states, the geometric H/D isotope effects imply a shortening of the covalent bond distance and a lengthening of the hydrogen bond [40]. In the transition state the deuterated system can be somewhat more compressed as compared to the protonated system, because the wavefunction of D is sharper than the wavefunction of H, i.e. D is closer to the H-bond center than H. The barrier height is larger for D than for H.

The mechanism of HH-transfer depends on whether the two hydrogen bonds involved are cooperative (Fig. 6.39(b)) or anti-cooperative (Fig. 6.39(c)). In the case of two cooperative H-bonds compression of one bond leads also to a compression of the second bond. Compression of one of two anti-cooperative bonds leads, however, to a lengthening of the other bond. In the case of non-cooperative H-bonds compression of the first bond has no effect on the second bond. When H in one bond is shifted to the H-bond center, assisted by compression of this hydrogen bridge, this compression will also lead to a compression of the second hydrogen bond, which in turn shifts also the hydrogen in this bond to the H-bond center. In other words, cooperative hydrogen bonds seem to favor a concerted or single-barrier HH-transfer. This may be the case in benzoic acid dimer, porphycene and pyrazole dimers and trimers. By contrast, in the case of anti- or non-cooperative H-bonds, only one H-bond can be suppressed but not the other, and only a single H is transferred, leading to a stepwise motion involving a metastable intermediate. This is the case in porphyrins, phthalocyanins, indigodiimine, tetraaza[14]annulenes. In the next section, other examples will follow.

WILEY-VCH
Schowen
2. UK
N. Denzau
Kühn & Weyh Satz und Medien
Freiburg
l:/Vch/Schowen/3b2/c06.3d
6.9.2006

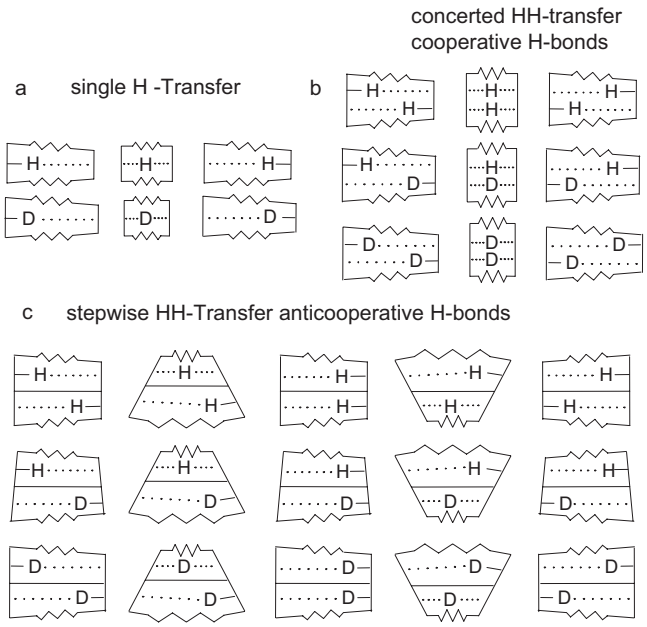

Figure 6.39 Simplified models of H- and D-substituted hydrogen transfer systems. The boxes containing springs symbolize the symmetries and the compressibilities of the hydrogen bonds. (a) Geometric H/D isotope effects during compression assisted H-transfer in a single hydrogen bond. (b) Geometric H/D isotope effects during compression assisted concerted HH-transfer in two cooperatively coupled hydrogen bonds. (c) Geometric H/D isotope effects during compression assisted stepwise HH-transfer in two anticooperatively coupled hydrogen bonds.

6.3.2
H-transfers Coupled to Major Heavy Atom Motions

In many H-transfer reactions in solution the reaction centers have first to form a reactive complex from non-reactive configurations or conformations i.e. they require a major molecular mobility. Therefore, it is understandable that complex H-transfers cannot take place in the solid state. In this section, various experimental published cases will be discussed.

6.3.2.1 H-transfers Coupled to Conformational Changes

Let us first discuss the intramolecular degenerate double proton transfers in azophenine [21] and in oxalamidines [22a]. By liquid state NMR of the ^{15}N labeled compounds the intramolecular pathways of the transfer processes were established and the rate constants k^{HH}, $k^{HD} = k^{DH}$ and when possible k^{DD} were measured. The Arrhenius diagrams are depicted in Fig. 6.40. In all cases, the reactions

WILEY-VCH
Schowen
2. UK
N. Denzau

Kühn & Weyh Satz und Medien
Freiburg
l:/Vch/Schowen/3b2/c06.3d
6.9.2006

in solution were suppressed in the solid state, indicating major heavy atom motions in addition to H-bond compression.

The kinetic HH/HD/DD isotope effects are given by Eq. (6.48) and are typical for stepwise degenerate reaction mechanisms involving metastable cis-intermediates reached by single H-transfers as illustrated by Fig. 6.11 and 6.12. In a similar case as described above for porphyrin, the observed rate constants k^{LL} could be converted into the rate constants k^{L} of the uphill single H-transfers. k^{H} and k^{D} were then calculated in terms of the Bell–Limbach tunneling model using the parameters included in Table 6.4 and converted back to k^{LL} using Eq.(6.48).

The reaction rates of tetraphenyloxalamidine (TPOA) dissolved in CD_2Cl_2 are only slightly larger than those of azophenine (AP) dissolved in $C_2D_2Cl_4$. The kinetic isotope effects are larger in the latter; moreover, they depend on temperature, whereas those of TPOA exhibit little temperature dependence. The tautomerism of the bicyclic oxalamidine OA7 is, on the other hand, substantially slower than that of TPOA. In the corresponding 6-membered bicyclic oxalamidine OA6

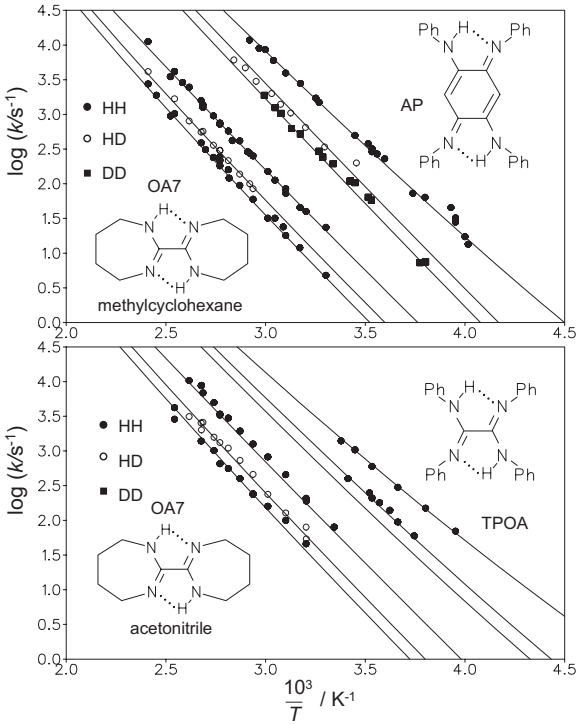

Figure 6.40 (a) Arrhenius diagrams of the tautomerism of azophenine (AP) dissolved in CD_2Cl_2 (top, [22a]) and of the seven-membered bicyclic oxalamidine OA7 (bottom) dissolved in methylcyclohexane [22b, 22c]. (b) Arrhenius diagrams of the tautomerism of tetraphenyloxalamidine (TPOA) dissolved in $C_2D_2Cl_4$ (top, [18b]) and of OA7 dissolved in acetonitrile (bottom, [22b, 22c]). The solid lines were calculated using the parameters listed in Table 6.4 as described in the text.

WILEY-VCH
Schowen
2. UK
N. Denzau
Kühn & Weyh Satz und Medien
Freiburg
l:/Vch/Schowen/3b2/c06.3d
6.9.2006

no double proton transfer was detectable [22c]. On the other hand, the tautomerism of OA7 was substantially faster in acetonitrile (dielectric constant 37.5) as compared to methylcyclohexane (dielectric constant 2.02), as illustrated in Fig. 6.40. These findings supported the formation of a zwitterionic intermediate according to the stepwise mechanism of Fig. 6.11. The small dependence of the kinetic isotope effects on temperature is confirmed for OA7 as the Arrhenius curves of the isotopic reactions are almost parallel. Note that a quantitative discussion of these parameters is difficult as the temperature range of the experimental data was limited. Therefore, the parameter sets obtained are not unique.

However, qualitatively, the above findings and the tunnel parameters obtained can be explained in terms of Fig. 6.41. In all cases, the total barrier heights E_d + E_m for each single reaction step are the same; in addition, it is assumed that the classical kinetic hydrogen/deuterium isotope effects for the over-barrier reactions are the same. Therefore, in the high temperature regime, the associated Arrhenius curves coincide. However, drastic differences are expected at lower temperatures, when tunneling becomes important. In this region, temperature independent kinetic isotope effects are expected, leading to parallel Arrhenius curves. Tunneling can occur only at energies indicated by the hatched areas. In Fig. 6.41(a) and (d) E_m is given by the energy of the intermediate E_i, whereas in Fig. 6.41(b) and (e) an additional reorganization energy E_r is required, mainly to compress the

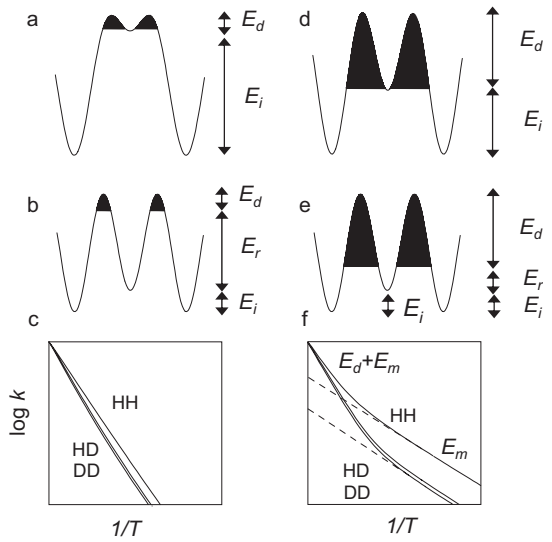

Figure 6.41 Visualization of a modified Bell tunneling model for degenerate, stepwise double proton transfers involving an intermediate. A minimum energy E_m is required for proton tunneling, which can take place only in the hatched regions. E_d barrier energy. (a) and (d) E_m is given by the energy of the intermediate, E_i . (b) and (e) E_m is given by E_i + E_r where E_r is associated with heavy atom reorganization preceding the proton transfer. (c) and (d) Corresponding Arrhenius curves (shown schematically) calculated in terms of the Bell–Limbach tunneling model. Adapted from Ref. [22c].

WILEY-VCH
Schowen
2. UK
N. Denzau

Kühn & Weyh Satz und Medien
Freiburg
l:/Vch/Schowen/3b2/c06.3d
6.9.2006

hydrogen bond, as discussed in the theoretical section. This hydrogen bond compression may involve additional molecular conformational changes. The corresponding Arrhenius curves are depicted in Fig. 6.41(c) and (d). The large changes in the experimental activation energies in the tautomerism of the oxalamidines and of azophenine, and at the same time the small changes in the kinetic isotope effects indicate then that the main differences arise from different values of $E_m = E_r + E_i$. It is plausible that the changes within the oxalamidines are then mainly due to different reorganization energies E_r.

This hypothesis was confirmed by semi-empirical calculations of various oxalamidines [22d]. The results are visualized in Fig. 6.42. In all cases, a substantial heavy atom reorganization precedes the H-transfer, which is strongly dependent on the chemical structure. This reorganization mainly involves a decrease in the nitrogen–nitrogen distances of the hydrogen bond in which the proton transfer takes place, thus lowering the barrier for the tautomerism. In contrast, in all other cases, hydrogen bond compression is associated with major conformational changes, requiring an additional reorganization energy. In TPOA and azophenine (not shown), H-bond compression is associated with a phenyl group reorientation.

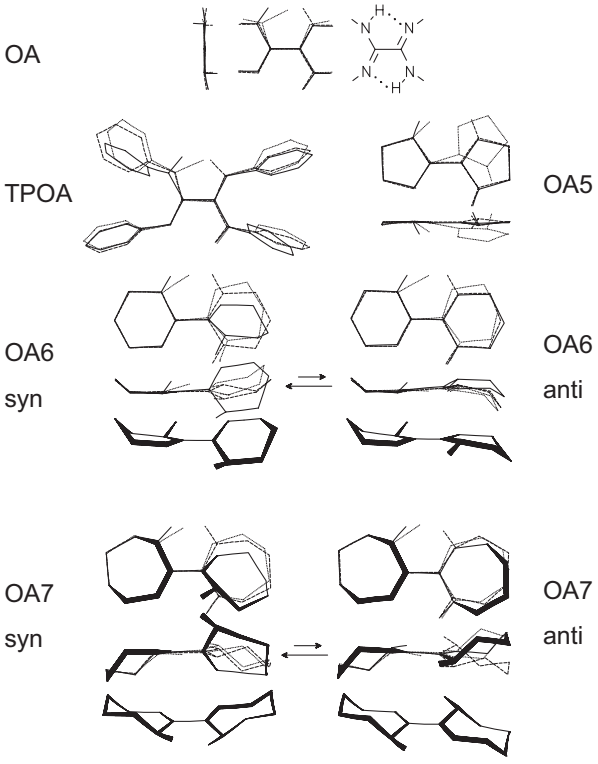

Figure 6.42 Heavy atom reorganization during the HH-transfer in oxalamidines calculated using the semiempirical PM3-MNDO method. Adapted from Ref. [22d].

WILEY-VCH
Schowen
2. UK
N. Denzau

Kühn & Weyh Satz und Medien
Freiburg
l:/Vch/Schowen/3b2/c06.3d
6.9.2006

This reorganization is not possible in the solid state, where only single tautomers are formed [21b, 22c]. The bicyclic oxalamidines also require a ring reorganization for H-bond compression to occur, which is smaller for OA7 than for OA5 and OA6, in accordance with experimental findings. For OA6 and OA7 syn- and anti-conformations were found, which both exhibited similar energies for the transition states. However, note that the ring reorganization did not involve a barrier leading to a pre-equilibrium for the tunneling step, as indicated in Fig. 6.20.

In all cases, the molecular structures do not allow for a simultaneous compression of both hydrogen bonds which would require a very high energy. Therefore, the transfers are stepwise, as indicated by Fig. 6.39(c).

The effects of small changes in the molecular structure can be observed in the case of the related diarylamidines which are the nitrogen analogs of formic acid and which represent models for nucleic acids. In tetrahydrofuran, for *N,N′*-di-(*p*-F-phenyl)amidine (DFFA) three forms were observed by NMR, a solvated s-cis-form and a solvated s-trans-form which is in fast equilibrium with a cyclic dimer in which a HH-transfer takes place [24] as illustrated in Fig. 6.43. Fortunately, at low temperatures, the s-cis- and the s-trans-forms were in slow exchange. The rate constants of the HH, HD and DD reactions were determined by dynamic ^{1}H and ^{19}F NMR as a function of concentration, deuterium fraction in the mobile proton sites and of temperature. The dependence of the observed rate constants of the s-trans-form on concentration is depicted in Fig. 6.44. The solid lines were calculated using Eq. (6.39) from which the rate constants in the dimer as well as the equilibrium constants of the dimer formation could be obtained. The Arrhenius

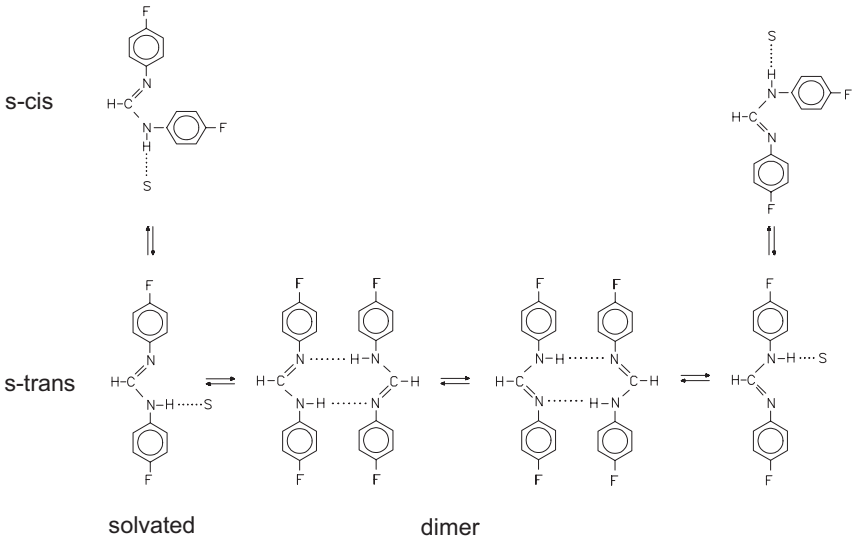

Figure 6.43 Conformational isomerism, hydrogen bond exchange and HH-transfer in *N,N′*-di-(*p*-F-phenyl)amidine (DFFA) dissolved in tetrahydrofuran (S) according to Ref. [24c].

WILEY-VCH
Schowen
2. UK
N. Denzau

Kühn & Weyh Satz und Medien
Freiburg
l:/Vch/Schowen/3b2/c06.3d
6.9.2006

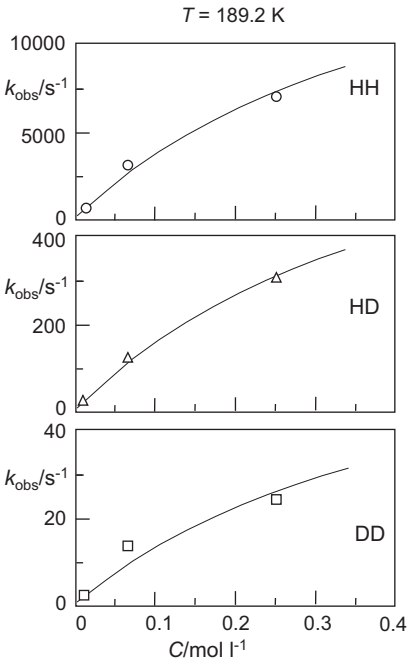

Figure 6.44 Pseudo-first order rate constants of the intermolecular HH, HD and DD transfers in cyclic dimers of *s-trans-N,N'*-di-(*p*-F-phenyl)amidine (DFFA) dissolved in tetrahydrofuran as a function of the concentration. The solid lines were calculated using an equilibrium constant of 1.12 L mol^{-1} of the monomer–dimer equilibrium. Adapted from Ref. [24c].

diagrams obtained are depicted in Fig. 6.45. Two large isotope effects are observed indicating a single barrier reaction according to Fig. 6.14(a). As the rate constants are intrinsic to the dimer, the contribution from the hydrogen bond equilibrium was eliminated from the minimum energy for tunneling to occur, but not contributions from heavy atom rearrangements, in particular from the expected aryl group conformations.

For that reason, symmetric diarylamidines with varying substituents in the *p*-position of the phenyl rings were studied by X-ray crystallography and dynamic solid state ^{15}N NMR [82]. The tendency to form cyclic dimers in the solid state was supported. In most cases, the angles α_N and α_{NH} between the phenyl groups and the molecular skeleton at the imino and the amino nitrogen atoms were different for a given molecule; the aryl ring at the imino nitrogen atom was often found to be coplanar with the molecular skeleton, but a substantial angle was observed at the amino nitrogen. This circumstance can be attributed to steric interactions of aromatic *o*-CH groups and the CH group of the amidine unit. It leads to a large preference for one of the two potentially degenerate tautomers, and suppresses the HH reaction in the solid. A degenerate HH-transfer was observed only in the OCH_3 substituted compound, where the two angles were similar but not coplanar with the molecular skeleton.

In solution the aryl groups of a cyclic dimer will not, therefore, be the same as lead to an asymmetry of the double well for the HH-transfer, as illustrated in Fig. 6.46. Reorientation of the phenyl groups to angles around 50° will symmetrize the

WILEY-VCH
Schowen
2. UK
N. Denzau

Kühn & Weyh Satz und Medien
Freiburg
l:/Vch/Schowen/3b2/c06.3d
6.9.2006

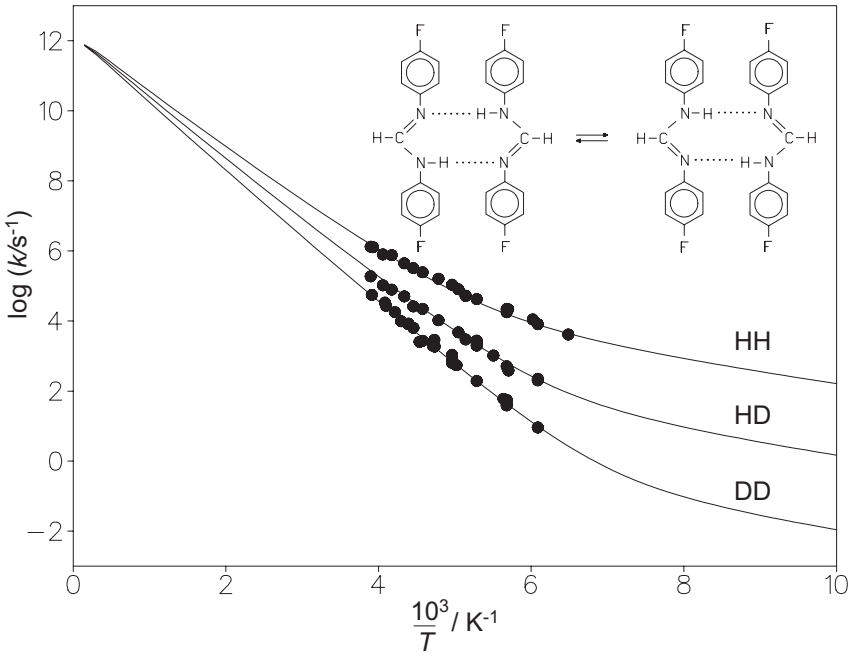

Figure 6.45 Arrhenius diagrams of the tautomerism of DFFA dissolved in THF. Adapted from Ref. [24c].

potential and minimize the barrier height of the HH-transfer. The latter is expected to take place in this configuration. Finally, the process is completed by a reorientation of the aryl groups. This means that the total barrier of the HH reaction in solution within the cyclic dimer will be slightly higher than in the symmetric configuration in the solid state. This is what was indeed observed for the rate constants of the OCH_3 substituted diarylamidine in the solid state.

6.3.2.2 H-transfers Coupled to Conformational Changes and Hydrogen Bond Pre-equilibria

Replacing the CH unit of diarylamidines with imino nitrogens leads to diaryltriazenes. As illustrated in Fig. 6.46, the aryl groups are found to be coplanar with the triazene unit. A consequence is that an intermolecular steric interaction between aromatic CH arises, which prevents the formation of cyclic dimers. Thus, diaryltriazenes are not able to exchange protons without the help of a catalyst, as has been shown recently [33]. In order to obtain more information about catalytic proton exchange, the base catalyzed transfer of 1,3-bis(4-fluorophenyl)[1,3-$^{15}N_2$]triazene was studied in more detail using ^1H and ^{19}F NMR. As catalysts dimethylamine, trimethylamine and water were studied, using tetrahydrofuran-d_8 and methylethylether-d_8 as solvents. The latter is liquid down to 130 K.

WILEY-VCH
Schowen
2. UK
N. Denzau

Kühn & Weyh Satz und Medien
Freiburg
l:/Vch/Schowen/3b2/c06.3d
6.9.2006

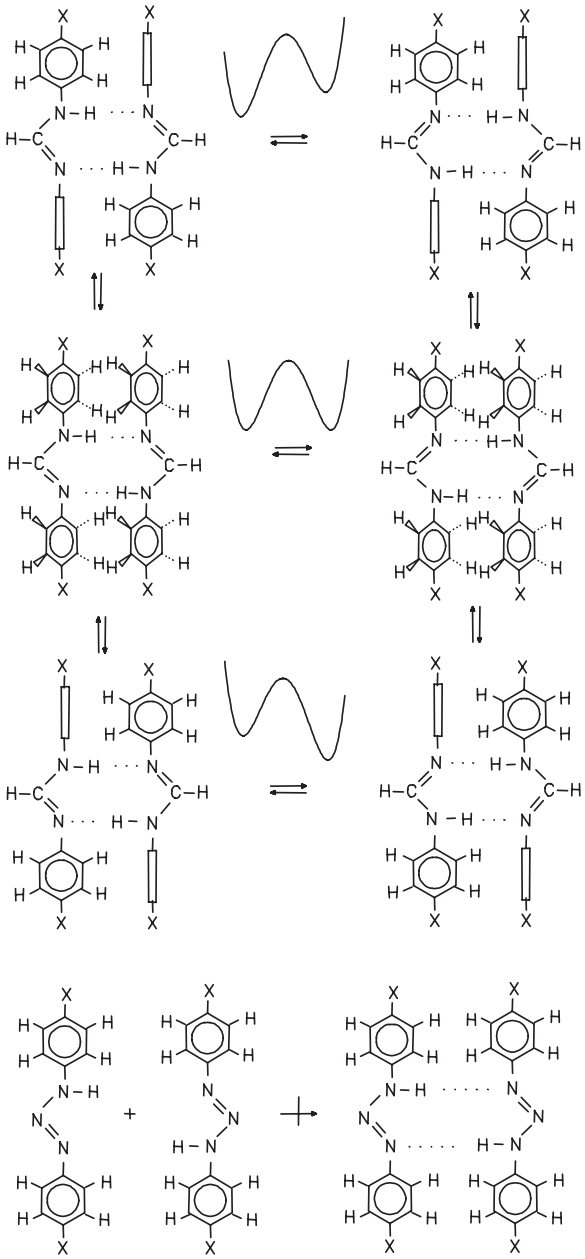

Figure 6.46 Coupling of the HH-transfer in cyclic dimers of diarylformamidines to the rearrangement of the aryl groups. Adapted from Ref. [82].

WILEY-VCH
Schowen
2. UK
N. Denzau

Kühn & Weyh Satz und Medien
Freiburg
l:/Vch/Schowen/3b2/c06.3d
6.9.2006

Surprisingly, both dimethylamine and trimethylamine were able to pick up the mobile proton of the triazene at one nitrogen atom and carry it to the other nitrogen atom, resulting in an intramolecular transfer process catalyzed each time by a different base molecule. Even more surprising is that the intramolecular transfer (Fig. 6.47(a)) catalyzed by dimethylamine is faster than the superimposed intermolecular double proton transfer (Fig. 6.47(b)).

The kinetic H/D isotope effects are small, especially in the catalysis by trimethylamine, indicating a major heavy atom rearrangement and absence of tunneling. This is because of the high asymmetry of the H-transfer from the triazene to the base. Semi-empirical PM3 and *ab initio* DFT calculations indicate a reaction pathway via a hydrogen bond switch of the protonated amine representing the transition state, where the imaginary frequency required by the saddle point corresponds to a heavy atom motion, as was illustrated schematically in Fig. 6.7. Tunneling is absent because of the very high tunneling masses involved, corresponding to the mass of the base.

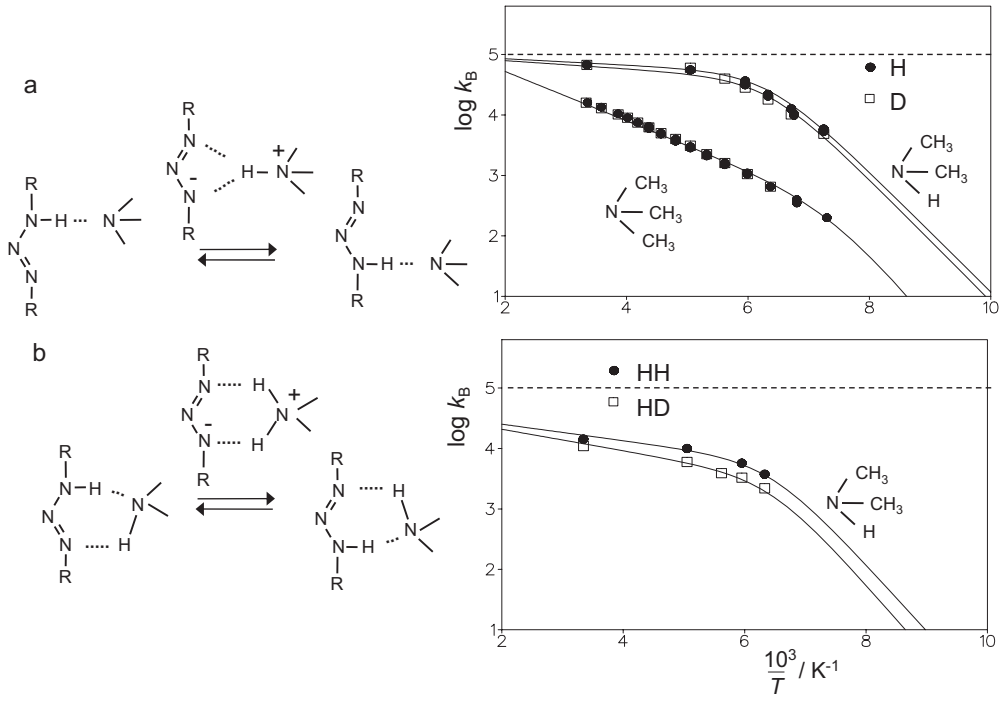

Figure 6.47 (a) Arrhenius diagrams of the intramolecular proton and deuteron transfer in 1,3-bis-(4-fluorophenyl)-[1,3-$^{15}N_2$]triazene dissolved at a concentration of 0.1 mol l^{-1} in methyl ethyl ether-d_8, catalyzed by the bases dimethylamine (0.0028 mol l^{-1} at $x_D = 0$ and 0.0041 mol l^{-1} at $x_D = 0.95$) and trimethylamine (0.02 mol l^{-1} at $x_D = 0$ and $x_D = 0.96$). k_B represents the average inverse life times of the base B between two exchange events. (b) Arrhenius diagrams of the intermolecular proton and deuteron transfer of 1,3-bis-(4-fluorophenyl)-[1,3-$^{15}N_2$]triazene catalyzed by dimethylamine. Adapted from Ref [33b].

WILEY-VCH
Schowen
2. UK
N. Denzau
Kühn & Weyh Satz und Medien
Freiburg
l:/Vch/Schowen/3b2/c06.3d
6.9.2006

The Arrhenius curves of all processes exhibit strong convex curvatures. This phenomenon is explained in terms of the hydrogen bond association of the triazene with the added bases, preceding the proton transfer. At low temperatures, all basic molecules form a hydrogen bonded reactive complex with the triazene, and the rate constants observed equal those of the reacting complex. However, at high temperatures, dissociation of the complex occurs, and the temperature dependence of the observed rate constants is affected also by the enthalpy of the hydrogen bond association according to Eqs. (6.37) and (6.46). As tunneling is not involved, the Arrhenius curves are not further discussed. For that the reader is referred to the original literature [53].

Al-Soufi et al. [83] have followed the kinetics of the intramolecular H- and D-transfer between the keto and the enol form of 2-(2′-hydroxy-4′-methylphenyl) benzoxazole (MeBO) dissolved in alkanes using optical methods. No dependence of the rate constants on the solvent viscosity could be found. The Arrhenius diagram obtained over a very wide temperature range is depicted in Fig. 6.48. At low temperatures, the very rare regime of temperature-independent rate constants is obtained, exhibiting a very large temperature independent kinetic H/D isotope effect of about 1400. At room temperature, still a quite large effect of about 14.5 is obtained.

Al-Soufi et al. [83] mentioned that the experimental pre-exponential factors obtained at high temperature were only about 10^9 s^{-1} instead of about 10^{13} s^{-1} as expected. Therefore, the Arrhenius curves of this reaction were recalculated here using Eq. (6.43), assuming an equilbrium between a reactive form and a non-reactive form. The parameters are listed in Table 6.2. Because of the large body of data all parameters could be determined.

At low temperatures, the intrinsic Arrhenius curves of the H- and the D-transfer, symbolized by the dashed lines, coincide with the observed ones, represented by the solid lines, as $k_{obs} = k$. However, at high temperature it was assumed that a non-reactive form of the molecule dominates because of its more positive entropy, leading to $k_{obs} = kK$. Thus, both the observed rate constants and the observed pre-exponential factors are smaller than expected.

Note that, at low temperatures, a very small minimum energy E_m for tunneling to occur is found, which refers to the reactive complex. This value could, therefore, be determined in addition to the values of ΔH and ΔS of the pre-equilibrium. In other cases, as discussed later, only the sum of $\Delta H + E_m$ can be determined. The barrier for the transfer is similar to that found for TTAA. The difference between the barriers for H and D is substantially large, of the order of that found for porphyrin. In addition, a contribution for heavy atom tunneling is observed.

At present, one can only speculate about the structure of the postulated non-reactive form. It could be that at low temperatures, the keto form may exhibit a zwitterionic aromatic character, and at high temperature a less polar but quinoid structure. Both structures are normally limiting structures. However, the zwitterionic structure is highly solvated and will exhibit, therefore, a much more negative entropy as compared to the zwitterionic structure. The entropy decrease is expected to be especially large in the case of apolar but polarizable solvents as has been shown by Caldin et al. [84]. Another possibility could be the formation of an

WILEY-VCH
Schowen
2. UK
N. Denzau
Kühn & Weyh Satz und Medien
Freiburg
l:/Vch/Schowen/3b2/c06.3d
6.9.2006

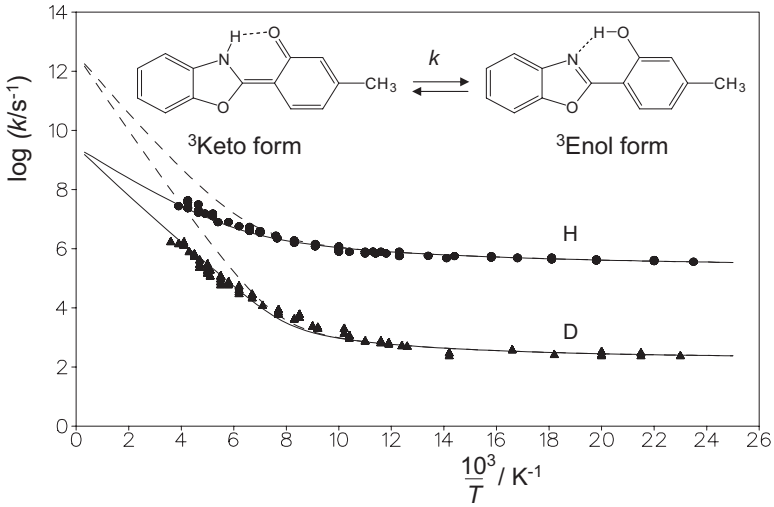

Figure 6.48 Arrhenius plot of the triplet state tautomerism of 2-(2′-hydroxy-4′-methylphenyl) benzoxazole (Me-BO, upper curve) and its deuterated analog (lower curve) dissolved in alkanes. The kinetic data were taken from Al-Soufi et al. [83]. The solid lines were calculated using the parameters listed in Table 6.4.

enolic conformer exhibiting an intramolecular OHO- instead of an OHN-hydrogen bond. However, further spectroscopic and kinetic measurements are necessary to clarify this problem.

Let us now discuss the well-studied case of the isomerization of the 2,4,6-tri-*tert*-butylphenyl radical to 3,5-di-*tert*-butylneophyl in apolar organic solvents, depicted in Fig. 6.49 which has been studied by Brunton et al. [8]. Various barrier types were used by these authors for Bell-type semiclassical tunneling calculations. It was shown that an inverted parabola could not give a satisfactory fit. The pre-exponential factors found for other barrier types were of the order of 8 to 12. As depicted in Fig. 6.49, a solution to the problem can be obtained in terms of an equilibrium where again a reactive form dominates at low and a non-reactive form at high temperature, as in the preceding case of Me-BO. In the case of the 2,4,6-tri-*tert*-butylphenyl radical one may interpret the reactive form with a configuration where the C–H bonds of the methyl groups are pointing in the direction of the aromatic acceptor carbon atom. Such a configuration could have a more negative entropy as compared to the non-reactive forms with unfavorable transfer geometries, dominating at high temperatures. The tunnel parameters used to calculate the Arrhenius curves are included in Table 6.4. No anomaly can be detected; the high barrier can be explained by the little capability for the formation of CHC-hydrogen bonds.

Let us discuss now some examples where non-reactive states are present at low temperatures, and reactive states at high temperatures.

WILEY-VCH
Schowen
2. UK
N. Denzau

Kühn & Weyh Satz und Medien
Freiburg
l:/Vch/Schowen/3b2/c06.3d
6.9.2006

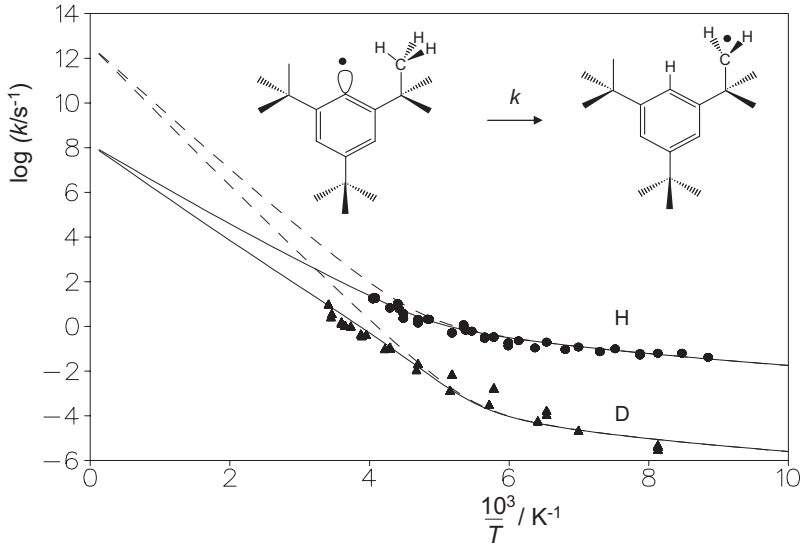

Figure 6.49 Arrhenius curves of the isomerization of the 2,4,6-tri-*tert*-butylphenyl radical to 3,5-di-*tert*-butylneophyl in apolar organic solvents. The solid and dashed lines were calculated as described in the text using the parameters listed in Table 6.4. Data from Brunton et al. [8].

The first two examples are the H-transfers in 2-hydroxyphenoxyl radicals which have been studied using dynamic EPR spectroscopy. When 3,6-di-*tert*-butyl-2-hydroxyphenoxyl and its deuterated analog are dissolved in heptane the Arrhenius diagram of Fig. 6.50 was obtained by Bubnov et al. [85]. The kinetic isotope effect is about 10 at room temperature. Setting the pre-exponential factor to $10^{12.6}$ (Table 6.4), leads to the concave Arrhenius curve depicted as solid lines. In contrast, Fig. 6.51 depicts the kinetic data of the parent compound 2-hydroxyphenoxyl in CCl_4/CCl_3F to which 0.11 mol l^{-1} dioxane had been added to increase the solubility [86]. Now, a kinetic isotope effect of about 56 is obtained at room temperature. This large difference between both molecules had been noted already some time ago by Limbach et al. [87]. In particular, it was noted that the two Arrhenius curves of the H and the D reaction are almost parallel. Application of the Bell–Limbach tunneling leads to unusually large pre-exponential factors of 10^{18} s^{-1}. As shown in Fig. 6.20(b) and the parameters of Table 6.4, the use of Eq. (6.43) improves the analysis, although the interpretation is similar to that obtained before.

The dashed lines in Fig. 6.51 indicate the intrinsic Arrhenius curve of the transfer, whereas the solid line indicates the one including the pre-equilibrium. The reduction of the rate constants as compared to the di-*tert*-butyl radical is explained by the formation of a non-reactive species at low temperatures, which is hydrogen bonded to the added dioxane. Thus, for the reaction to occur, the intramolecular H-bonded species has first to be formed, which exhibits a higher energy but also a

WILEY-VCH
Schowen
2. UK
N. Denzau

Kühn & Weyh Satz und Medien
Freiburg
l:/Vch/Schowen/3b2/c06.3d
6.9.2006

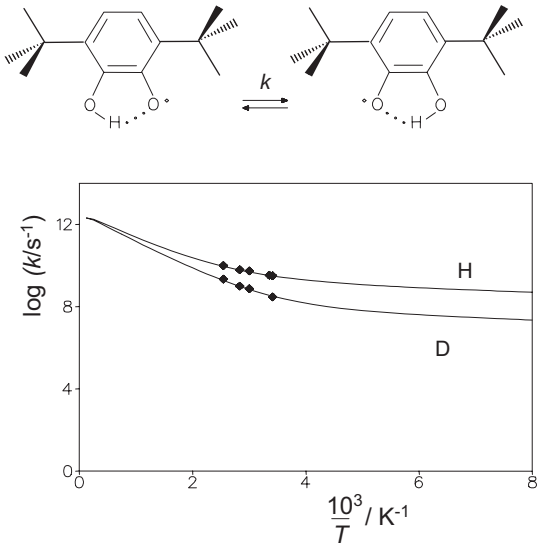

Figure 6.50 Arrhenius curves of the tautomerism of 3,6-di-*tert*-butyl-2-hydroxyphenoxyl dissolved in heptane according to Bubnov et al. [85]. The solid lines were calculated using the parameters listed in Table 6.4.

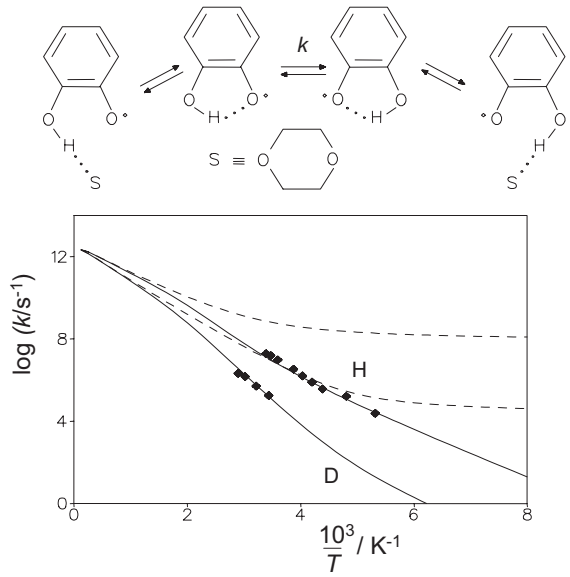

Figure 6.51 Arrhenius curves of the tautomerism of 2-hydroxyphenoxyl dissolved in CCl_4/CCl_3F/dioxane according to Loth et al. [86]. The solid lines were calculated using the parameters listed in Table 6.4.

WILEY-VCH
Schowen
2. UK
N. Denzau

Kühn & Weyh Satz und Medien
Freiburg
l:/Vch/Schowen/3b2/c06.3d
6.9.2006

more positive entropy. A comparison of the Arrhenius curves in Fig. 6.20(b) indicates that the desolvated intramolecular H-bonded species is never dominant over the whole temperature range, as the interaction with dioxane is stronger because of the linear intermolecular H-bond, in comparison with the weaker intramolecular H-bond.

The larger kinetic H/D isotope effects in the parent radical can be explained in terms of the higher symmetry of the parent radical as compared to the di-*tert*-butyl radical. In the latter, the methyl groups on both sides of the ring are not ordered, leading to effective asymmetric double well potentials of the H-transfer. These examples show how subtle structural effects can lead to very different H-transfer properties.

A related solvent effect was found for the proton exchange between acetic acid and methanol in tetrahydrofuran by Bureiko et al [88] and by Gerritzen et al. [9]. Hydrogen bonding to the solvent prevents the formation of the cyclic complexes in which the proton exchange takes place. Unfortunately, these complexes could not be seen directly. The rate constants were measured as a function of concentra-

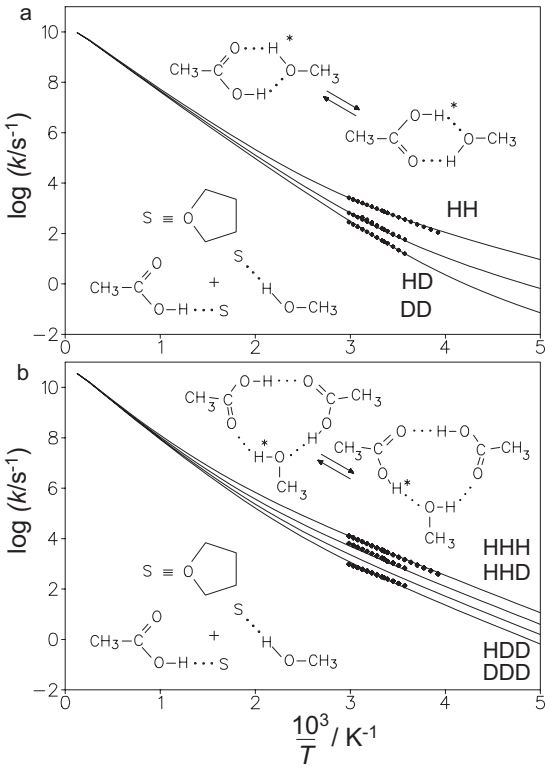

Figure 6.52 Arrhenius curves of the HH and HHH-transfer between acetic acid and methanol dissolved in tetrahydrofuran. Adapted from Ref. [9].

WILEY-VCH
Schowen
2. UK
N. Denzau
Kühn & Weyh Satz und Medien
Freiburg
l:/Vch/Schowen/3b2/c06.3d
6.9.2006

tion. At low concentration a second-order rate law was obtained indicating a HH-transfer in a cyclic 1:1 hydrogen bonded complex between acetic acid and methanol. At higher concentrations, the rate law changed indicating the participation of two acetic acid molecules, i.e. a HHH process. The multiple kinetic isotope effects were measured as a function of the inverse temperature as illustrated in Fig. 6.52.

For the double proton transfer two large kinetic HH/HD and HD/DD isotope effects of about 5 and 3 were observed, consistent with the pattern of Fig. 6.14(a) expected for a single barrier process. In the latter, tunneling was not yet included, which leads to the observed deviation from the Rule of the Geometric Mean. Recently, this reaction has been modeled using the instanton approach by Fernández-Ramos et al. [89]. The Arrhenius curves could be reproduced. The calculated geometries of the initial and the transition state are depicted in Fig. 6.53. In the latter, a proton is shifted towards the oxygen atom of methanol, but it is not completely transferred, rather, a strong hydrogen bond is formed.

The Arrhenius diagram of the HHH-transfer in the 2:1 complex is depicted in Fig. 6.52(b). The kinetic isotope effects are similar to those expected for a single barrier process according to Fig. 6.16(a). They exhibit little dependence on temperature, indicating a rather narrow barrier. Unfortunately, the reacting complex could not be observed directly and its structure studied in more detail. Note, however, that this complex represents a model for the catalytic sites of proteases as proposed by Northrop [90].

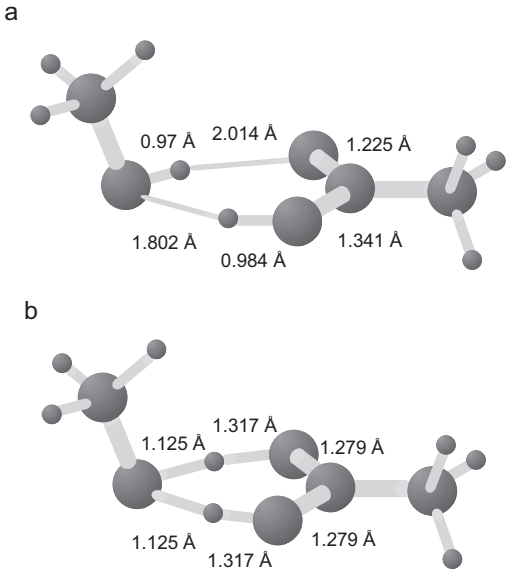

Figure 6.53 Structures of the initial state (a) and of the transition state (b) of the 1:1 complex between acetic acid and methanol according to Fernández-Ramos et al. [89]. The geometries were fully optimized at QCISD (quadratic configuration interaction including single and double substitutions) level of theory.

WILEY-VCH
Schowen
2. UK
N. Denzau

Kühn & Weyh Satz und Medien
Freiburg
l:/Vch/Schowen/3b2/c06.3d
6.9.2006

6.3.2.3 H-transfers in Complex Systems

Although the model systems of the previous section already involved major molecular motions, the latter can be even much more complex in living systems. Here, only two extreme examples are considered, i.e. hydride transfer in an enzyme and proton transfer in pure methanol.

6.3.2.3.1 The Case of H-transfer in Thermophilic Alcohol Dehydrogenase (ADH)

Firstly, let us discuss the example of a thermophilic alcohol dehydrogenase from *Bacillus stearothermophilus* (*bs*ADH) studied by Kohen et al. [91, 92]. This enzyme catalyzes the abstraction of a hydride to the nicotinamide cofactor NAD^+ as depicted in Fig. 6.54. The Arrhenius diagram is depicted in Fig. 6.54(a); a sudden decrease in the apparent slope and the apparent intercept of the Arrhenius curves is observed around room temperature (Fig. 6.54(b)). The puzzling observation is that the kinetic isotope effects are independent of temperature in the high-temperature regime but dependent on temperature in the low-temperature regime.

The solid lines in Fig. 6.54 were calculated recently [54] assuming the simple reaction network of Fig. 6.55. It is assumed that the enzyme adopts two different

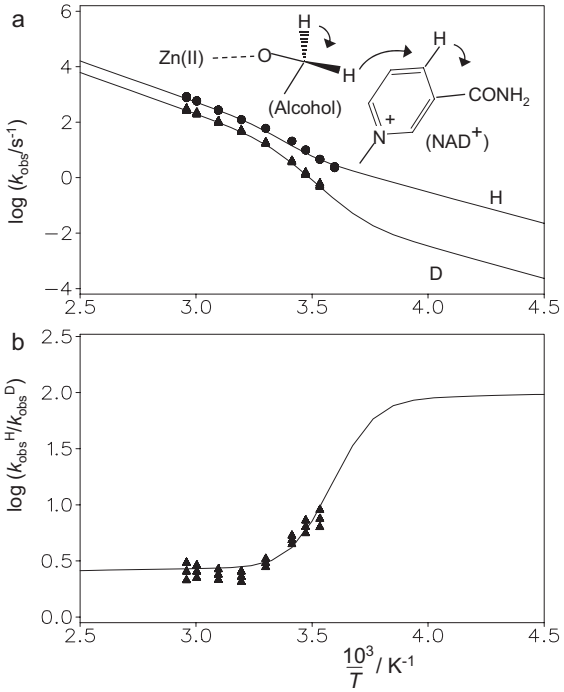

Figure 6.54 Arrhenius curves (a) and kinetic H/D isotope effects (b) of the intrinsic H-transfer in a thermophilic alcohol dehydrogenase (ADH) according to Kohen et al. [91]. The solid lines were calculated using the parameters listed in Table 6.4.

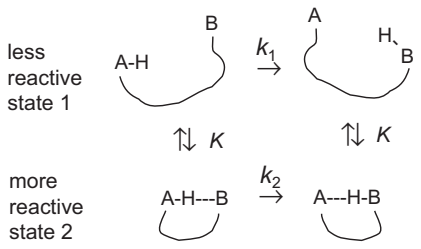

Figure 6.55 Conformational dependent H-transfer in a biomolecule.

states 1 and 2 at equilibrium (K), where 1 is less reactive than 2. In the less reactive state 1, dominating at lower temperatures, the rate constant of H-transfer is given by k_1, but in the more reactive state, dominating at higher temperatures, it is given by k_2. Assuming again that the H-transfer is slower than the conversions between the states the following expression is obtained by modification of Eq. (6.43), i.e.

$$k = x_1 k_1 + x_2 k_2 = k_1 \frac{1}{1+K} + k_2 \frac{K}{1+K} \tag{6.55}$$

x_1 and x_2 correspond to the mole fractions of states 1 and 2 and K is again the equilibrium constant of the formation of state 2 from state 1. According to Table 6.4, state 2 dominates at higher temperatures, in spite of its higher energy, because of its very large positive entropy. This state could be one where the protein has become ideally flexible for proper activity, in contrast to the low-temperature regime. This conclusion is in accordance with the fact that this *bs*ADH was evolved to function at ~65 C and with qualitative suggestions proposed in the past to rationalize the curved Arrhenius plot [91].

The tunnel parameters included in Table 6.4 indicate a ground state tunneling situation at high and at low temperatures, with temperature-independent kinetic isotope effects. The apparent temperature dependence observed at low temperatures is then the result of the transition between the two regimes, but does not arise from intrinsic temperature-dependent kinetic isotope effects. Note that in both states the pre-exponential factor of $10^{12.6}$ s^{-1} employed throughout this study was consistent with the data. The minimum energy for tunneling to occur is larger in the high-temperature state 2, but the barrier height and the barrier width are smaller than in the low temperature state 1. Thus, there seems to be a substantial change in the barrier parameters upon flexibilization of the enzyme at higher temperatures.

6.3.2.3.2 **The Case of H-transfer in Pure Methanol and Calix[4]arene**

As a second case of high complexity, let us discuss how protons are exchanged in pure protic liquids. This problem has been studied by Gerritzen et al. [93] who studied the inverse proton lifetimes τ_{AH}^{-1} of $CH_3OH \equiv AH$ in the pure liquid and

WILEY-VCH
Schowen
2. UK
N. Denzau

Kühn & Weyh Satz und Medien
Freiburg
l:/Vch/Schowen/3b2/c06.3d
6.9.2006

of CH_3OH present as isotopic impurity in chemically pure $CH_3OD \equiv AD$ as a function of temperature. A mechanism involving the transfer of a small number n of protons in relatively stable cyclic hydrogen bonded intermediates $(AH)_n$ according to Fig. 6.10 to 6.18 was discarded. One reason was the finding that the addition of an organic solvent to methanol immediately quenches the proton exchange observed for the pure liquid. This would not be the case if the transfer takes place in cyclic hydrogen bonded intermediates.

Therefore, an autoprotolysis mechanism was proposed consisting of dissociation:

$$AH + AH \underset{k_n}{\overset{k_d}{\rightleftharpoons}} A^- + AH_2^+ \tag{6.56}$$

$$\text{cation propagation } AH_2^+ + AH \underset{\longleftarrow}{\overset{k_1}{\longrightarrow}} AH + AH_2^+ \tag{6.57}$$

$$\text{anion propagation } AH^- + AH \underset{\longleftarrow}{\overset{k_2}{\longrightarrow}} AH^- + AH \tag{6.58}$$

$$\text{neutralization } A^- + AH_2^+ \underset{k_d}{\overset{k_n}{\rightleftharpoons}} AH + AH \tag{6.59}$$

The concentration of methoxonium and methoxide ions in the pure liquid is given by the autoprotolysis constant

$$K^H = \frac{k_d}{k_n} = c_{AH_2^+} c_{AH^-} \tag{6.60}$$

where K^H represents the autoprotolysis constant, which is 2.76×10^{-17} mol^2 l^{-2} at 298 K, i.e. $c_{AH_2^+} = c_{AH^-} = 5.2 \times 10^{-9}$ mol l^{-1} [94]. The autoprotolysis mechanism is immediately suppressed by adding an organic solvent as it reduces the dielectric constant and hence the autoprotolysis constant.

The following expression for the inverse proton life times follows from the autoprotolysis mechanism in CH_3OH a straightforward way [93]

$$\tau_{AH}^{-1} = (k_1^H c_{AH_2^+} + k_2^H c_{AH^-}) = (k_1^H + k_2^H)\sqrt{K^H} \tag{6.61}$$

For 1% CH_3OH in CH_3OD it was shown that

$$\tau_{AH}^{-1}(CH_3OD) = (k_1^H(CH_3OD) + k_2^H(CH_3OD))\sqrt{K^D} \tag{6.62}$$

where K^D represents the autoprotolysis constant of CH_3OD. Let E_{a1}^H and E_{a2}^H be the energies of activation describing the temperature dependence of k_1^H and k_2^H. By assuming that $E_{a1}^H \cong E_{a2}^H$ it follows then from Eq. (6.61) that the effective energy of activation of proton exchange is given by

$$E_a^H = E_{a1}^H + \frac{\Delta H^H}{2} \tag{6.63}$$

where ΔH^H represents the enthalpy of autoprotolysis of CH_3OH. In other words, if the cation and the anion are not created by autoprotolysis but stem from acid

WILEY-VCH
Schowen
2. UK
N. Denzau

Kühn & Weyh Satz und Medien
Freiburg
l:/Vch/Schowen/3b2/c06.3d
6.9.2006

and basic impurities, their concentration will be temperature independent and E_a^H is equal to E_{a1}^H. When the impurities are, however, removed, E_a^H is substantially increased. This is indeed observed, as illustrated in the Arrhenius plot of Fig. 6.56(a). The solid lines are given by

$$\begin{aligned}\tau_{AH}^{-1}(CH_3OH) &= 10^{6.1}\exp(-28.5\,\mathrm{kJmol^{-1}}/RT)\\ \tau_{AH}^{-1}(CH_3OD) &= 10^{5.7}\exp(-29.3\,\mathrm{kJmol^{-1}}/RT)\end{aligned} \tag{6.64}$$

The kinetic isotope effects observed are given by [93]

$$\frac{\tau_{AH}^{-1}(CH_3OH)}{\tau_{AH}^{-1}(CH_3OD)} = \frac{(k_1^H(CH_3OH)+k_2^H(CH_3OH))}{(k_1^H(CH_3OD)+k_2^H(CH_3OD))} \times \sqrt{\frac{K^H}{K^D}} = 3.2 \text{ at } 298\text{ K} \tag{6.65}$$

This overall kinetic isotope effect represents the product of an average kinetic isotope effect of the two propagation steps times the equilibrium isotope effect of the

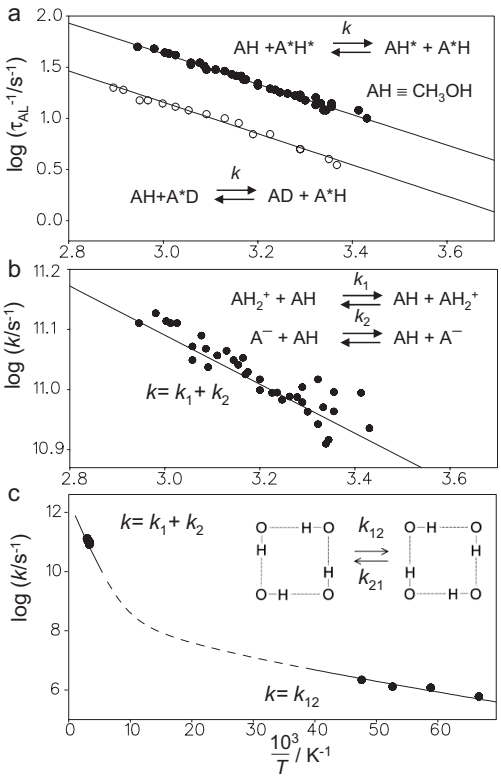

Figure 6.56 Arrhenius curves of (a) proton exchange in pure CH_3OH and CH_3OD. Adapted from Gerritzen et al. [93]. (b) Arrhenius curves of the elementary proton transfers in methanol calculated from the data of Fig. 6.56(a) and the known ionization constant. (c) Kinetic data of the HHHH-transfer in solid *p-tert*-butyl calix[4]arene reported by Horsewill et al. [80] combined with those of Fig. 6.56(a).

WILEY-VCH
Schowen
2. UK
N. Denzau
Kühn & Weyh Satz und Medien
Freiburg
l:/Vch/Schowen/3b2/c06.3d
6.9.2006

autoprotolysis. The value for water solutions was shown to be $K^H/K^D = 5$ at 298 K [95], whereas for methanol solutions a value of 6.5 was predicted [96]. Thus, the average kinetic isotope effect of the propagation is between 1.3 and 1.4. This effect corresponds to the usual isotope ratio expected for the reorientation of CH_3OH and CH_3OD.

Using Eq. (6.61), the inverse life times $\tau_{AH}^{-1}(CH_3OH)$ were converted into the sum $k_1^H + k_2^H = k_1^H(CH_3OH) + k_2^H(CH_3OH)$ plotted in Fig. 6.56(b) as a function of the inverse temperature. The solid line was given by [93]

$$k_1^H + k_2^H = 10^{12.3}\exp(-7.7\,\mathrm{kJmol^{-1}}/RT),\ k_1^H + k_2^H = 9.3\times10^{10}\mathrm{s^{-1}}\ \text{at 298 K} \qquad (6.66)$$

It follows that $\Delta H^H \cong 40$ kJ mol^{-1}. Note that Grunwald et al. [97] measured values of $k_1 = 8.8\times10^{10}$ s^{-1} and $k_2 = 1.85\times10^{10}$ s^{-1} for buffered solutions; their sum is in very good agreement with the value obtained for pure methanol.

The values of $k_1^H + k_2^H$ for water are very close to those of methanol. Using the known dependence of K^H as a function of temperature, the proton lifetimes in pure water were estimated [93]

$$\tau_{AH}^{-1}(H_2O) = 10^{9.9}\exp(-39\,\mathrm{kJmol^{-1}}/RT) = 15000\ \mathrm{s^{-1}}\ \text{at 298 K} \qquad (6.67)$$

Thus, proton exchange is faster than in pure methanol because of the larger autoprotolysis constant.

For comparison, let us compare the methanol data with those obtained by Horsewill et al. [80] who have reported an intramolecular quadruple proton transfer in the solid state between the four OH groups of solid calix[4]arene. Almost temperature independent rate constants were observed, which are again indicative of tunneling. An Arrhenius curve can be calculated using reasonable parameters (Table 6.4) which can reproduce both the pure methanol and the calix[4]arene data. It would be interesting to know more about the kinetic isotope effects in both systems.

6.4 Conclusions

In this chapter, the Bell–Limbach tunneling model has been applied to describe the Arrhenius curves of a number of single and multiple hydrogen transfer reactions. This model contains a number of parameters which can be obtained by simulation of the Arrhenius curves when enough experimental data are available. It is proposed to describe concerted multiple H-transfers in terms of a single barrier process. Multiple kinetic isotope effects of stepwise transfers can be treated in terms of formal kinetic reaction theory, where in each step one or more protons can be transferred, again in a concerted way. This approach is justified if each step can be described in terms of rate constants. This may not be the case for very strong hydrogen bonds, where H can be delocalized. Each reaction step can be

WILEY-VCH
Schowen
2. UK
N. Denzau
Kühn & Weyh Satz und Medien
Freiburg
l:/Vch/Schowen/3b2/c06.3d
6.9.2006

treated as a first approach in terms of the Bell–Limbach or any other tunneling model, or in terms of a more sophisticated quantum-mechanical theory.

A main result of the examples discussed above is that pre-exponential factors of H-transfers coupled to only minor heavy atom motions are of the order of $kT/h \cong 10^{12.6}$ s^{-1}, the value predicted by Eyring's transition state theory for the high-pressure limit [5]. Deviations are then a first and important diagnostic tool for detecting so far unrecognized heavy atom motions and pre-equilibria such as conformational isomerism and hydrogen bond equilibria. Two types of heavy atom motions are considered, i.e. those which precede the H tunnel process and those which take place during the tunnel process. The latter give rise to an increased tunneling mass which reduces kinetic H/D isotope effects arising from tunneling. Thus, this model helps experimentalists to interpret their kinetic data, but does not preclude further quantum-mechanical studies of the hydrogen transfer steps.

Acknowledgements

This research has been supported by the Deutsche Forschungsgemeinschaft, Bonn, and the Fonds der Chemischen Industrie (Frankfurt). I am indebted to Professors Maurice Kreevoy, Minneapolis, Minnesota, USA; R. L. Schowen, Lawrence, Kansas, USA and G. S. Denisov, St. Petersburg, Russian Federation for stimulating discussions over three decades. I also thank Professors G. S. Denisov and R. L. Schowen for carefully reading the manuscript and for their helpful comments.

References

1 E. Caldin, V. Gold (Eds.), *Proton Transfer Reactions*, Chapman and Hall: London, 1975.

2 R. A. Marcus, *J. Chem. Phys.* **1966**, *45*, 4493–4499.

3 P. Schuster, G. Zundel, C. Sandorfy (Eds.), *The Hydrogen Bond*, North Holland, Amsterdam, 1976, Vol 1–3.

4 (a) H. H. Limbach, Dynamic NMR Spectroscopy in the Presence of Kinetic Hydrogen/ Deuterium Isotope Effects, in *NMR Basic Principles and Progress, Deuterium and Shift Calculation*, Springer-Verlag, Heidelberg 1991, Vol. 23, pp. 66–167; (b) H. H. Limbach, Dynamics of Hydrogen Transfer in Liquids and Solids, in *Encyclopedia of Nuclear Magnetic Resonance*, D. M. Grant, R. K. Harris (Eds.), *Advances in NMR*, John Wiley & Sons, Chichester, 2002, Suppl. Vol. 9, pp. 520–531.

5 S. Glasstone, K. J. Laidler, H. Eyring, *The Theory* of *Rate Processes*. McGraw-Hill, New York 1941.

6 (a) J. Bigeleisen, *J. Chem. Phys.* **1949**, *17*, 675–678; (b) J. Bigeleisen, *J. Chem. Phys.* **1955**, *23*, 2264–2267; (c) L. Melander, W. H. Saunders, *Reaction Rates of Isotopic Molecules*, Krieger, Malabar, FL, 1987.

7 (a) R. P. Bell, *The Proton in Chemistry*, 2nd edn. Chapman and HalI, London, **1973**; (b) R. P. Bell, *The Tunnel Effect*, Chapman and Hall, London, **1980**.

8 G. Brunton, J. A. Gray, D. Griller, L. R. C. Barclay, K. U. Ingold, *J. Am. Chem. Soc.* **1978**, *100*, 4197–4200.

WILEY-VCH
Schowen
2. UK
N. Denzau

Kühn & Weyh Satz und Medien
Freiburg
l:/Vch/Schowen/3b2/c06.3d
6.9.2006

9 (a) D. Gerritzen, H. H. Limbach, *J. Am. Chem. Soc.* **1984**, *106*, 869–879; (b) H. H. Limbach, W. Seiffert, *J. Am. Chem. Soc.* **1980**, *102*, 538–542.

10 J. Basran, S. Patel, M. J. Sutcliffe, N. S. Scrutton, *J. Biol. Chem.* **2001**, *276*, 6234–6242.

11 (a) N. Bruniche-Olsen, J. Ulstrup, *J. Chem. Soc., Faraday Trans. 1* **1979**, *75*, 205–226; (b) E. D. German, A. M. Kuznetsov, R. R. Dogonadze, *J. Chem. Soc., Faraday Trans. 2* **1980**, *76*, 1128–1146.

12 (a) A. M. Kuznetsov, J. Ulstrup, *Can. J. Chem.* **1999**, *77*, 1085–1096; (b) A. M. Kuznetsov, J. Ulstrup, *Proton Transfer and Proton Conductivity in Condensed Matter Environment.* In *Isotope Effects in the Biological and Chemical Sciences*, A. Kohen, H. H. Limbach (Eds.) Taylor & Francis, Boca Raton FL, 2005, Ch. 26, pp. 691–724.

13 M. J. Knapp, K. Rickert, J. P. Klinman, *J. Am. Chem. Soc.* **2002**, *124*, 3865–3874.

14 (a) W. Siebrand, T. A. Wildman, M. Z. Zgierski, *J. Am. Chem. Soc.* **1984**, *106*, 4083–4089; (b) W. Siebrand, T. A. Wildman, M. Z. Zgierski, *J. Am. Chem. Soc.* **1984**, *106*, 4089–4096.

15 D. Truhlar, Variational Transition-State Theory and Multidimensional Tunneling for Simple and Complex Reactions in the Gas Phase, Solids, Liquids, and Enzymes, in Ref. [12b], Ch. 22, pp. 579–620.

16 Z. Smedarchina, W. Siebrand, A. Fernández-Ramos, Kinetic Isotope Effects in Multiple Proton Transfer, in Ref. [12b], Ch. 22, pp. 521–548.

17 O. Brackhagen, Ch. Scheurer, R. Meyer, H. H. Limbach, *Ber. Bunsenges. Phys. Chem.* **1998**, *102*, 303–316.

18 (a) H. H. Limbach, J. Hennig, D. Gerritzen, H. Rumpel, *Faraday Discuss., Chem. Soc.* **1982**, *74*, 229–243; (b) M. Schlabach, B. Wehrle, H. Rumpel, J. Braun, G. Scherer, H. H. Limbach, *Ber. Bunsenges. Phys. Chem.* **1992**, *96*, 821–833; (c) B. Wehrle, H. H. Limbach, M. Köcher, O. Ermer, E. Vogel, *Angew. Chem.* **1987**, *99*, 914–917; *Angew. Chem. Int. Ed. Engl.* **1987**, *26*, 934–936; (d) J. Braun, M. Schlabach, B. Wehrle, M. Köcher, E. Vogel, H. H. Limbach, *J. Am. Chem. Soc.* **1994**, *116*, 6593–6604; (e) J. Braun, H. H. Limbach, P. G. Williams, H. Morimoto, D. Wemmer, *J. Am. Chem. Soc.* **1996**, *118*, 7231–7232.

19 (a) M. Schlabach, H. Rumpel, H. H. Limbach, *Angew. Chem.* **1989**, *101*, 84–87; *Angew. Chem. Int. Ed. Engl.* **1989**, *28*, 76–79; (b) M. Schlabach, G. Scherer, H. H. Limbach, *J. Am. Chem. Soc.* **1991**, *113*, 3550–3558.

20 (a) M. Schlabach, B. Wehrle, H. H. Limbach, E. Bunnenberg, A. Knierzinger, A. Shu, B. R. Tolf, C. Djerassi, *J. Am. Chem. Soc.* **1986**, *108*, 3856–3858; (b) M. Schlabach, H. H. Limbach, E. Bunnenberg, A. Shu, B. R. Tolf, C. Djerassi, *J. Am. Chem. Soc.* **1993**, *115*, 4554–4565.

21 (a) H. Rumpel, H. H. Limbach, *J. Am. Chem. Soc.* **1989**, *111*, 5429–5441; (b) H. Rumpel, H. H. Limbach, G. Zachmann, *J. Phys. Chem.* **1989**, *93*, 1812–1818.

22 (a) G. Otting, H. Rumpel, L. Meschede, G. Scherer. H. H. Limbach, *Ber. Bunsenges. Phys. Chem.* **1986**, *90*, 1122–1129; (b) G. Scherer, H. H. Limbach, *J. Am. Chem. Soc.* **1989**, *111*, 5946–5947; (c) G. Scherer, H. H. Limbach, *J. Am. Chem. Soc.* **1994**, *116*, 1230–1239; (d) G. Scherer, H. H. Limbach. *Croat. Chem. Acta,* **1994**, *67*, 431–440.

23 (a) J. Braun, C. Hasenfratz, R. Schwesinger, H. H. Limbach, *Angew. Chem.* **1994**, *106*, 2302–2304; *Angew. Chem. Int. Ed. Engl.* **1994**, *33*, 2215–2217; (b) J. Braun, R. Schwesinger, P. G. Williams, H. Morimoto, D. E. Wemmer, H. H. Limbach, *J. Am. Chem. Soc.* **1996**, *118*, 11101–11110.

24 (a) L. Meschede, D. Gerritzen, H. H. Limbach, *Ber. Bunsenges. Phys. Chem.* **1988**, *92*, 469–485; (b) H. H. Limbach, L. Meschede, G. Scherer, *Z. Naturforsch.a* **1989**, *44*, 459–471; (c) L. Meschede, H. H. Limbach, *J. Phys. Chem.* **1991**, *95*, 10267–10280.

25 (a) F. Aguilar-Parrilla, O. Klein, J. Elguero, H. H. Limbach, *Ber. Bunsenges. Phys. Chem.* **1997**, *101*, 889–901; (b) O. Klein, M. M. Bonvehi, F. Aguilar-Parrilla, J. Elguero, H. H. Limbach, *Isr. J. Chem.* **1999**, *34*, 291–299.

WILEY-VCH
Schowen
2. UK
N. Denzau

Kühn & Weyh Satz und Medien
Freiburg
l:/Vch/Schowen/3b2/c06.3d
6.9.2006

26 H. H. Limbach, O. Klein, J. M. Lopez Del Amo, J. Elguero, *Z. Phys. Chem.* **2004**, *217*, 17–49.

27 O. Klein, F. Aguilar-Parrilla, J. M. Lopez, N. Jagerovic, J. Elguero, H. H. Limbach, *J. Am. Chem. Soc.* **2004**, *126*, 11718–11732.

28 J. Brickmann, H. Zimmermann, *Ber. Bunsenges. Phys. Chem.* **1966**, *70*, 157–165; **1966**, *70*, 521–524; **1967**, *71*, 160–1964; J. Brickmann, H. Zimmermann, *J.Chem.Phys.* **1969**, *50*, 1608–1618.

29 P. M. Morse, E. C. G. Stückelberg, *Helv. Phys. Acta* **1931**, *4*, 335–354; R. L. Somorjai, D. F. Hornig, *J.Phys.Chem.* **1962**, *36*, 1980–1987; J. Laane, *Appl. Spectrosc.* **1970**, *24*, 73–80.

30 W. F. Rowe, R. W. Duerst, E. B. Wilson, *J. Am. Chem. Soc.* **1976**, *98*, 4021–4023; S. L. Baughcum, R. W. Duerst, W. F.Rowe, Z. Smith, E. B. Wilson, *J. Am. Chem. Soc.* **1981**, *103*, 6296–6393; S. L. Baughcum, Z. Smith, E. B. Wilson, R. W. Duerst, *J. Am. Chem. Soc.* **1984**, *106*, 2260–2265.

31 R. L. Redington, R. L. Sams, *J. Phys. Chem. A* **2002**, *106*, 7494–7511.

32 F. Madeja, M. Havenith, *J. Chem. Phys.* **2002**, *117*, 7162–7168.

33 D. W. Firth, P. F. Barbara, H. P. Trommsdorff, *Chem.Phys.* **1989**, *136*, 349–360.

34 J. D. McDonald, *Annu. Rev. Phys. Chem.* **1979**, *30*, 29–50.

35 D. Borgis, J. T. Hynes, *J. Chem. Phys.* **1991**, *94*, 3619–3628; D. Borgis, J. T. Hynes, *Chem. Phys.* **1993**, *170*, 315–346.

36 H. H. Limbach, G. Buntkowsky, J. Matthes, S. Gründemann, T. Pery, B. Walaszek, B. Chaudret, *Chem. Phys. Chem.* **2006**, *7*, 551–554; G. Buntkowsky, B. Walaszek, A. Adamczyk, Y. Xu, H. H. Limbach, B. Chaudret, *Phys. Chem. Chem. Phys.* **2006**, *8*, 1929–1935.

37 R. P. Bell, *J. Chem. Soc., Faraday Discuss.* **1965**, *39*, 16–24.

38 (a) L. Pauling, *J. Am. Chem. Soc.* **1947**, *69*, 542–553; (b) I. D. Brown, *Acta Crystallogr., Sect. B* **1992**, *48*, 553–572.

39 (a) T. Steiner, *J. Chem. Soc., Chem. Commun.* **1995**, 1331–1332; (b) T. Steiner, *J. Phys. Chem. A* **1998**, *102*, 7041–7052; (c) T. Steiner, *Angew. Chem. Int. Ed. Engl.* **2002**, *41*, 48-76.

40 H. H. Limbach, G. S. Denisov, N. S. Golubev, Hydrogen Bond Isotope Effects Studied by NMR, in Ref [12b], Ch. 7, pp. 193–252.

41 (a) H. S. Johnston, *Gas Phase Reaction Rate Theory. Modern Concepts in Chemistry*, The Ronald Press Company, New York 1966; (b) D. G. Truhlar, *J. Am. Chem. Soc.* **1972**, *94*, 7584–7586; (c) N. Agmon, *Chem. Phys. Lett.* **1977**, *45*, 343–345.

42 H. H. Limbach, M. Pietrzak, H. Benedict, P. M. Tolstoy, N. S. Golubev, G. S. Denisov, *J. Mol. Struct.* **2004**, *706*, 115–119.

43 H. H. Limbach, M. Pietrzak, S. Sharif, P. M. Tolstoy, I. G. Shenderovich, S. N. Smirnov, N. S. Golubev, G. S. Denisov, *Chem. Eur. J.* **2004**, *10*, 5195–5204.

44 K. F. Wong, T. Selzer, S. J. Benkovic, S. Hammes-Schiffer, *Proc. Nat. Acad. Sci. USA* **2005**, *102*, 6807–6812.

45 F. H. Westheimer, *Chem. Rev.* **1961**, *61*, 265–273.

46 R. A. More O'Ferrall, *Substrate Isotope Effects*. in Ref. [1], Ch. 8, pp. 201–262.

47 (a) G. Wentzel, *Z. Phys.* **1926**, *138*, 518–529; (b) H. A. Kramers, *Z. Phys.* **1926**, *39*, 828–840; (c) L. Brillouin, *C. R. Acad. Sci*, **1926**, *153*, 24–26.

48 Ref. [7a], p. 275.

49 U. Langer, L. Latanowicz, Ch. Hoelger, G. Buntkowsky, H. M. Vieth, H. H. Limbach, *Phys. Chem. Chem. Phys.* **2001**, *3*, 1446–1458.

50 S. N. Smirnov, H. Benedict, N. S. Golubev, G. S. Denisov, M. M. Kreevoy, R. L. Schowen, H. H. Limbach, *Can. J. Chem.* **1999**, *77*, 943–949.

51 S. Schweiger, G. Rauhut, *J. Phys. Chem. A* **2003**, *107*, 9668–9678.

52 M. Eigen, *Angew. Chem. Int. Ed. Engl.* **1964**, *3*, 1–23.

53 (a) F. Männle, H. H. Limbach, *Angew. Chem. Int. Ed. Engl.* **1996**, *35*, 441–442; (b) H. H. Limbach, F. Männle, C. Detering, G. S. Denisov, *Chem. Phys.* **2005**, *319*, 69–92.

WILEY-VCH
Schowen
2. UK
N. Denzau

Kühn & Weyh Satz und Medien
Freiburg
l:/Vch/Schowen/3b2/c06.3d
6.9.2006

54 H. H. Limbach, J. M. Lopez del Amo, A. Kohen, *Philos. Trans. B*. **2006**, *361*, 1399–1415.

55 R. M. Claramunt, J. Elguero, A. R. Katritzky, *Adv. Heterocycl. Chem.* **2000**, *77*, 1–50.

56 D. K. Maity, T. N. Truong, *J. Porph. Phthal.* **2001**, *5*, 289–299.

57 C. B. Storm, Y. Teklu, *J. Am. Chem. Soc.* **1974**, *94*, 1745–1747; C. B. Storm, Y. Teklu, *Ann. N. Y. Acad. Sci.* **1973**, *206*, 631–640.

58 (a) J. Hennig, H. H. Limbach, *J. Chem. Soc., Faraday Trans.2* **1979**, *75*, 752–766; (b) H. H. Limbach, J. Hennig, R. Kendrick, C. S. Yannoni, *J. Am. Chem. Soc.* **1984**, *106*, 4059–4060.

59 P. Stilbs, M. E. Moseley, *J. Chem. Soc., Faraday Trans. 2* **1980**, *76*, 729–731.

60 J. Hennig, H. H. Limbach, *J. Magn. Reson.* **1982**, *49*, 322–328.

61 A. A. Bothner-By, R. L. Stephens, J. Lee, C. D. Warren, R. W. Jeanloz, *J. Am. Chem. Soc.* **1984**, *106, 811–813*.

62 A. Bax, D. G. Davis, *J. Magn. Reson.* **1985**, *63*, 207–213.

63 H. H. Limbach, J. Hennig, *J. Chem. Phys.* **1979**, *71*, 3120–3124; H. H. Limbach, J. Hennig, J. Stulz, *J. Chem. Phys.* **1983**, *78*, 5432–5436 ; H. H. Limbach, *J. Chem. Phys.* **1984**, *80*, 5343–5345.

64 A. Sarai, *Chem. Phys. Lett.* **1981**, *83*, 50–54 ; A. Sarai, *J. Chem. Phys.* **1982**, *76*, 5554–5563; A. Sarai, *J. Chem. Phys.* **1984**, *80*, 5341–5343.

65 D. K. Maity, R. L. Bell, T. N. Truong, *J. Am. Chem. Soc.* **2000**, *122*, 897–906.

66 (a) R. D. Kendrick, S. Friedrich, B. Wehrle, H. H. Limbach, C. S. Yannoni, *J. Magn. Reson.* **1985**, *65*, 159–161; (b) B. Wehrle, H. H. Limbach, *Chem. Phys.* **1989**, *136*, 223–247.

67 T. J. Butenhoff, C. B. Moore, *J. Am. Chem. Soc.* **1988**, *110*, 8336–8341.

68 J. D. Thoburn, W. Lüttke, C. Iber, H. H. Limbach, *J. Am. Chem. Soc.* **1996**, *118*, 12459–12460.

69 C. G. Hoelger, B. Wehrle, H. Benedict, H. H. Limbach, *J. Phys. Chem.* **1994**, *98*, 843–851.

70 U. Langer, C. Hoelger, B. Wehrle, L. Latanowicz, E. Vogel, H. H. Limbach, *J. Phys. Org. Chem.* **2000**, *13*, 23–34.

71 B. Wehrle, H. Zimmermann, H. H. Limbach, *J. Am. Chem. Soc.* **1988**, *110*, 7014–7024.

72 (a) B. H. Meier, F. Graf, R. R. Ernst, *J. Chem. Phys.* **1982**, *76*, 767–774; (b) A. Stöckli, B. H. Meier, R. Kreis, R. Meyer, R. R. Ernst, *J. Chem. Phys.* **1990**, *93*, 1502–1520; (c) A. Heuer, U. Haeberlen, *J. Chem. Phys.* **1991**, *95*, 4201–4124.

73 (a) J. L. Skinner, H. P. Trommsdorff, *J. Phys. Chem. A* **1988**, *89*, 897–907; (b) R. Meyer, R. R. Ernst, *J. Chem. Phys.* **1990**, *93*, 5518–5532; (c) Y. Kim, *J. Am. Chem. Soc.* **1996**, *118*, 1522–1528; (d) Y. Kim, *J. Phys. Chem. A* **1998**, *102*, 3025–3036.

74 Q. A. Xue, A. J. Horsewill, M. R. Johnson, H. P. Trommsdorff, *J. Chem. Phys.* **2004**, *120*, 11107–11119.

75 P. M. Tolstoy, P. Schah-Mohammedi, S. N. Smirnov, N. S. Golubev, G. S. Denisov, H. H. Limbach, *J. Am. Chem. Soc.* **2004**, *126*, 5621–5634.

76 F. Aguilar-Parrilla, G. Scherer, H. H. Limbach, M. C. Foces-Foces, F. H. Cano, J. A. S. Smith, C. Toiron, J. Elguero, *J. Am. Chem. Soc.* **1992**, *114*, 9657–9659.

77 (a) A. Baldy, J. Elguero, R. Faure, M. Pierrot, E. J. Vicent, *J. Am. Chem. Soc.* **1985**, *107*, 5290–5291; (b) J. A. S. Smith, B. Wehrle, F. Aguilar-Parrilla, H. H. Limbach, M. C. Foces-Foces, F. H. Cano, J. Elguero, A. Baldy, M. Pierrot, M. M. T. Khurshid, J. B. Larcombe-McDouall, *J. Am. Chem. Soc.* **1989**, *111*, 7304–7312; (c) F. Aguilar-Parrilla, C. Cativiela, M. D. Diaz de Villegas, J. Elguero, M. C. Foces-Foces, J. I. G. Laureiro, F. H. Cano, H. H. Limbach, J. A. S. Smith, C. Toiron, *J. Chem. Soc., Perkin 2* **1992**, 1737–1742; (d) J. Elguero, G. I. Yranzo, J. Laynez, P. Jiménez, M. Menédez, J. Catalán, J. L. G. De Paz, F. Anvia, R. W. Taft, *J. Org. Chem.* **1991**, *56*, 3942; (e) J. Elguero, F. H. Cano, M. C. Foces-Foces, A. Llamas-Saiz, H. H. Limbach, F. Aguilar-Parrilla, R. M. Claramunt, C. Lopez, *J. Heterocycl. Chem.* **1994**, *31*, 695–700; (f) F. Aguilar-Parrilla, F. Männle, H. H. Limbach, J. Elguero, N. Jagerovic, *Magn. Reson. Chem.* **1994**,

32, 699–702; (g) A. Llamaz-Saiz, M. C. Foces-Foces, F. H. Cano, P. Jimenez, J. Laynez, W. Meutermans, J. Elguero, H. H. Limbach, F. Aguilar-Parrilla, *Acta Crystallogr., Sect. B* **1994**, *50*, 746–762; (h) F. Aguilar-Parrilla, H. H. Limbach, M. C. Foces-Foces, F. H. Cano, N. Jagerovic, J. Elguero, *J. Org. Chem.* **1995**, *60*, 1965–1970; (i) J. Elguero, N. Jagerovic, M. C. Foces-Foces, F. H. Cano, M. V. Roux, F. Aguilar-Parrilla, H. H. Limbach, *J. Heterocycl. Chem.* **1995**, *32*, 451–456; (j) C. Lopez, R. M. Claramunt, A. Llamas-Saiz, M. C. Foces-Foces, J. Elguero, I. Sobrados, F. Aguilar-Parrilla, H. H. Limbach, *New J. Chem.* **1996**, 20, 523–536; (k) C. Hoelger, H. H. Limbach, F. Aguilar-Parrilla, J. Elguéro, O. Weintraub, S. Vega, *J. Magn. Res.* **1996**, *A120*, 46–55; (l) J. Catalan, J. l. M. Abboud, J. Elguero, *Adv. Heterocycl. Chem.* **1987**, *41*, 187; (m) F. Toda, K. Tanaka, M. C. Foces-Foces, A. Llamas-Saiz, H. H. Limbach, F. Aguilar-Parrilla, R. M. Claramunt, C. Lopez, J. Elguero, *J. Chem. Soc., Chem. Commun.* **1993**, 1139–1142; (n) F. Aguilar-Parrilla, R. M. Claramunt, C. Lopez, D. Sanz, H. H. Limbach, J. Elguero, *J. Phys. Chem.* **1994**, *98*, 8752–6760; (o) C. Foces-Foces, A. Echevarría, N. Jagerovic, I. Alkorta, J. Elguero, U. Langer, O. Klein, M. Minguet-Bonvehí, H. H. Limbach, *J. Am. Chem. Soc.* **2001**, *123*, 7898–7906.

78 J. L. G. de Paz, J. Elguero, M. C. Foces-Foces, A. Llamas-Saiz, F. Aguilar-Parrilla, O. Klein, H. H. Limbach, *J. Chem. Soc. Perkin Trans. 2* **1997**, 101–109.

79 (a) S. Schweiger, B. Hartke, G. Rauhut, *J. Phys. Chem. A* **2003**, *107*, 9668–9878; (b) S. Schweiger, B. Hartke, G. Rauhut, *Phys. Chem. Chem. Phys.* **2005**, 7, 493–500.

80 D. F. Brougham, R. Caciuffo, A. J. Horsewill, *Nature* **1999**, *397*, 241–243.

81 T. Vangberg, A. Ghosh, *J. Phys. Chem. B* **1997**, *101*, 1496–1497.

82 (a) F. Männle, I. Wawer, H. H. Limbach, *Chem. Phys. Lett.* **1996**, *256*, 657–662; (b) R. Anulewicz, I. Wawer, T. M. Krygowski, F. Männle, H. H. Limbach, *J. Am. Chem. Soc.* **1997**, *119*, 12223–12230.

83 W. Al-Soufi, K. H. Grellmann, B. Nickel, *J. Phys. Chem.* **1991**, *95*, 10503–10509.

84 E. F. Caldin, S. Mateo, *J. Chem. Soc., Faraday Trans.1* **1975**, *71*, 1876–1904.

85 (a) A. I. Prokofiev, N. N. Bubnov, S. P. Solodnikov, M. I. Kabachnik, *Tetrahedron Lett.* **1973**, 2479–2480; (b) N. N. Bubnov, S. P. Solodnikov, A. I. Prokofiev, M. I. Kabachnik, *Russ. Chem. Rev.* **1978**, *47*, 549–571.

86 K. Loth, F. Graf, H. Günthardt, *Chem. Phys.* **1976**, *13*, 95–113.

87 H. H. Limbach, D. Gerritzen, *Faraday Discuss. Chem. Soc.* **1982**, *74*, 279–296.

88 S. F. Bureiko, G. S. Denisov, N. S. Golubev, I. Y. Lange, *React. Kinet. Catal. Lett.* **1979**, *11*, 35–38.

89 A. Fernández-Ramos, Z. Smedarchina, J. Rodríguez-Otero, *J. Chem. Phys.* **2001**, *114*, 1567–1574.

90 D. B. Northrop, *Acc. Chem. Res.* **2001**, *34*, 790–797.

91 A. Kohen, R. Cannio, S. Bartolucci, J. P. Klinman, *Nature* **1999**, *399*, 496–499.

92 A. Kohen, *Kinetic Isotope Effects as Probes for Hydrogen Tunneling in Enzyme Catalysis*. In *Isotope Effects in the Biological and Chemical Sciences*, A. Kohen, H. H. Limbach (Eds.) Taylor & Francis, Boca Raton FL 2005, Ch. 28, pp. 743–765.

93 D. Gerritzen, H. H. Limbach, *Ber. Bunsenges. Phys. Chem.* **1981**, *85*, 527–535.

94 C. S. Leung and E. Grunwald, *J. Phys. Chem.* **1970**, *74*, 696–701.

95 E. J. King, in *Physical Chemistry of Organic Solvent Systems*, A. Covington, T. Dickinson (Eds.), Plenum Press, New York 1973, Ch. 3, pp. 331–403.

96 V. Gold, S. Grist, *J. Chem. Soc. B*, **1971**, 1665–1670.

97 E. Grunwald, C. F. Jumper, S. Meiboom, *J. Am. Chem. Soc.* **1963**, *84*, 4664–4671.

WILEY-VCH
Schowen
2. UK
N. Denzau

Kühn & Weyh Satz und Medien
Freiburg
l:/Vch/Schowen/3b2/c06.3d
6.9.2006